UNIVERSIDADE FEDERAL DO CEARÁ
CENTRO DE CIÊNCIAS
PROGRAMA DE PÓS-GRADUAÇÃO EM QUÍMICA
GRUPO DE ELETROQUÍMICA E CORROSÃO

LUÍS PAULO MOURÃO DOS SANTOS

ELECTRODEPOSITION OF TELLURIUM AND CADMIUM TELLURIDE ON GOLD FROM DEEP EUTECTIC SOLVENTS BASED ON CHOLINE CHLORIDE

FORTALEZA
2019

LUÍS PAULO MOURÃO DOS SANTOS

ELECTRODEPOSITION OF TELLURIUM AND CADMIUM TELLURIDE ON GOLD FROM DEEP EUTECTIC SOLVENTS BASED ON CHOLINE CHLORIDE

Doctoral thesis submitted to the Graduate Program in Chemistry in partial fulfillment of the requirements to obtain the Doctor degree in Chemistry. (Concentration area: Physical Chemistry)

Advisor: Prof. Dr. Pedro de Lima-Neto

FORTALEZA

2019

Dados Internacionais de Catalogação na Publicação
Universidade Federal do Ceará
Sistema de Bibliotecas
Gerada automaticamente pelo módulo Catalog, mediante os dados fornecidos pelo(a) autor(a)

S236e Santos, Luís Paulo Mourão dos.
Electrodeposition of tellurium and cadmium telluride on gold from deep eutectic solvents based on choline chloride / Luís Paulo Mourão dos Santos. – 2019.
101 f. : il. color.

Tese (doutorado) – Universidade Federal do Ceará, Centro de Ciências, Programa de Pós-Graduação em Química, Fortaleza, 2019.
Orientação: Prof. Dr. Pedro de Lima Neto.

1. tellurium. 2. cadmium telluride. 3. deep eutectic solvent. 4. electrodeposition. 5. semiconductor. I. Título.

CDD 540

LUÍS PAULO MOURÃO DOS SANTOS

ELECTRODEPOSITION OF TELLURIUM AND CADMIUM TELLURIDE ON GOLD FROM DEEP EUTECTIC SOLVENTS BASED ON CHOLINE CHLORIDE

Doctoral thesis submitted to the Graduate Program in Chemistry in partial fulfillment of the requirements to obtain the Doctor degree in Chemistry. (Concentration area: Physical Chemistry)

Advisors: Prof. Dr. Pedro de Lima-Neto

Approved in: 27/11/2019

DEFENSE COMMITTEE

_____

Prof. Dr. Pedro de Lima-Neto (Advisor)
Universidade Federal do Ceará (UFC)

_____

Prof. Dr. Paulo Naftali da Silva Casciano
Universidade Federal do Ceará (UFC)

_____

Prof. Dr. Walney Silva Araújo
Universidade Federal do Ceará (UFC)

_____

Prof. Dr. Elton Patrick Barbano
Universidade Estadual do Vale do Acaraú (UVA)

_____

Prof. Dr. Marcelo Monteiro Valente Parente
Instituto Federal de Educação, Ciência e Tecnologia do Ceará (IFCE)

I would like to dedicate this dissertation to:

My mother, who has spared no efforts for my education and for every single Brazilian whom, believes that a great nation is built under light of education.

ACKNOWLEDGEMENT

I would like to express my acknowledgments and gratitude to all those who gave me the support to complete this work. I would like to say thanks to …

The funding agencies CNPq (Conselho Nacional de Desenvolvimento Científico e Tecnológico), CAPES (Coordenação de Aperfeiçoamento de Pessoal de Nível Superior), and Finep (Financiadora de Estudos e Projetos) for their financial support.

My family for unconditional support until here, particularly to my mother for her the invaluable care and love.

Eva Jordana my lovely fiancée for her patience and constant encouragement during the preparation of this work.

My advisor Prof. Pedro de Lima-Neto (Department of Analytical Chemistry and Physical Chemistry, UFC) for all the support and guidance in the course of this research. In addition to his patience and generosity in offering me many opportunities in this period as doctoral a student which prepared me for the new challenges in my career. Finally, for the long discussions about physical chemistry and about daily life itself.

Profa. Adriana N. Correia (Department of Analytical Chemistry and Physical Chemistry, UFC) for support me in difficult moments. Also for the collaboration which allowed me to possible complete this work.

UFC and the Graduate Program in Chemistry, especially to Grupo de Eletroquímica e Corrosão (GELCORR) for host me as student over the last four years.

All researchers that contributed to this work without which this thesis would not have been possible. Therefore, I would like express my gratitude to Prof. Hosiberto Sant'Ana, Prof. Felipe Feitosa, and Dra. Regiane Silva Pinheiro (Department of Chemical Engineering, UFC) for their support with the measurements densities and viscosities of eutectic mixtures, my friend Dr. Rafael Freire and his colleagues (The Universidad de Santiago de Chile, Chile) for their collaboration with the TEM analyses, Prof. Marcelo José Gomes da Silva (Department of Materials Science and Engineering, UFC) for provided me access to the XRD equipment, Prof. Igor Vasconcelos (Department of Materials Science and Engineering, UFC) for his valuable time to discussions, Prof. Eduardo B. Barros and his doctoral student Daniel Araújo (Department of Physics, UFC) for their support with the AFM measurements, the colleagues at the Central Analítica UFC/CT-INFRA/MCTI-SISNANO/Pró-Equipamentos CAPES (Department of Physics, UFC) for their valuable support with the SEM investigation, Mrs. Nádia Pitombeira (Department of Organic Chemistry and Inorganic Chemistry, UFC)

for friendship and support with UV-vis measurements. Profa. Helena Becker and Profa. Elisane Longhinotti (Department of Analytical Chemistry and Physical Chemistry, UFC) and Prof. Walney Araújo (Department of Materials Science and Engineering, UFC) for hosted the members of GELCORR during the reform of our laboratory's building.

Good friends Jorge Luiz Cardozo, Wydson Martins, João Rodrigues Neto, Mohammed Masoumi, Natan Lima, Francisco Oliveira, Francisco Gilvane Sampaio, Francisco Iran de Sousa, Kleyton Camelo, Maurício de Sousa Pereira, Tiago Ribeiro, Anderson, Daniel Girão, Archimedes Avelino, Vinícius, Darley, Úrsula Cid and Samuel (Department of Materials Science and Engineering, UFC) for the friendship, endless discussions and fellowship at days and nights at UFC, at least for silence present that let me know that I am not alone.

The group mates Francisco Avelino Figueiredo-Sobrinho, Natália Vieira, Natália Gomes, Raíssa Costa, Raiane Nunes, Rodolfo, Carlos Pedro, Flaviana, Carla Manuela, Vanessa, Janmille Aragão, Henrique Jorge, Ana Aline Alcanfor, Evellin Enny, Erineldo, Uilson Alves, Danivo Machado, Stefany Costa, David Alves, José Joelson, Julierme Pereira, João Rufino Bezerra-Neto, and Wagner Neto for the companionship at this journey. Also, I would like to say thank you to Dr. Othon Campos for the friendship and endless discussion.

Colleagues and friends at Department of Organic Chemistry and Inorganic Chemistry Ana Rosa Richter, Rodrigo Costa, Fabrício, Everton, Ramon, Irisvan, Vinicius Sombra, and Dieric Abreu for the good moments of distractions and companionship.

My dear friend Lucas Vasconcelos and his family for their friendship over the last two decades.

Always the eyes watching you and the voice enveloping you. Asleep or awake, working or eating, indoors or out of doors, in the bath or in bed - no escape. Nothing was your own except the few cubic centimetres inside your skull.

(ORWELL, 1984, p. 18)George Orwell

ABSTRACT

Te is one of the most important for the production of materials in sectors, such as clean energy, electronics, and defense. On the other hand, over the last decade, tremendous attention has been given to the Deep Eutectic Solvents (DESs) because of their physical and chemical properties, which become these solvents one of the most important agent chemicals to electrodeposition of metals and alloys. Therefore, the main goal of this investigation was the electrodeposition of Te in choline chloride-ethylene glycol and choline chloride-urea based eutectic mixtures, at a molar ration of 1:2, at several temperatures. In both DESs, the electrochemical study revealed two cathodic waves for the Te plating solutions; the first associated with Te^{4+}/Te and the second one to Te/Te^{2-} redox couple on the Au substrate. AFM analyses demonstrated that Te electrocrystalisation on Au electrode proceeded by three-dimensional progressive nucleation mechanism in both eutectic solvents. These results corroborated with predicted by the Scharifker-Hills model. In addition, SEM micrographs of Te electrodeposits from both solvents revealed a large-scale Te rods-like morphology with a hexagonal cross-section in nanoscale regime uniformly distributed on electrode surface. TEM investigation suggested that Te single-crystalline grew perpendicular direction of (100) planes which implied in the preferential growth direction of [001]. Furthermore, the electrodeposition and characterisation of CdTe semiconductor were performed in choline chloride-ethylene glycol-based DES. The electrochemical results have shown that the formation of CdTe occurs at the same region of reduction of Cd^{2+} to Cd. XRD suggested that CdTe films grew with the crystallite in nanosize regime preferentially oriented along the (111) and (311) planes. SEM examination demonstrated that surface morphology of CdTe coatings exhibited a uniform distribution of spherical-like clusters with large agglomerated crystallite increasing as the temperature goes up. Finally, it was found a blue shift in the optical bandgap of the CdTe films which could be associated with the quantum-confinement effects.

Keywords: tellurium; cadmium telluride; deep eutectic solvent; electrodeposition; semiconductor;

RESUMO

O Te é um dos mais importantes para a produção de materiais em setores como energia limpa, eletrônica e defesa. Por outro lado, na última década, grande atenção foi dada aos solventes eutéticos (DESs) por causa de suas propriedades físicas e químicas, que tornam esses solventes um dos agentes químicos mais importantes na eletrodeposição de metais e ligas. Portanto, o principal objetivo desta investigação foi à eletrodeposição de Te em misturas eutéticas à base de cloreto de colina-etileno glicol e cloreto de colina-uréia, na proporção molar de 1: 2, a várias temperaturas. Em ambos os DESs, o estudo eletroquímico revelou duas ondas catódicas para as soluções de deposição de Te; o primeiro associado ao Te^{4+}/ Te e o segundo ao par redox Te/Te^{2-} sobre o substrato Au. As análises AFM demonstraram que a eletrocristalização de Te sobre o eletrodo Au procedeu por um mecanismo de nucleação progressiva tridimensional em ambos os solventes eutéticos. Estes resultados corroboram com os resultados previstos pelo modelo de Scharifker-Hills. Além disso, micrografias SEM de eletrodepositados de Te de ambos solventes revelaram uma morfologia semelhante a bastões de Te em grande escala com seção hexagonal em regime de nanoescala uniformemente distribuídos na superfície do eletrodo. A investigação do MET sugeriu que o Te cresceu como monocristais orientados ao longo dos perpendicularmente aos planos (100), o que implicava na direção preferencial de crescimento [001]. Além disso, a eletrodeposição e caracterização do semicondutor CdTe foram realizadas em DES à base de cloreto de colina-etileno glicol. Os resultados eletroquímicos mostraram que a formação de CdTe ocorre na mesma região de redução de Cd^{2+} para Cd. O DRX revelou que os filmes de CdTe cresceram com o cristalito em regime de nanométrico, orientado preferencialmente ao longo dos planos (111) e (311). A investigação com SEM demonstrou que a morfologia dos filmes CdTe exibeu uma distribuição uniforme de grupos esféricos com grande cristalito aglomerado, os quais aumentam à medida que a temperatura aumenta. Finalmente, foi constatada um desvio para o azul no intervalo da banda óptica dos filmes de CdTe que poder estar associado aos efeitos do confinamento quântico.

Palavras-chave: telúrio; telureto de cádmio; solventes eutéticos; eletrodeposição; semicondutor;

List of Figures

Figure 1 - Shares of global primary energy consumption by fuel. 16

Figure 2 - Schematic illustration showing the crystal structure of Te (a) spiral chains of the crystals arrange in a crystal structure and (b) view along the c-axis indicating spiral chains of Te atomic structures with an angle of 120°. 19

Figure 3 - Cyclic voltammograms (a) of the blank 1ChCl:2EG (dash line) and containing 0.05 mol L^{-1} $TeCl_4$ and (b) of the blank 1ChCl:2U (short dashed line) and containing 0.05 mol L^{-1} $TeCl_4$..... 37

Figure 4 - Cyclic voltammograms recorded on Au disk in DESs (a) 1ChCl:2EG and (b) 1ChCl:2U containing 0.05 mol L^{-1} $TeCl_4$ at several temperatures. 38

Figure 5 - AFM micrograph of Te electrodeposits on Au-coated FTO electrode from either 1ChCl:2EG at (a) 30 °C and (b) 80 ºC or 1ChCl:2U at (c) 30 °C and (d) 60 °C (E = –0.22 V for 0.50 s) both solutions containing 0.05 mol L^{-1} $TeCl_4$. 39

Figure 6 - Histogram showing the diameter distribution of the electrodeposited Te islands obtained from 1ChCl:2EG mixture at (a) 30 °C and (b) 80 ºC and from 1ChCl:2U at (c) 30 °C and (d) 60 °C and observed in the AFM micrographs. 40

Figure 7 - Collection of current-time transients for the reduction of Te^{4+}/Te on Au substrate obtained from 1ChCl:2EG containing 0.05 mol L^{-1} $TeCl_4$ at (a) 30, (b) 45, (c) 60 and (d) 80 °C. 42

Figure 8 - Current-time transients for the reduction of Te^{4+}/Te on Au substrate obtained from 1ChCl:2U containing 0.05 mol L^{-1} $TeCl_4$ at (a) 30, (b) 45 and (c) 60 °C..... 43

Figure 9 - Comparison of the dimensionless experimental curves derived from Fig. 4.5a-d with those simulated by S-H model for electrodeposition of Te on Au from 1ChCl:2EG containing 0.05 mol L^{-1} $TeCl_4$ and at (a) 30°C, (b) 45°C, (c) 60 °C, and (d) 80 °C. 44

Figure 10 - Comparison of the dimensionless experimental curves derived from Fig. 4.6a-c with those simulated by S-H model for electrodeposition of Te on Au from 1ChCl:2U containing 0.05 mol L^{-1} $TeCl_4$ and at (a) 30, (b) 45, and (c) 60 °C. 45

Figure 11 - Current-time transients for the reduction of Te^{4+}/Te on Au substrate obtained from 1ChCl:2EG at diffusional control (a) 30, (b) 40, (c) 60 and (d) 80 °C. Cottrell plots are showed as insert. 51
Figure 12 - Current-time transients for the reduction of Te^{4+}/Te on Au substrate obtained from 1ChCl:2U at diffusional control at (a) 30, (b) 40, and (c) 60 °C. Cottrell plots are showed as insert. 51
Figure 13 - Arrhenius' plot for dynamic viscosity of (a) 1ChCl:2EG and (b) 1ChCl:2U containing 0.05 mol L^{-1}. 53
Figure 14 - Stokes-Einstein plots of (a) 1ChCl:2EG and (b) 1ChCl:2U both contains 0.05 mol L^{-1} $TeCl_4$. 54
Figure 15 - Arrhenius' plots showing for the Te^{4+} species diffusion coefficient in (a) 1ChCl:2EG and (b) 1ChCl:2U solutions. 56
Figure 16 - SEM micrographs of Te nanorods arrays on Au-coated FTO substrate grew under potentiostatic control from either 1ChCl:2EG at (a) 30 °C (E_{peak}= –0.22 V), (b) 100 °C (E_{peak}= –0.07 V), (c) 30 °C (E_{peak}= –0.48 V) and (d) 60 °C (E_{peak}= –0.43 V). 58
Figure 17 - Histogram of diameter distribution of the Te nanorods arrays on Au-coated FTO substrate obtained from DESs (a) 1ChCl:2EG and (b) 1ChCl:2U at several temperatures. 59
Figure 18 - XRD pattern of the Te nanorods arrays on Au-coated FTO substrate obtained from (a) 1ChCl:2EG and (b) 1ChCl:2U at several different temperatures. The (*) is corresponding to FTO peaks and (‡) is indicating the Au peaks position. 60
Figure 19 - TEM of Te nanorods obtained in 1ChCl:2EG (a), (b), and (c) and in 1ChCl:2U. 62
Figure 20 - Cyclic voltammograms obtained for Au electrode in 1ChCl:2EG blank electrolyte (dashed line) and containing 0.2 mmol L^{-1} $TeCl_4$ (solid line). 68
Figure 21 - Cyclic voltammograms obtained for Au electrode in 1ChCl:2EG (a) blank electrolyte (dashed line) and containing 20 mmol L^{-1} $CdCl_2$ (solid line). 69
Figure 22 - Cyclic voltammograms obtained for Au electrode in 1ChCl:2EG containing a mixture of 20 mmol L^{-1} $CdCl_2$ + 0.2 mmol L^{-1} $TeCl_4$ at 30 °C. 70
Figure 23 - (a) Arrhenius' plot of dynamic viscosity and (b) density as function of absolute temperature for 1ChCl:2EG containing either 20 mmol L^{-1} $CdCl_2$

(hollow circle), 0.2 mmol L^{-1} $TeCl_4$ (hollow triangle), and 20 mmol L^{-1} $CdCl_2$ + 0.2 mmol L^{-1} $TeCl_4$ (hollow) 73
Figure 24 - Current-time transients for the reduction of Cd^{2+}/Cd on Au/FTO substrate obtained from DES 1ChCl:2EG containing 0.02 mol L^{-1} $CdCl_2$. 75
Figure 25 - Arrhenius' plot for experimental of $D_{Cd^{2+}}$ (hollow circle) and $D_{Cd^{2+}/Te^{4+}}$ (hollow square) in 1ChCl:2EG. 76
Figure 26 - Stokes-Einstein's plots for 1ChCl:2EG containing either 20 mmol L^{-1} $CdCl_2$ (hollow circle) or 20 mmol L^{-1} $CdCl_2$ + 0.2 mmol L^{-1} $TeCl_4$ (hollow square). 77
Figure 27 - SEM micrographs of CdTe electrodeposited on Au-coated FTO substrate from 1Ch:2EG at (a) 30 °C (E_{peak} = –1.02 V), (b) 60 °C (E_{peak} = –0.97 V), (c) 80 °C (E_{peak} = –0.95 V), and (d) EDS spectrum for sample showed in (a). Inset: SEM micrographs of high magnification. 79
Figure 28 - Histogram of CdTe clusters size electrodeposited on Au-coated FTO substrate from 1Ch:2EG at (a) 30, (b) 60, and (c) 80 °C. 80
Figure 29 - XRD pattern CdTe thin film electrodeposited on Au-coated FTO substrate from 1Ch:2EG at (a) 30 °C (E_{peak} = –1.02 V), (b) 60 °C (E_{peak} = –0.97 V), and (c) 80 °C (E_{peak} = –0.95 V). The (*) is corresponding the SnO_2 phase from FTO. 81
Figure 30- Texture coefficient of the CdTe thin film electrodeposited on Au/FTO from 1ChCl:2EG. 82
Figure 31 - (a) UV–vis absorption spectra of CdTe thin films electrodeposited on Au-coated FTO substrate from 1Ch:2EG and (b) Tauc´s plot. 84

List of Tables

Table 1 - Experimental data extracted from the current-time transients for Te nucleation on Au substrate from DESs…….. .. 48

Table 2 - Deposition charge for the reduction of Te^{4+}/Te on Au substrate calculated from the integration of current-times curves. 49

Table 3 - Comparison between the diffusion coefficients of Te^{4+} species obtained in this Thesis with those already reported in the literature. 50

Table 4 - Effect of temperature on diffusion coefficients of Te^{4+} species, density and viscosity of 1ChCl:2EG and 1ChCl:2U. 55

Table 5 - Effect of temperature on density, dynamic viscosity, diffusion coefficient of metals species of 1ChCl:2EG electrolytes. 71

Table 6 - Values of fitting parameters for density of 1ChCl:2EG electrolytes. 73

Table 7 - Elemental chemical composition of CdTe films electrodeposited in 1ChCl:2EG. 80

Table 8 - Values of crystallite size, thickness, absorption coefficient at absorption edge, and the optical band gap energy of CdTe films eletrodeposited on Au/FTO in 1ChCl:2EG. 83

Contents

1	**INTRODUCTION**.....	**16**
2	**OBJECTIVES**.....	**26**
2.1	**General objectives**.....	**26**
2.2	**Specific objectives**.....	**26**
3	**MATERIALS AND METHODS**.....	**27**
3.1	**Chemicals and preparation of electrolytes**.....	**27**
3.2	**Dynamic viscosity and density**.....	**28**
3.3	**Atomic force microscopy**.....	**28**
3.4	**Electrochemical experiments**.....	**28**
3.4.1	***Cyclic voltammetry***.....	**29**
3.4.2	***Cronoamperometry***.....	**29**
3.5	**Physical chracterisation of films**.....	**30**
3.5.1	***X-ray diffraction***.....	**30**
3.5.2	***Scanning electron microscopy***.....	**30**
3.5.3	***Transmission electron microscopy***.....	**30**
3.5.4	***Optical characterisation***.....	**31**
4	**ELECTRODEPOSITION OF Te ON Au FROM EUTETIC MIXTURES BASED ON CHOLINE CHLORIDE**.....	**32**
4.1	**Introduction**.....	**32**
4.2	**Results and discussion**.....	**36**
4.2.1	***Cyclic voltammetry***.....	**36**
4.2.2	***Atomic force microscopy***.....	**38**
4.2.3	***Cronoamperometry***.....	**40**
4.2.4	***Dynamic viscosity***.....	**52**
4.2.5	***SEM examination***.....	**57**
4.2.6	***XRD analyses***.....	**59**
4.2.7	***TEM examination***.....	**60**
4.3	**Conclusions**.....	**63**
5	**ELECTRODEPOSITION OF CdTe ON Au FROM CHLORIDE-ETHYLENE GLYCOL BASED EUTETIC MIXTURE**.....	**64**
5.1	**Introduction**.	**64**
5.2	**Results and discussion**.....	**67**

5.2.1 Cyclic voltammetry studies..... **67**
5.2.2 Viscosity and density of the electrolytes..... **72**
5.2.3 SEM examination of CdTe films..... **78**
5.2.4 X-ray diffraction analysis of CdTe films..... **80**
5.2.5 Optical characterization of CdTe films..... **83**
5.3 Conclusion..... **87**
6 CONCLUSIONS..... **88**
7 SCIENTIFIC PRODUCTION..... **89**
REFERENCES..... **90**

1. INTRODUCTION

The evolution in materials science and its technologies over a half of century enabled the development of several products for modern life (GRAEDEL *et al.*, 2015), such as smart televisions, high performance computers, practical mobile phones, electrical vehicles, and services for technology like software to apps, further medical and healthcare devices. The scientific development in this period allows the establishment of the electronics and photonics industries as a main part of the global economies. The American standards and trace organisation, namely the Consumer Technology Association (CTA) (THE CONSUMER TECHNOLOGY ASSOCIATION, 2016) reported that the consumer technology sector is among the most vibrant and innovative parts of the United State (U.S.) economy that was directly responsible for 5.2% of U.S. gross domestic product (GDP) in 2015. In the Europe Union (EU), the information and communication sector (service and manufacture) was just over EUR 580 billion in 2016 which was equivalent to 3.75% of the EU's GDP in that year (EUROSTAT, 2018). Moreover, the impact of the Asian technological sector in world economy is terrific, Yeung (YEUNG, 2007) point out that the investments a long of last three decades in high-tech industry lead the Asian companies are in control of around 70% of world's annual shipment of computer notebooks, set up two of the world's largest semiconductor manufacturers and stamped Samsung® and Hyundai®, for instance, as household brand names worldwide among others.

Therefore, it has been demonstrated that it is indisputable that modern life is enabled by the use of materials in its technologies. One of the main pillars of such industrial development is energy which its demand is growing faster due the global industrialisation (ENERGY INFORMATION ADMINISTRATION, 2019; PETROLEUM, 2019; U.S. DEPARTMENT OF ENERGY, 2005). The projections of the U.S. Department of Energy (U.S. DEPARTMENT OF ENERGY, 2005) revealed that the because of the increase of the Earth's population, rapid technology development and economic growth worldwide, the demand for energy in world more than double by 2050 from 2005 when the world produced the power of 13 terawatt. Furthermore, according to the Annual Energy Outlook 2019 reported by the U.S. Energy Information Administration (EIA) (ENERGY INFORMATION ADMINISTRATION, 2019), the U.S. industrial energy consumption in reference to 2018 grows by 50% over the same period. Currently, the world's energy matrix is strictly based on fossil fuels, as reported by the British Petroleum (PETROLEUM, 2019). The Figure 1 shows

global energy consumption by fuel. As can be seen, oil remains the most used fuel in the global energy matrix, although it is the lowest level since the 1980s. Coal is the second largest fuel consumed but lost share in 2018 to account for 27%. The share of natural gas increased to 24% such that the gap between coal and gas has narrowed to three percentage points. The contribution of hydro and nuclear sources remained relatively flat in 2018 at 7% and 4%, respectively. Strong growth pushed up renewable energy sources which share to 4% over the last two decades, just behind nuclear (PETROLEUM, 2019).

Figure 1 - Shares of global primary energy consumption by fuel.

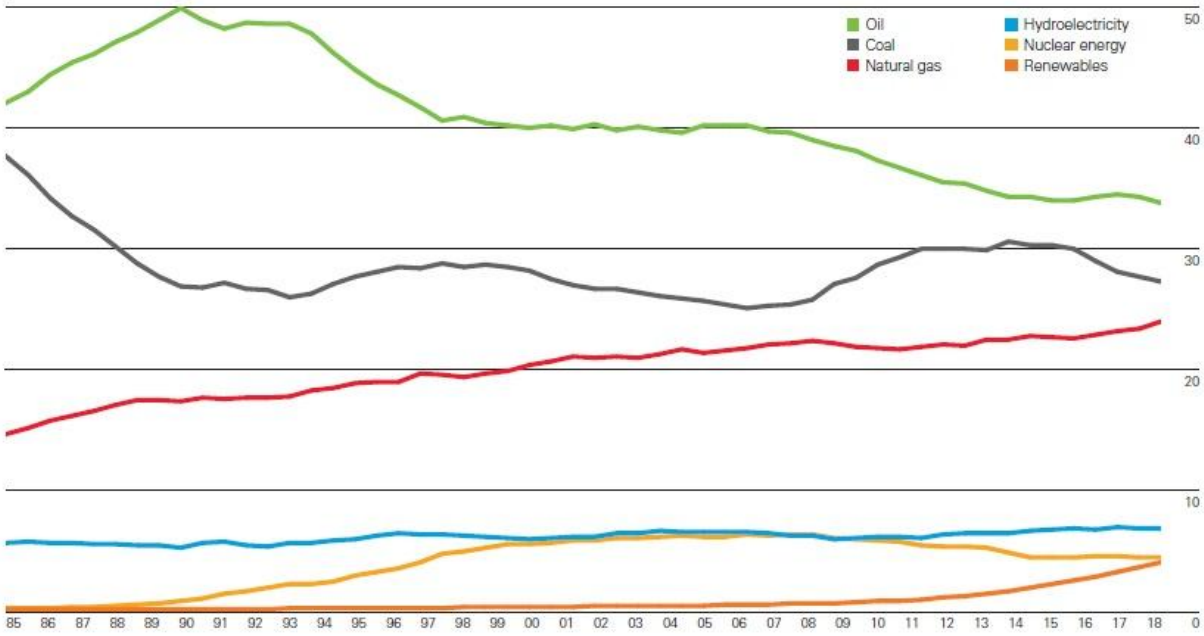

Source: (PETROLEUM, 2019).

Therefore, approximately 85% of the energy consumed in 2018 came from fossil fuels, see Figure 1. However, the dependency on this energy source has provoked serious consequences, such as global warming and climate changes. In order to revert this scenario, over the last two decades a tremendous attention have been given on clear energy technologies. The British Petroleum (PETROLEUM, 2019) reported that at the global level in 2018, the share of renewable sources were 9.3% of global electricity generation which represented a power generation increased by 14% (excluding hydro contribution), mainly due to the contributions of wind and solar sources. Solar energy has constantly increased its share and now represents 24% among the renewable sources (PETROLEUM, 2019). Over the same period, the report also indicated that the Europe has the highest penetration at 18.7%, followed by South & Central America at 12% and North America at 10%. When investigated by country, China was again the largest contributor to renewable growth, accounting for 45%

of the global growth in renewable power generation, substantially higher than the entire nations of the Organisation for Econimic Co-oparation and Development (OECD) combined (PETROLEUM, 2019). The EIA (ENERGY INFORMATION ADMINISTRATION, 2019) point out that the electricity generation from both coal and nuclear should be decline by 2050, notwithstanding, the continuous reduction in the cost and increase in performance of renewables can make these energies source competitive in near future. Furthermore, the projection leads also to expect that the share of renewable energy generation increases from 18% to 31% in that period. Among the renewable electricity generation the solar photovoltaic, wild, and hydroelectric could be represent the share of 48%, 25%, and 18% by 2050, respectively (ENERGY INFORMATION ADMINISTRATION, 2019). On the world stage, Brazil has a unique energy matrix with significant share of renewable energy source. According to the Brazilian National Energy Balance reported by the Ministry of Mines and Energy (BRASIL, 2019), the renewable energy sources represent 83.2% of the energy matrix in 2018. Actually, the impact of the solar photovoltaic on Brazilian Energy Balance is humble, although the sector has been gaining ground, increasing from 0.1% of the energy matrix in 2017 to 0.5% in 2018 (BRASIL, 2019).

On the frontier of the global revolution for development of clean energy technologies are some critical materials. In the Critical Materials Strategy report by U.S. Department of Energy (U.S. DEPARTMENT OF ENERGY, 2011) the materials criticality was categorised two-dimensionally taking into account their importance to clean energy and supply risk. Basically, 16 elements were mentioned in this document which revealed that five of them were considered critical; yttrium, europium, terbium, neodymium, and dysprosium, while tellurium together with lithium were assessed near-critical in a medium-term perspective (2015-2025) (U.S. DEPARTMENT OF ENERGY, 2011). Moreover, the German Öko-Institut e.V. (ÖKO-INSTITUT E.V., 2009) two years earlier had performed a larger investigation concerning on future sustainable technologies that use metals, earth-rare metals, and metalloids for generate renewable energy. The study included a total of 26 elements which were evaluated as their global demand, supply risk, and recycling restrictions. The results estimated that in the photovoltaic sector; tellurium, indium, and gallium were as most critical materials due to rapid demand growth as well as serious supply risks combined with moderate recycling restrictions (ÖKO-INSTITUT E.V., 2009). Therefore, the rapidly growing demand of these elements could be represent a risk for the clean energy market. Bustamante and Gaustad (BUSTAMANTE; GAUSTAD, 2014) analysed the imapacts of scarcity, supply

risks, and recycling of tellurium on thin film photovoltaic. They purposed that improvements in byproduct yield, end-use recycling rate, and end-use material intensity exhibit significant leverage to minimise risk in the energy-critical tellurium supply-chain (BUSTAMANTE; GAUSTAD, 2014).

The technological importance of materials based on tellurium was announced by National Science and Technology Council through the Materials Genome Initiative for Global Competitiveness (HOLDREN, John P., 2011) which claimed that tellurium is one of the most important elements for the manufacture of products in key high-growth sectors, including clean energy, consumer electronics, and defense. Furthermore, Jin and co-workers (JIN, Y.; KIM, J.; GUILLAUME, 2016) conducted a extensive review dated from 1974 to 2014 in several scientific databases and that highlighted tellurium (Te) and cadmium (Cd) as critical elements for clean technology, such as thin film semiconductors, electric vehicles, photovoltaic, and energy-efficient lighting. In addition, these elements were also assessed indispensible to design materials often designated critical for general industrial activities (JIN, Y.; KIM, J.; GUILLAUME, 2016), for instance; opto-electronic sector.

Te is a metalloid element located in the *p*-block of the periodic Table that has an atomic number of 52, atomic mass of 127.60 u, and electron configuration [Kr] $4d^{10}5s^{2}5p^{4}$ (REZENDE, 2004). Of the six outer electrons in the configuration, two of them are paired in the *s*-orbital, occupying the lower energetic level in the shell while four electrons are distributed between three *p*-orbitals, two are paired in one of these orbitals and the remaining two are available for covalent bonding in half filled *p*-orbitals (WEIDMANN; ANDERSON, 1971). The crystal structure of Te was first determined in 1924 by Bradly (BRADLEY, 1924) that proposed the helical chains of atoms through covalent bonds which are bounded together by the van der Waals interactions among the chains to form a hexagonal (*t*-trigonal) lattice (STUKE, 1969). These chains of Te atoms in crystal structure are oriented along the [001] direction, suggesting a highly anisotropic growth tendency along of c-axis (HE *et al.*, 2017; XIA, Y *et al.*, 2003), as shown in Fig. 2a (ZHU, W. *et al.*, 2006). In this network, every Te atom touches two other ones in the same spiral by a rotating of 120° and four atoms in adjacent spirals, as seen in Fig. 2b (LIU, J. W. *et al.*, 2016).

Figure 2 - Schematic illustration showing the crystal structure of Te (a) spiral chains of the crystals arrange in a crystal structure and (b) view along the c-axis indicating spiral chains of Te atomic structures with an angle of 120°.

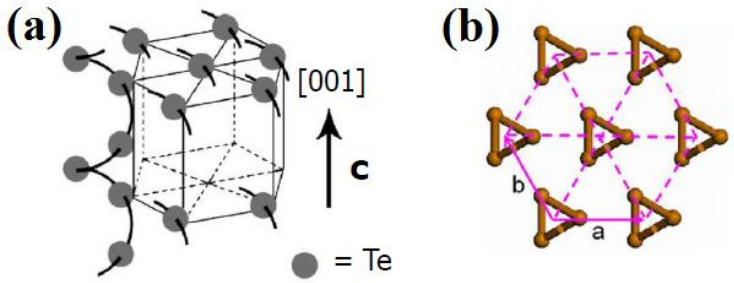

Source: Adapted from (ZHU, W. *et al.*, 2006) and (LIU, J. W. *et al.*, 2016).

At room temperature, elemental Te is a *p*-type semiconductor material with narrow direct band-gap energy around 0.35 eV (STUKE, 1969). Furthermore, Te presents wealth and unique properties, such as piezoelectricity, photoconductivity, thermoelectricity, and nonlinear optical responses, which allow its application in gas sensing, photoconductors, thermoelectric, solar cells, electronic and optoelectronic devices (ABAD *et al.*, 2015; LIANG, F.; QIAN, H., 2009; LIN, S. *et al.*, 2016; LIU, J.-W. *et al.*, 2010). Some important materials based on Te reported in the literature include the semiconductors, such as PbTe (MOKARI; ZHANG, Minjuan; YANG, Peidong, 2007) and CdTe (TOMA *et al.*, 2014), thermoelectric alloys, for instance; Bi_2Te_3 (MAMUR *et al.*, 2018) and Ce_3T_4 (LI, J.-P. *et al.*, 2017), and optical alloys HgTe (CHEN, Q.; SANDERSON; ZHANG, C., 2015).

Cd is a post-transition metallic element which has an atomic number of 48, atomic mass of 112.41 u and electron configuration [Kr] $4d^{10}5s^2$ (REZENDE, 2004). The two outer electrons in the configuration are paired in the *s*-orbital. The crytal structure of this element is found to be hexagonal close-packed (REZENDE, 2004). Cd is not considered a transition metal, since it does not present *d* or *f* shells partially filled. Thereby, Cd is found in the most of its compounds in the oxidation state of +2. Although, Cd has widely known as toxic metal that poses serious environmental health hazards to both humans and wildlife, as well as, its compounds have been classified as human carcinogens (epidemiological data show causal associations with prostate, breast and lung cancer) (LUEVANO; DAMODARAN, 2014), Cd and its alloys continue explored in industrial applications, such as an alloying element in soft solders, in fusible alloys, wear resistance materials (VISWANATH; JACHAK, 2013), and in nickel-cadmium rechargeable batteries (GOODENOUGH, 2012). Currently, Cd-semiconductors (II-VI compounds), such as CdS (WANG, Y. *et al.*, 2019), CdSe (KUMARI

et al., 2019) and CdTe (CAMACHO-ESPINOSA *et al.*, 2019) are one of the most exciting researched materials because of their opto-electronic properties.

Over the last decades, the synthesis of nanostructured materials with size and shape-controlled have been a great scientific interest due to their potential technological applications (GE, M. *et al.*, 2016; GORIPARTI *et al.*, 2014; HU, J.; ODOM; LIEBER, 1999; WU, Yiying *et al.*, 2002; XIA, Y *et al.*, 2003). It has been demonstrated that precise control of the size of materials in the nanoscale regime can produce tremendous changes in their physical properties (DORANTES-DÁVILA; PASTOR, 1998; GAMBARDELLA *et al.*, 2000, 2002; ROSS, 2001) which allowed the widening the technological edge in strategic fields for modern life, such as opto-communication devices (XIA, Y *et al.*, 2003), renewable energy sources (GE, M. *et al.*, 2016; GORIPARTI *et al.*, 2014), , storage information, and microelectronic (DORANTES-DÁVILA; PASTOR, 1998; GAMBARDELLA *et al.*, 2002; ROSS, 2001).

Currently, terrific development has been given to the synthesis of chalcogen materials, particularly in II-VI semiconductors alloys based on Te (HE *et al.*, 2017; XIA, Y *et al.*, 2003) due to their wide applications in the high technology industry. These materials are crucial for the manufacture of lasers, radiation detectors, light-emitting diodes, photovoltaic, optoelectronic, magnetic, and thermoelectric devices (BRITT; FEREKIDES, 1993; HE *et al.*, 2017; MINGO, 2004; MIROV, S. *et al.*, 2013). Among these materials, cadmium telluride (CdTe) is one of the most promise semiconductors because of its direct band-gap energy around 1.45 – 1.50 eV at room temperature and its high absorption coefficient around 10^4 – 10^5 cm^{-1}, which leads to its utilisation in the photovoltaic field (ADACHI; KIMURA; SUZUKI, 1993; FENG, L. *et al.*, 2005; HERNANDEZ-CALDERON, 2002; MYERS; EDWARDS; SCHETZINA, 1981; TOMA *et al.*, 2014). CdTe has been highlighted in the market of thin-film photovoltaic technology. In 2016, the American Company First Solar confirmed the recorded of conversion efficiency for thin films of CdTe solar cells when achieved 22.1% for cells in laboratory scale and 18.6% for terrestrial modules (GREEN *et al.*, 2018). Therefore, CdTe is setting down as a prominent and competitive material to the traditional multicrystalline Si technology that reported in a record efficiency of 22.3% and 19.9% for lab-scale cells and modules, respectively (GREEN *et al.*, 2018).

There are several strategies for preparation Te and CdTe nanostructures are available in the literature, including the well-established the vacuum-based technique (CHEN, H. *et al.*, 2007; MOHAMED *et al.*, 2014; SCHAFFNER *et al.*, 2011; SEN *et al.*, 2008; TOMA *et al.*, 2014). Independently, Chen *et al.*, (CHEN, H. *et al.*, 2007) and Sen *et al.*, (SEN *et al.*, 2008) reported the growth of Te nanowires under vacuum and high temperature (~300–450 °C) conditions. Mohamed *et al.*, (MOHAMED *et al.*, 2014) deposited CdTe nanocrystals and CdTe/Co stacked nanolayers by electron beam evaporation technique. Toma and co-workers (TOMA *et al.*, 2014) demonstrated the formation of CdTe thin films with nanosized grains for photovoltaic applications. These deposition methods allow the accuracy control of shape, size and thickness of thin films; however, its require processes operating at high vacuum and temperature, additionally, expensive instrumental is needed which is not attractive under industrial point of view.

On the other hand, equally important the chemical routes also lead the preparation of Te and CdTe nanostructures (CAO, X. *et al.*, 2008; LI, G. *et al.*, 2014; LIU, J. W. *et al.*, 2016; SONG, J.-M. *et al.*, 2008; WANG, Z. *et al.*, 2010b; YONG *et al.*, 2010; ZHANG, B. *et al.*, 2007; ZHOU, B. *et al.*, 2006; ZHU, Y.-J. *et al.*, 2004). Liu *et al.*, (LIU, J. W. *et al.*, 2016) reported a systematic study on the synthesis of Te nanostructure from nanoparticles to nanorods, nanowires, and nanotubes by a solvothermal processes. They observed a red shift from 388 nm of nanoparticles to 639 nm of nanowires attributed to the growth and increase in length of the Te nanostructures. Wang *et al.*, (WANG, Z. *et al.*, 2010) demonstrated the growth of single-crystal Te nanowires and nanotubes by through a hydrothermal recrystallization route. According to these researchers, the morphologies of the Te nanostructure could be controlled by tuning the amount of hydrochloric acid added in the hydrazine hydrate solution. Li and co-workers (LI, G. *et al.*, 2014) reported the formation of Te polycrystalline nanoplates with thickness 100-300 nm using a solvothermal method, as well as, the transformation from nanoplates to single nanorods driven by reaction temperature. In addition, solution-phase approaches have been also proposed, such as assisted with visible-light (ZHANG, B. *et al.*, 2007), ultrasonic (ZHOU, B. *et al.*, 2006), and micro-wave (ZHU, Y.-J. *et al.*, 2004). Furthermore, Yong *et al.*, synthesised CdTe nanowires with carbon sheaths via a one-step hydrothermal process at 180 °C. The authors used ascorbic acid as a reducing agent and carbonization source and cetyltrimethylammonium bromide as growth agent (YONG *et al.*, 2010). Cao *et al.*, (CAO, X. *et al.*, 2008) proposed a hydrothermal method from CdTe nanoparticles stabilised with thioglycolic acid for preparation of ultra long

nanowires and nanoribbons morphologies with lengths up to 100 μm after reaction of time 12 h at 140 °C.

Although these solution-based approaches are considered efficient and inexpensive strategies when comparison to vacuum based techniques, in spite of that, long deposition time and/or annealing treatment are demanded. Therefore, a low-cost and quick deposition technique is essential.

In this scenario, among the low-cost deposition methods of materials electrodeposition is one of the most attractive techniques, since it has large-scale coatings production, low temperature operating processes, and handle-easily, additionally, it can be an environmentally friendly strategy. According to Lincot and co-workers (LINCOT, 2005; LINCOT *et al.*, 2004) electrodeposition is already a major technology for mass production of large area metallic protective coatings in the industry, such as zinc electroplating and to most advanced electronic industries, for instance; for Cu plating in the Damascene process for integrated circuits and magnetic heads.

Over the 1990s years, electrodeposition turns up as powerful tool to growth of semiconductor materials at large scale, such as II-VI compounds (CdSe, ZnSe, CdS, ZnS, , ZnTe, CdTe, including some ternary alloys) and chalcopyrite ($Cu(In,Ga)(S,Se)_2$) (LINCOT, 2005; LINCOT *et al.*, 2004). Readers more interested on the electrodeposition of semiconductors a complete view of the field can be found in refs. (PANDEY, R Kumar; CHANDRA; SAHU, 1996; SCHLESINGER; PAUNOVIC, 2011). Lee *et al.*, (LEE, Y.-C. *et al.*, 2002) demonstrated that II-VI compounds can be electrochemically deposited in nanometer regime. Furthermore, the size, shape and morphology of the nanostructures can be controlled by deposition parameters, such as the concentration of the electroactive species, applied electrode potentials (potentiostatic control), applied current density (galvanostatic control), mechanical stirring of the electroplating bath and bath temperature (LEE, Y.-C. *et al.*, 2002; LINCOT, 2005). Therefore, the electrodeposition is a convenient route for manufacture nanostructured semiconductors materials.

Traditionally, electrodeposition is carried out aqueous plating solutions (ABAD *et al.*, 2015b; KOWALIK *et al.*, 2016; KUMAR, N. *et al.*, 2015; SHE *et al.*, 2009; ZHAO, A. *et al.*, 2005). The growth of ordered Te nanowires have already reported by direct

electrodeposition in 1.0 mol L^{-1} KOH aqueous solution (SHE *et al.*, 2009). Furthermore, templete-assisted electrodeposition has been demonstrated an efficient method to preparation Te nanowires vertically orientated along of the [001] direction either in acid solutions (ZHAO, A. *et al.*, 2005) or alkaline electrolytes (KUMAR, N. *et al.*, 2015). Kanagaraj *et al.*, (KANAGARAJ *et al.*, 2019) also demonstrated the growth of vertical arrays of CdTe nanowires on flexible/transparent substrates by template electrodeposition from an acid plating solution. Moreover, Wang *et al.*, (WANG, J. *et al.*, 2017) electrodeposited uniform CdTe nanorods films on a flexible nickel substrate in acid electrolyte, additionally, they observed that conversion efficiency of solar cells manufactured with these films was significantly influenced by the length of CdTe. On the flip side, Shan and co-authors (SHAN *et al.*, 2016) claimed that CdTe films were successfully electrodeposited in alkaline bath containing nitrilotriacetic acid. However, aqueous plating solutions have some drawbacks, such as a narrow electrochemical window that limit the deposition of metals because of hydrogen gas evolution during electrolysis, affecting the quality of coatings, low thermal stability and evaporation which lead the liberation of toxic vapor during the operation (SIMKA; PUSZCZYK; NAWRAT, 2009).

Room Temperature Ionic liquids (RTILs) are an alternative to aqueous electroplating baths to electrodeposition of metals and alloys. RTILs are a new class of salts which are entirely composed ions and existing in liquid state at temperature below 100 °C (ENDRES, Frank.; ABBOTT, A.; MACFARLANE, 2017). In general, RTILs formed by an organic cations with organic or inorganic anions (ENDRES, Frank.; ABBOTT, A.; MACFARLANE, 2017). Historically, the first RTIL synthesised was the ethylammonium nitrate, $[C_2H_5NH_3]NO_3$ by Walden (WALDEN, 1914) in 1914, but in that time no attention was given to this solvents. A major breakthrough in the RTILs was achieved only in 1970s and 1980s with investigation performed on chloroaluminate ($AlCl_3$) with organic halogen ionic mixtures at room temperature (APPLEBY *et al.*, 1986; CHUM *et al.*, 1975). The RTILs based on $AlCl_3$ are considered the first generation of ionic liquids (ILs). The $AlCl_3$ based RTILs are still employing to electrodeposition of aluminium (SU, C. J. *et al.*, 2013). However, the hygroscopic nature these RTILs has limiting their use for further applications (ENDRES, Frank; ABEDIN, Sherif Zein EL, 2006). Another major development in RTILs was conducted by Wilkes and Zaworoko (WILKES, J. S; ZAWOROTKO, M. J., 1992) when these researchers synthesised air- and water-stable RTILs based on alkyl-imidazolium cation with either tetrafluoroborate or hexafluorophosphate as anions which could be prepared at

ambient conditions. These solvents are considered the second generation of ILs. In general, these generation of RTILs are prepared by cations of quaternary ammonium salts, such as tetraalkylammonium or cyclic amines, for example; pyridinium, imidazolium, piperidinium, pyrrolidinium with inorganic or organic anions, such as halides, $[BF_4]^-$, $[PF_6]^-$, $[AsF_6]^-$ or amide $[N(CN)_2]^-$, $[C_4F_9SO_3]^-$, trifluoroacetic $[CF_3CO_2]^-$, amides $[N(CF_3SO_2)_2]^-$, and $[CF_3CONCF_3SO_2]^-$ (GALIŃSKI; LEWANDOWSKI; STEPNIAK, 2006). RTILs are usually non-volatile, non-flammable, less toxic, and present high solubility of metal salts, high electrical conductivity and a wide range of potential which allows the electrodeposition of metals and alloys that are difficult to obtain in aqueous plating electrolytes. Abedin *et al.*, (ABEDIN, S Zein El *et al.*, 2007) demonstrated the potential of RTILs in preparation of nanomaterials by electrodeposition. Imidazolium based RTILs have been widely used to electrodeposited single-metal and alloys nanowires, Se (STEICHEN; DALE, P., 2011), Sn (AL-SALMAN *et al.*, 2015), Co (HSIEH, Y. T. *et al.*, 2014), and Ni-Zn (YANG, J.-M.; GOU; SUN, I-Wen, 2010), while piperidinium based RTILs has been employed to electrodeposition of Te nanorods (SZYMCZAK *et al.*, 2012). Nevertheless, Endres and Abedin (ENDRES, Frank; ABEDIN, Sherif Zein EL, 2006) explained that although these RTILs are moisture insensible the exposure to moisture for a long time can cause some changes in their physical and chemical properties. In addition, it is important to observed that tetrafluoroborate RTILs can suffer hydrolysis to form HF (hydrofluoric acid) (ENDRES, Frank; ABEDIN, Sherif Zein EL, 2006; WILKES, J. S.; ZAWOROTKO, M. J., 1992). Further, Romero *et al.*, (ROMERO *et al.*, 2008) investigated the toxicity and biodegradability of

several imidazolium based ILs in aqueous phase and pointed out that RTILs are poor biodegradable and perhaps hazardous to aquatic environments.

Abbott and co-workers (ABBOTT, A. P. *et al.*, 2003; ABBOTT, A. P.; BOOTHBY; *et al.*, 2004) proposed the namely Deep Eutectic Solvents (DESs) as alternative RTILs. The physical and chemical properties of DESs are quit close to RTILs, therefore, sometimes they are considered a new class of ILs analogues (SMITH; ABBOTT, A. P.; RYDER, 2014). Strictly speaking, the DESs can be distinguished from ILs by the fact that they also contain an organic molecular component (WAGLE; ZHAO, H.; BAKER, 2014). Moreover, DESs are biodegradable, nontoxic, and present superior insensible to presence of water and lower price in comparison to RTILs (ZHANG, Q. *et al.*, 2012). DESs are obtained by simply mixing a quaternary ammonium salts (hydrogen bond acceptor - HBA) with the

hydrogen bonding donor (HBD) molecule, such as amides, alcohols, carboxylic acids (SMITH; ABBOTT, A. P.; RYDER, 2014; WAGLE; ZHAO, H.; BAKER, 2014; ZHANG, Q. *et al.*, 2012). The interaction between the HBA and HBD decrease the freezing point of the mixture forming a single liquid phase at room temperature. The most popular and well-studied eutectics mixtures involve the choline chloride (ChCl) with either urea (U) or ethylene glycol (EG), at molar ratio of 1:2 (SMITH; ABBOTT, A. P.; RYDER, 2014; WAGLE; ZHAO, H.; BAKER, 2014; ZHANG, Q. *et al.*, 2012). Because of the their high ionic conductivity, high thermal stability, good solubility to metal salts, and wide potential range of electrochemical stability DESs have been employed in several electrochemistry applications, such as electrodepolishing, electroextraction, and electrodeposition of metals and alloys (SMITH; ABBOTT, A. P.; RYDER, 2014). Zhang and Xua (ZHANG, Q. B.; HUA, 2014) employed ChCl-U based DES, at molar ratio of 1:2, for the electrochemical growth of Cu nanoparticles on Ni substrate. Moreover, Wei *et al.*, (WEI, L. *et al.*, 2013) claimed that shape-controlled Pt nanocrystals with high-index facets, exhibiting higher catalytic activity than commercial Pt material can be electrodeposited in ChCl-U based DES. On the other hand, Alcanfor *et al.*, reported the template-free electrodeposition of In nanorods arrays on Cu electrode from a ChCl-EG based eutectic mixture, at molar ratio of 1:2.

In addition, several researchers have been dedicated to employ DES as electrolyte for the electrodeposition of semiconductor materials. Shivigan and co-workers (SHIVAGAN, D D *et al.*, 2007) and Malaquias (MALAQUIAS *et al.*, 2013) revealed that ChCl-U based DES is a promising low-cost electrolyte for the electrodeposition of Cu-In, Cu-In-Se, and Cu-In-Ga-Se precursor thin films which can be used to form chalcopyrite absorber layers CIS and CIGS. Dale (DALE, Phillip J. *et al.*, 2007) reported the successful electrodeposition of II-IV semiconductors compounds (CdS, CdSe, and ZnS) on on fluorine-doped tin oxide (FTO) substrate using eutectic mixture based on ChCl-U at 100 °C for photovoltaic applications. Furthermore, CuTe and SbTe semiconductor alloys have been electrodeposition from a eutectic mixture based ChCl with oxalic acid (OxA), in 1:1 molar ratio. DESs have been used as electrolytes for electrodeposition (CATRANGIU, A.-S. *et al.*, 2016).

Therefore, this Thesis presented a study performed on the electrochemical of Te^{4+} and Te films electrodeposition in ChCl-EG and ChCl-U based electrolytes. Moreover, the electrodeposition of CdTe films from eutectic mixture based on ChCl-EG is presented and discussed.

2. OBJECTIVES

2.1 General objectives

The mean goal of this thesis was obtain and characterise the Te and CdTe films Au substrate deposited by electrodeposition from deep eutectic solvents based on choline chloride.

2.2 Specific objective

- The first specific objective was to investigate the electrochemical behaviour of Te^{4+} and Cd^{2+} species on Au electrode in deep eutectic solvents based on choline chloride.
- The second one was to perform electrochemical synthesis of Te and CdTe films on Au substrate from DESs by electrodeposition.
- The third one was probe the nucleation and growth mechanism of Te on Au surface taking into account the AFM analyses and theoretical model developed by Scharifker-Hills.
- Another one was to determine the diffusion coefficient of Te^{4+} and Cd^{2+} species in both DESs by the well-known Cottrell´s equation.
- Finally, the last specific objective was perform a morphological, structural and optical chracterisation of the Te and CdTe thin films electrodeposited on Au-coated FTO substrate using conventional techniques.

3. MATERIALS AND METHODS

In this chapter are presented all chemicals used during this study, as well as, the procedure for sample preparation. In addition, the electrochemical methods employed to investigate electrochemistry of the Te^{4+} and Cd^{2+} species in solution and for electrodeposition of films are described. Moreover, a complete description of the techniques utilised to obtain structural, morphological, and spectroscopy information are presented, further, the procedure for study physical properties of the electrolytes solution are also described.

3.1. Chemicals and preparation of electrolytes

ChCl ($HOC_2H_4N(CH_3)_3Cl$, Sigma-Aldrich, ≥ 98%), EG ($HOCH_2CH_2OH$, Sigma-Aldrich, ≥ 99.8%), and U ($(NH_2)_2CO$ Sigma-Aldrich, ≥ 99%) were used as received without more purification. The eutectic mixtures used in this work were synthesised following the method described by Abbott et al., (ABBOTT, A. P. *et al.*, 2003; ABBOTT, A. P.; BOOTHBY; *et al.*, 2004). The ChCl was mixed with either EG (1ChCl:2EG) or U (1ChCl:2U), at a molar ration of 1:2 in baker. Next, the mixtures were heated at 80 °C until the formation of a homogeneous colourless liquid phase.

In order to investigate the electrochemistry of Te^{4+} species in 1ChCl:2EG and 1ChCl:2U the electrolytes were obtained by the dissolution of a mass of anhydrous tellurium tetrachloride ($TeCl_4$, Sigma-Aldrich®, ≥ 99%) in both DESs, ultrasonic bath assisted (Quimis® 0335D) and at room temperature (≅ 25 °C), to produce 0.05 mol L^{-1} $TeCl_4$. The electroplating solutions with the same concentration of $TeCl_4$ were used to electrodeposit the Te films.

On the other hand, before the electrodeposition of CdTe films the electrochemical behaviour of individual metals in 1ChCl:2EG was carried out from the electrochemical baths containing either 20 mmol L^{-1} $CdCl_2$ (Sigma-Aldrich®, ≥ 99%) or 0.2 mmol L^{-1} $TeCl_4$ (Sigma-Aldrich®, ≥ 99%). The films were obtained using the electrolytes containing together Te^{4+} and Cd^{2+} (20 mmol L^{-1} $CdCl_2$ + 0.2 mmol L^{-1} $TeCl_4$).

The amount of water in the all electrolytes was determined using Karl-Fischer (Metrohm-Eco Chemie®) Titration and it was to found less than 0.5%.

3.2. Dynamic viscosity and density

The dynamic viscosity and density measurements of the electrolytes were done at using an Anton Paar's Stabinger viscometer, model SVM 3000. For the 1ChCl:2EG solutions, the measurements were performed in the range temperature from 20 up to 100 °C, whereas in 1ChCl:2U electrolytes the analysis were done in the range from 20 up to 60 °C, since, for higher temperatures, a white precipitate was formed.

3.3. Atomic force microscopy

The nucleation and growth mechanism of the Te films on Au surface was characterised using an Asylum Research Scanning Probe Atomic Force Microscopy (AFM) under ambient conditions. AFM images were collected in tapping mode using a Nanoworld Innovative Technologies®Pt/Ir coating probe with a spring constant of 2.8 N/m at resonance frequency of 75 kHz. The obtained AFM images were analysed by ImageJ software.

3.4. Electrochemical experiments

The cyclic voltammetry technique was used to investigate the electrochemical behaviour of Te^{4+} species in both DESs and Cd^{2+} ions in 1ChCl:2EG whereas the chronoamperometry was used to the electrodeposition of both Te and CdTe films. All the electrochemical measurements were performed in a conventional three-electrode electrochemical cell under atmospheric conditions using a potentiostat/galvanostat (AUTOLAB PGSTAT30, Metrohm-Eco Chemie®) controlled by NOVA software version 1.11. The electrochemical experiments were conducted using a Pt plate (15 × 10 × 0.2 mm^3, 99.5%, Heraues Vectra do Brasil Ltda) and $Ag_{(s)}/AgCl_{(s)}$ immersed in the DESs as the counter-electrode and pseudo-reference electrode, respectively.

3.4.1. Cyclic voltammetry

Cyclic voltammetry technique was employed in pure DESs (as prepared) in order to probe the electrochemical window of both eutectic mixtures. In addition, the Faradaic (cathodic and anodic) processes of the electroactive species were determined using cyclic voltammetry measurements on Au electrode in 1ChC:2EG and 1ChCl:2U, respectively.

The effect of temperature in electrochemical reduction of electroative species in DESs was also investigated. In case of systems containing only Te^{4+} ions, the experiments were performed at temperatures of 30, 45, 60, 80 and 100 °C in 1ChC:2EG, however, in the system of 1ChCl:2U the temperatures were 30, 45 and 60 °C, since that a white precipitate was observed after heating the electrolyte above 60 °C, as mentioned above. The temperature control of each experiment was done using an ultra-thermostatic bath (CIENLAB), otherwise, a hot plate was used control the temperature at 100 °C.

In the system containing together Te^{4+} and Cd^{2+} species in 1ChC:2EG, the experiments were performed at 30, 60 and 80 °C, respectively. The working electrode used in all cyclic voltammetry measurements was an Au disc (Ø = 1.0 mm, 99.99%, Heraues Vectra do Brasil Ltda). Before each measurement, the Au disc surface was ground with 1200 mesh emery paper and then rinsed with Milli-Q water. The cyclic voltammetry was carried out at a scan rate of 50 mV s^{-1}.

3.4.2. Chronoamperometry

The chronoamperometry technique was used to investigate the nucleation-growth mechanism of Te on Au substrate, the Scharifker–Hills model employed in the chronoamperometric transients curves (SCHARIFKER; HILLS, 1983).

Furthermore, the electrodeposition experiments were carried out using Au-coated fluorine-doped tin oxide (FTO) coated glass (20 × 10 × 2.5 mm^3) as working electrodes. The Au coatings (~100 nm) were deposited on FTO surface by sputtering using a Q150T turbo-pumped sputter coater (Quorum technologies®). Prior to the electrodeposition Au-coated substrates were cleaned for 10 min with acetone, ethanol alcohol and Milli-Q water, respectively, in ultrasonic bath (Quimis® model 0335D) and dry under air.

The films were electrodeposited at several temperature potentiostatically at peak potential which were determined in cyclic voltammetry measurements. The Te films were electrodeposited with a fixed coulombic charge density of 0.5 C cm^{-2} at each temperature but the CdTe films were grown employing a constant potential for a period of 0.5 h. Afterwards, the films were carefully rinsed with Milli-Q water and dry with blow air.

3.5. Physical characterisation of films

3.5.1. X-ray diffraction

X-ray diffraction (XRD) of the Te and CdTe films were recorded in range 20 to 80° with step 0.013°/min at 40 kV and 40 mA using a PANalytical® diffractometer model X-Pert PRO with $Co_{K\alpha}$ (λ = 1.788Å) radiation. X-Pert HighScore Plus version 3.0.4 (PANalytical®) software was used to data treatment and the crystallography card files were obtained from Inorganic Crystal Structure Database (ICSD).

3.5.2 Scanning electron microscopy

A high resolution field emission gun scanning electron microscope (FEG-SEM, FEI-Quanta 450) coupled to energy dispersive X-ray spectroscopy (EDS, Oxford Instruments INCA X-MAX) operating at an accelerating voltage of 20 kV was used to analyse the morphology and the chemical composition of as-deposited films.

3.5.3. Transmission electron microscopy

Transmission electron microscope (TEM) micrographs of Te electrodeposits were also recorded using a Hitachi® HT7700 TEM system operating at an accelerating voltage of 120 kV. The selected area electron diffraction (SAED) patterns were used to determine the growth direction of Te nanorods. Before the acquisition of TEM images, the Te films were mechanically scraped from the substrate surface with a sterilized scapel, disperse in ethanol, and finally, drop onto a carbon grid.

3.5.4. Optical characterisation

The optical properties of the CdTe films were investigated by ultraviolet-visible (UV-vis) spectroscopy at room temperature in the diffuse reflectance mode using a UV 2600 Shimadzu spectrophotometer coupled to an integrating sphere ISR 2600 Plus.

4. ELECTRODEPOSITION OF Te ON Au FROM EUTECTIC MIXTURES BASED ON CHOLINE CHLOLINE

In this Chapter, the electrodeposition of Te on Au substrate was investigated in either choline chloride-urea, or choline chloride-ethylene glycol deep eutectic solvent, at a molar ration of 1:2, containing 0.05 mol L^{-1} $TeCl_4$ as source of Te. The results revealed that electrodeposition of Te on Au electrode proceeded by three-dimensional progressive nucleation mechanism in both eutectic solvents. The diffusion coefficients of Te^{4+} species as a function of temperature were well fitted by an Arrhenius-like equation in both eutectic mixtures. The apparent activation energies were 22.20 and 22.55 kJ mol^{-1} for Scharifker-Hills and Cottrell´s models, respectively, in 1ChCl:2EG. On the other hand, in 1ChCl:2U these values were 59.20 and 57.80 kJ mol^{-1}. In addition, SEM micrographs of Te electrodeposits from both revealed a large-scale Te rods-like morphology with hexagonal cross-section in nanoscale regime uniformly distributed on electrode surface. TEM investigation suggested that Te single-crystalline grew perpendicular direction of (100) planes which implied in the preferential growth direction of [001].

4.1. INTRODUCTION

Trigonal tellurium (Te) is a *p*-type semiconductor material with narrow direct band-gap energy around 0.35 eV at room temperature (STUKE, 1969). Its crystal structure is formed by helical chains of covalently bound atoms maintained together by the van der Waals interactions among the chains forming a hexagonal lattice, which suggests a highly anisotropic growth tendency (DEVILLANOVA; DU MONT, 2013; HE *et al.*, 2017; STUKE, 1969; XIA, Younan *et al.*, 2003). In addition, Te presents unique properties, such as piezoelectricity, photoconductivity, thermoelectricity and nonlinear optical responses (ABAD *et al.*, 2015; DEVILLANOVA; DU MONT, DU, 2013a, 2013b; LIANG, F.; QIAN, H., 2009; LIN, S. *et al.*, 2016a; LIU, J.-W. *et al.*, 2010; STUKE, 1969), which allow its application in gas sensing, photoconductors, thermoelectric, solar cells, electronic and optoelectronic devices (ABAD *et al.*, 2015a; DEVILLANOVA; DU MONT, 2013b, 2013a; JIAN-MIN *et al.*, 2009; LIANG, F.; QIAN, H., 2009; LIN, S. *et al.*, 2016a; LIU, J.-W. *et al.*, 2010; QIAN, H. S. *et al.*, 2006; RHEEM *et al.*, 2010; TSIULYANU, D. *et al.*, 2005; WANG, Z. *et al.*, 2010a; XIA, Younan *et al.*, 2003).

In technological terms, the importance of this semiconductor was evidenced in 2011, when the United States of Americas' Government announced in the Materials Genome Initiative report, that Te was one of the most important materials to the manufacture of products in key high-growth sectors, including clean energy, consumer electronics and defense(HOLDREN, J P, 2011). Moreover, it has been demonstrated that, at nanometric size, their physical properties change, allowing a range of new applications in high technological devices, for instance: chemical transformations templates, batteries, ion detection and removal among others (HE *et al.*, 2017).

Over the last two decades, the synthesis of nanostructured materials, with controlled size and format, has arouses great scientific interest due to the potential in applied nanostructured materials for the development of new technologies (GE, M. *et al.*, 2016b; GORIPARTI *et al.*, 2014; HU, J.; ODOM; LIEBER, 1999a; WU, Yiying *et al.*, 2002a; XIA, Younan *et al.*, 2003).

Currently, a considerable effort has been conducted to synthesise Te nanostructures including: nanoparticles, nanoplates, nanobelts, nanowires and nanotubes (HE *et al.*, 2017), by chemical routes (GAUTAM; RAO, 2004; LI, G. *et al.*, 2014; QIAN, H. S. *et al.*, 2006; SONG, J.-M. *et al.*, 2008a; WANG, Z. *et al.*, 2010a), solution-phase assisted with visible-light (ZHANG, B. *et al.*, 2007b), ultrasonic (ZHOU, B. *et al.*, 2006) or microwave (ZHU, Y.-J. *et al.*, 2004a), and vacuum vapour deposition (CHEN, H. *et al.*, 2007). However, these techniques either require a long synthesis time and elevated temperatures or are based on high vacuum technology, which become very expensive at industrial scale.

Among the various synthesis methods used to produce nanostructured materials, the electrodeposition is very attractive, since it has low-cost, large-scale production, low temperature processing and handle-easily (LINCOT, 2005). Furthermore, the size, shape and morphology of the nanostructures can be controlled by electrodeposition parameters, such as the concentration of the electroactive species, deposition potentials, deposition current density, and bath temperature. Therefore, the electrodeposition is a convenient route to manufacture nanostructured semiconductors materials (LINCOT, 2005).

The aqueous plating baths are the most traditional way to electrodeposited Te coating (ABAD *et al.*, 2015a; KOWALIK *et al.*, 2016a; LINCOT, 2005; WU, L.-K. *et al.*,

2017). Additionally, it has been demonstrated the possibility to obtain Te nanostructures from aqueous electrolytes. For instance, Zhao and co-workers (ZHAO, A. *et al.*, 2005) electrodeposited ordered Te nanowires on Au substrate using aluminium membrane (AAM) as template in acid electrochemical bath at room temperature; Kumar *et al.*, (KUMAR, N. *et al.*, 2015) have been employed a polycarbonate membrane to produce vertically orientated Te nanowires, with preferential growth along the [001] direction, in a sulfuric acid solution at pH = 0.8; She *et al.*, (SHE *et al.*, 2009) reported the direct grown of Te nanowire on ITO-coated glass by dissolving TeO_2 in 1.0 mol L^{-1} KOH aqueous solution.

Room temperature ionic liquids (RTILs) is an alternative to aqueous electroplating baths to electrodeposition of metals and alloys, because they are electrochemically stable in a wide range of potential, allowing the production of the metals that are not electrodeposited in aqueous bath, such as aluminium (SU, C. J. *et al.*, 2013) and there is no reduction of the solvent occurring simultaneously with the metal electrodeposition, as observed for several metals in aqueous-based electrolyte, which are electrodeposited in the same potential range of the hydrogen evaluation reaction (ABBOTT, A. P.; FRISCH; RYDER, 2013; ENDRES, Frank.; ABBOTT, A.; MACFARLANE, 2017; ZEIN EL ABEDIN; ENDRES, F., 2009). Furthermore, the solubility of metals salts are high in RTILs and they present low toxicity (ABBOTT, A. P.; FRISCH; RYDER, 2013; ENDRES, Frank.; ABBOTT, A.; MACFARLANE, 2017; ENDRES, Frank; ABEDIN, Sherif Zein EL, 2006). It has been reported the possibility of deposition of nanostructured materials using RTILs baths (ABEDIN, S Zein El *et al.*, 2007; AL-SALMAN *et al.*, 2015).

Recently, special attention has been given to free-template electrodeposition of Te nanostructures in ionic liquids. For example: Szymczak *et al.*, (SZYMCZAK *et al.*, 2012) reported template-free electrodeposition of single crystalline Te nanowires with diameter ranging from 30 to 200 nm grown along the [001] direction in a piperidinium-based ionic liquid mixture; Thiebaud *et al.*, (THIEBAUD; LEGEAI; STEIN, 2016) performed a study concerning the influence of deposition parameters on the morphology of the electrodeposits in ionic liquid based on piperidinium and showed that the shape and dimensions of the nanostructures were controlled by the applied potential. Furthermore, Thiebaud *et al.*, (THIEBAUD *et al.*, 2016) used piperidinium-based ionic liquid containing low bromide concentration to obtain hair-like Te nanowires, it means, low diameter and high aspect ratio, which is very interesting for thermoelectric applications.

However, the physical and chemical properties of RTILs change under exposition to moisture, some of them are very corrosive and release hydrofluoric acid in presence of water, which can be an environmental problem in the waste disposal of industries and laboratories (ENDRES, Frank; ABEDIN, Sherif Zein EL, 2006). As alternative, the Deep Eutectic Solvents (DESs) have been proposed (ABBOTT, A. P. *et al.*, 2003; ABBOTT, A. P.; BOOTHBY; *et al.*, 2004), since they are nontoxic, biodegradable and considered environmentally friendlier, and, finally, cheaper than RTILs (SMITH; ABBOTT, A. P.; RYDER, 2014; WAGLE; ZHAO, H.; BAKER, 2014; ZHANG, Q. *et al.*, 2012). The most widespread combination used for the formation of DESs are choline chloride (ChCl), a quaternary ammonium salt, with either ethylene glycol (EG) or urea (U), in molar ratio of 1:2, which are hydrogen bond-donor components (SMITH; ABBOTT, A. P.; RYDER, 2014; WAGLE; ZHAO, H.; BAKER, 2014; ZHANG, Q. *et al.*, 2012). Additionally, these solvents present a wide potential range of electrochemical stability, high solubility of metals salts, appreciable ionic conductivity (SMITH; ABBOTT, A. P.; RYDER, 2014; WAGLE; ZHAO, H.; BAKER, 2014; ZHANG, Q. *et al.*, 2012).

It was already reported in literature that Te alloys can be electrodeposited from DES electrolytes. Golgovici *et al.*, (GOLGOVICI, Florentina *et al.*, 2011) successfully employed DES based on ChCl with malonic acid in molar ratio of 1:1 for electrodeposited BiTe, SbTe and BiSbTe alloys on Pt electrode at temperature of 85 °C. In addition, Catrangiu *et al.* (CATRANGIU, A.-S. *et al.*, 2016) used an eutectic mixture based on ChCl with oxalic acid (OxA), in 1:1 molar ration, to obtain Sb_xTe_y semiconductor alloy on Cu electrode at bath temperature 60-70 °C. Moreover, they also reported the electrodeposition of Cu_xTe_y semiconductor material on carbon steel in ChCl and EG and in ChCl with OxA mixtures, with 1:1 molar ratio for both solutions and at 60°C [48]. Agapescu *et al.*, (AGAPESCU *et al.*, 2013) reported that the DES based on combination of ChCl and OxA is a promise bath to electrodeposition of the thermoelectric Bi_2Te_3 alloy.

Therefore, this Chapter explore the Te electrodeposition in nanostructured regime on Au substrate from plating solutions based on eutectic mixtures. In addition, the Chapter reports the investigation carried out to understand the electrochemical behaviour of Te in either ChCl-EG or ChCl-U eutectic mixtures, at a molar ration of 1:2, as well as, the effects of temperature range from 30 up to 100 °C.

4.2. RESULTS AND DISCUSSION

4.2.1. Cyclic voltammetry

Cyclic voltammetry experiments were performed to establish the working electrochemical potential range for the Te electrodeposition in both plating solutions at scan rate of 50 mV s^{-1}. Cyclic voltammograms recorded at 30 °C for the freshly prepared 1ChCl:2EG and 1ChCl:2U solutions, with and without Te^{4+} species, are shown in Figure 3. For 1ChCl:2EG solution, without Te^{4+} ions, no peaks related to the Faradaic process are displayed between 0.6 and –1.25 V (Fig. 3a, dashed line), while an increase in the background current is showed for potentials more negative than –1.25 V, which is associated to the reduction of choline ions (Ch^+), hydroxyl groups of EG and trace of water (VIEIRA, L; SCHENNACH; GOLLAS, B., 2016; VIEIRA, Luciana; WHITEHEAD; GOLLAS, B. R., 2014; YUE *et al.*, 2012). On the other hand, a meaningful broad peak current, located around –1.27 V is observed in the cyclic voltammogram recorded for 1ChCl:2U solution without Te^{4+} species (Fig. 3b, dashed line). This process is attributed to the electrochemical reduction of traces of water dissolved in 1ChCl:2U solution, as demonstrated by Urcezino *et al.*, (URCEZINO *et al.*, 2017). Finally, both plating solutions displayed a significant increase of the background current for applied potential more positive than 0.60 V. The anodic limit is attributed to the oxidation of chloride to form chlorine ions (Cl_3^-) (HAERENS *et al.*, 2009). Therefore, for both 1ChCl:2EG and 1ChCl:2U plating solutions, the cyclic voltammograms were obtained sweeping the potential between 0.6 and –1.0 V.

Figure 3 - Cyclic voltammograms (a) of the blank 1ChCl:2EG (dash line) and containing 0.05 mol L^{-1} $TeCl_4$ and (b) of the blank 1ChCl:2U (short dashed line) and containing 0.05 mol L^{-1} $TeCl_4$.

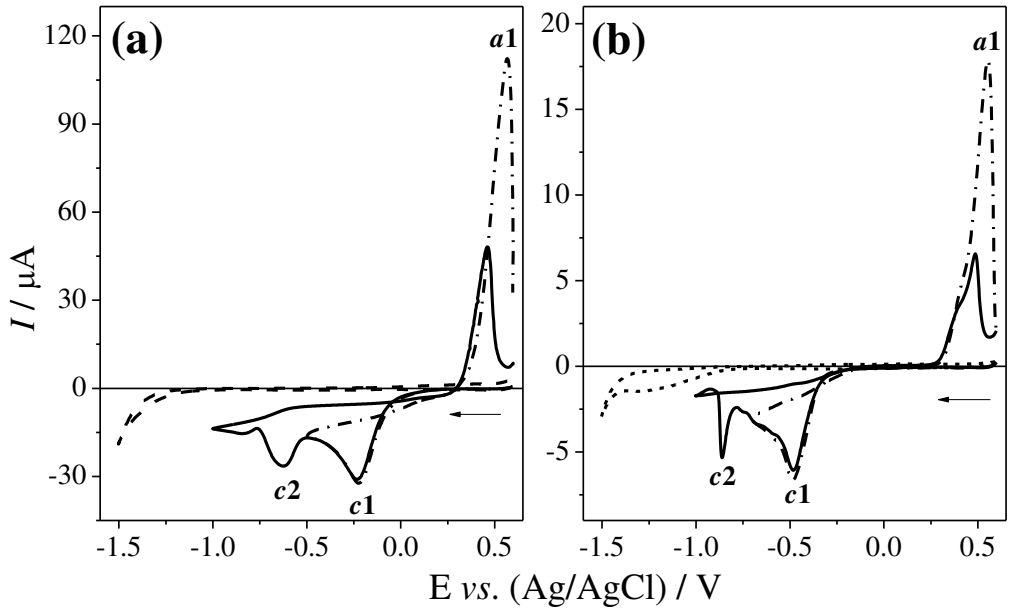

Source: Author

Figure 3 also gives the cyclic voltammogram recorded for Te^{4+} species dissolved in 1ChCl:2EG and 1ChCl:2U eutectic mixtures. As can be seen, the voltammetric peaks profiles of Te^{4+} species on Au electrode were very similar in both electrolytes. For 1ChCl:2EG solution with Te^{4+} species, peaks around –0.22 and –0.62 V are displayed in the forward scan (Fig. 3a, peaks *c*1 and *c*2, solid line), while for 1ChCl:2U solution, containing Te^{4+} species, peaks at –0.49 and at –0.86 V are displayed in the forward sweep (Fig. 3b, peaks *c*1 and *c*2, solid line). Some authors have already reported the occurrence of two electrochemical reduction process for Te^{4+} species in other non-aqueous plating solutions, such as molten salt (JENG; SUN, I-Wen, 1997), imidazolium-based (HSIU; SUN, I.-W., 2004; TSAI *et al.*, 2014) and piperidinium-based (SZYMCZAK *et al.*, 2012; THIEBAUD *et al.*, 2016; THIEBAUD; LEGEAI; STEIN, 2016) ionic liquids. Following these authors, the peak named *c*1 is attributed to the reduction of Te^{4+} species to Te *via* one-step of four electrons transfer, whereas occurrence of the peak *c*2 is attributed to the Te stripping to the surface due to the reduction of metallic Te to Te^{2-} species (HSIU; SUN, I.-W., 2004; JENG; SUN, I-Wen, 1997; SZYMCZAK *et al.*, 2012).

Furthermore, the cyclic voltammograms recorded at different temperatures for the plating solutions containing Te^{4+} species, are shown in Figure 4. For both electrolytes, it is

clearly seen that the peak current related to the Te electrodeposition increases with the bath temperature. Moreover, the existence of a current crossover-loop between the forward and reverse scans, in each cyclic voltammogram, indicates that the Te electrodeposition on Au surface follows a nucleation-growth controlled process.

Figure 4 - Cyclic voltammograms recorded on Au disk in DESs (a) 1ChCl:2EG and (b) 1ChCl:2U containing 0.05 mol L^{-1} $TeCl_4$ at several temperatures.

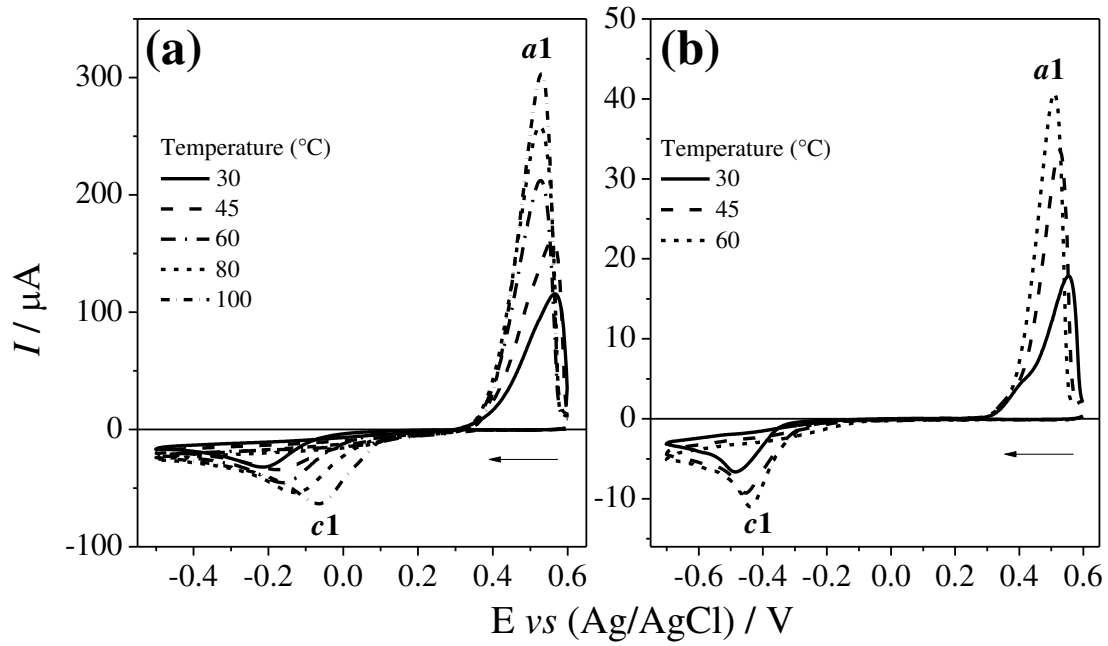

Source: Author

4.2.2. Atomic force microscopy

Nucleation and growth mechanism of Te on Au substrate was investigated by AFM analyses. In 1ChCl:2EG, the electrodeposition was conducted applying the potential of -0.04 V for 1.20 s at 30 °C, while the potential of 0.16 V for 0.50 s was used at 80 °C. On the other hand, the following conditions were used for electrodeposition carried out in 1ChCl:2U; deposition potential of –0.28 V for 0.80 s at 30 °C whereas at 60 °C the potential of –0.22 V for 0.50 s. Therefore, AFM topographic images obtained in the initial stages of the Te electrodeposition Au-coated FTO electrode, from both DESs based electrolytes are shown in Figure 5.

Figure 5 - AFM micrograph of Te electrodeposits on Au-coated FTO electrode from either 1ChCl:2EG at (a) 30 °C and (b) 80 °C or 1ChCl:2U at (c) 30 °C and (d) 60 °C (E = –0.22 V for 0.50 s) both solutions containing 0.05 mol L^{-1} $TeCl_4$.

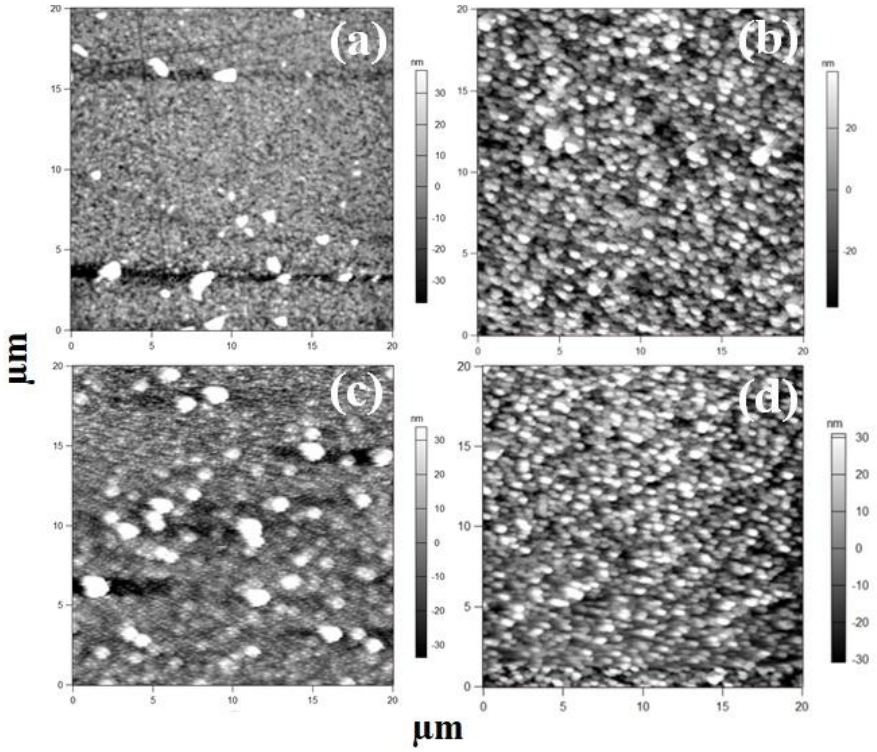

Source: Author.

It shows that, in the early stages, the electrodeposited Te deposits appeared to have a nanometer thickness around 30 nm, as can be seen in the side bar in the Fig. 5. The nanostructures presented a three-dimensional nodular morphology islands-like of varying diameter sizes and randomly distributed over the Au-coated FTO electrode surface in all investigated conditions. The number of spherical particles per unit of area increase with temperature, presumably, due to the decrease of viscosity and increase in the availability of Te^{4+} species at the electrode surface.

Furthermore, a histogram of these spherical nanostructures obtained from AFM micrograph is displayed in Fig. 6. In 1ChCl:2EG electrolyte at 30 °C (Fig. 6a) Te nanostructures with diameter size between 0.13 and 1.50 µm were obtained, while agglomerates with diameter ranging from 0.27 up to 1.33 µm were observed at 80 °C (Fig. 6b). On the other hand, the Te electrodeposition conducted in 1ChCl:2U solution at 30 °C (Fig. 6c) produced nanostructures with diameter varying from 0.27 to 1.60 µm. Similar range in diameter size were seen in Te nanostructures deposited in 1ChCl:2U mixture at 60 °C (Fig.

6d). Therefore, these histograms reveal a disparate in diameters range of Te nanostructures in both DES medium, it suggests that the Te nuclei are gradually created on the substrate's surface at varying rates depending on time. Thereby, the AFM analysis indicated that the electrocrystallisation of Te on Au electrode proceeded via a three-dimensional progressive nucleation and growth mechanism.

Figure 6 - Histogram showing the diameter distribution of the electrodeposited Te islands obtained from 1ChCl:2EG mixture at (a) 30 °C and (b) 80 °C and from 1ChCl:2U at (c) 30 °C and (d) 60 °C and observed in the AFM micrographs.

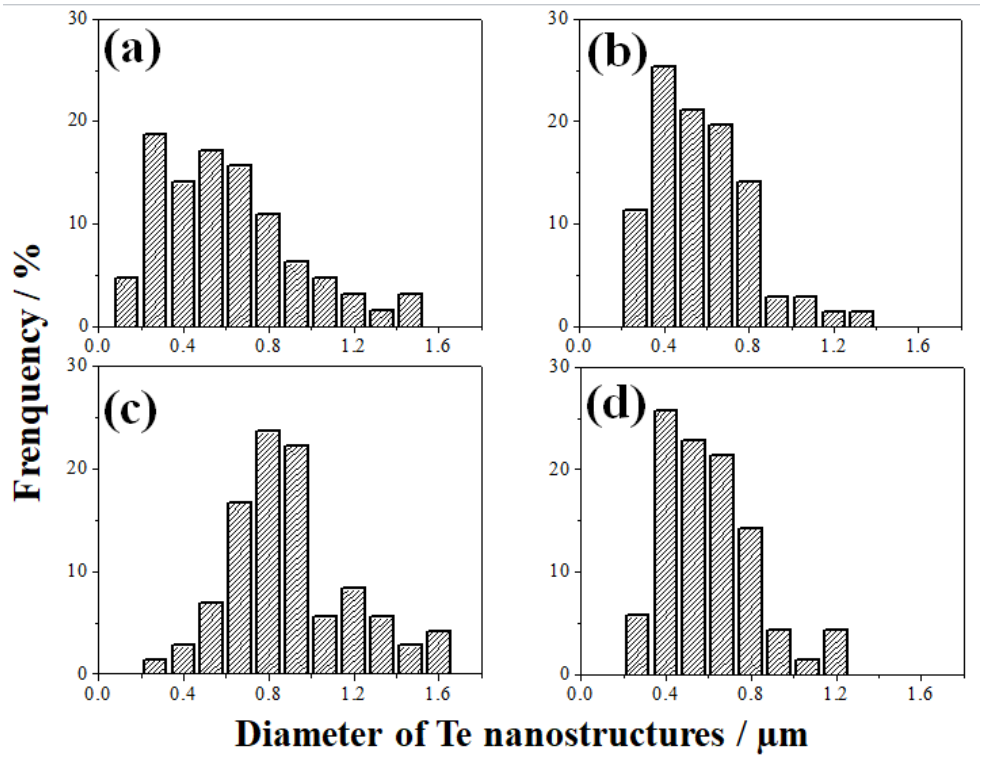

Source: Author.

4.2.3. Chronoamperometry

In addition, the nucleation and growth mechanism of Te on Au substrate was also studied by chronoamperometry experiments, employing the model proposed by Scharifker and Hill model (S-H model) (SCHARIFKER; HILLS, 1983). This theoretical calculation allows parameters related to early stages of metal deposition on substrate.

According to S-H model the metal electrochemical nucleation on foreign substrate can be splitting in two limiting cases either instantaneous or progressive mechanisms. In the instantaneous mechanism all nucleation sites are activated at onset potentiostatic current transient, thereby, the nuclei formed on electrode surface at beginning of the applied nucleation potential grow at a constant rate depending on the applied potential. In contrast, in the progressive mechanism the nucleation sites are gradually activated as the potentiostatic experiment pursues, therefore, the nuclei formation and grow proceeds at varying rates depending on time. For the purpose to distinguish between the instantaneous and progressive mechanisms the chronoamperometric data are normalized to $(I/I_m)^2$ and (t/t_m) and compared with the dimensionless models that can be mathematically described by the following equations (SCHARIFKER; HILLS, 1983):

Instantaneous mechanism

$$\left(\frac{I}{I_m}\right)^2 = \frac{1.9542}{(t/t_m)}\left\{1-\exp\left[-1.2564\left(\frac{t}{t_m}\right)\right]\right\}^2 \qquad 4.1$$

Progressive mechanism

$$\left(\frac{I}{I_m}\right)^2 = \frac{1.2254}{(t/t_m)}\left\{1-\exp\left[-2.3367\left(\frac{t}{t_m}\right)^2\right]\right\}^2 \qquad 4.2$$

in the equations above, I is current recorded at time t whereas I_m is maximum current value at maximum time t_m obtained from potentiostatic current transients.

The collection of current-time transients recorded at different working temperatures for 1ChCl:2EG and 1ChCl:2U mixtures, containing 0.05 mol L^{-1} $TeCl_4$, are shown in Figs. 7 and 8, respectively. All current transient curves presented a typical behaviour of three-dimensional nucleation mechanism with diffusion-controlled growth. The chronoamperometric curves were characterised by a sharp current decaying at the beginning of the of the applied nucleation potential owing of the electrode double-layer charging, subsequently, the current rises gradually, which is due to the formation and growth of Te

nuclei on the Au surface. Thereby, the current reaches the maximum value (I_m) at a corresponding maximum time (t_m) and then the current decay slowly until reaches the diffusion-controlled regime to a planar electrode (SCHARIFKER; HILLS, 1983). It is worth mentioning that an increasing in the values of I_m followed by a decreasing in the t_m when the applied overpotential was shifted in direction to more negative values. This can be explained based on decreasing in the time required for the diffusion layer to overlap (SCHARIFKER; HILLS, 1983) due to an increased nucleation density of Te nuclei on Au electrode.

Figure 7 - Collection of current-time transients for the reduction of Te^{4+}/Te on Au substrate obtained from 1ChCl:2EG containing 0.05 mol L^{-1} $TeCl_4$ at (a) 30, (b) 45, (c) 60 and (d) 80 °C.

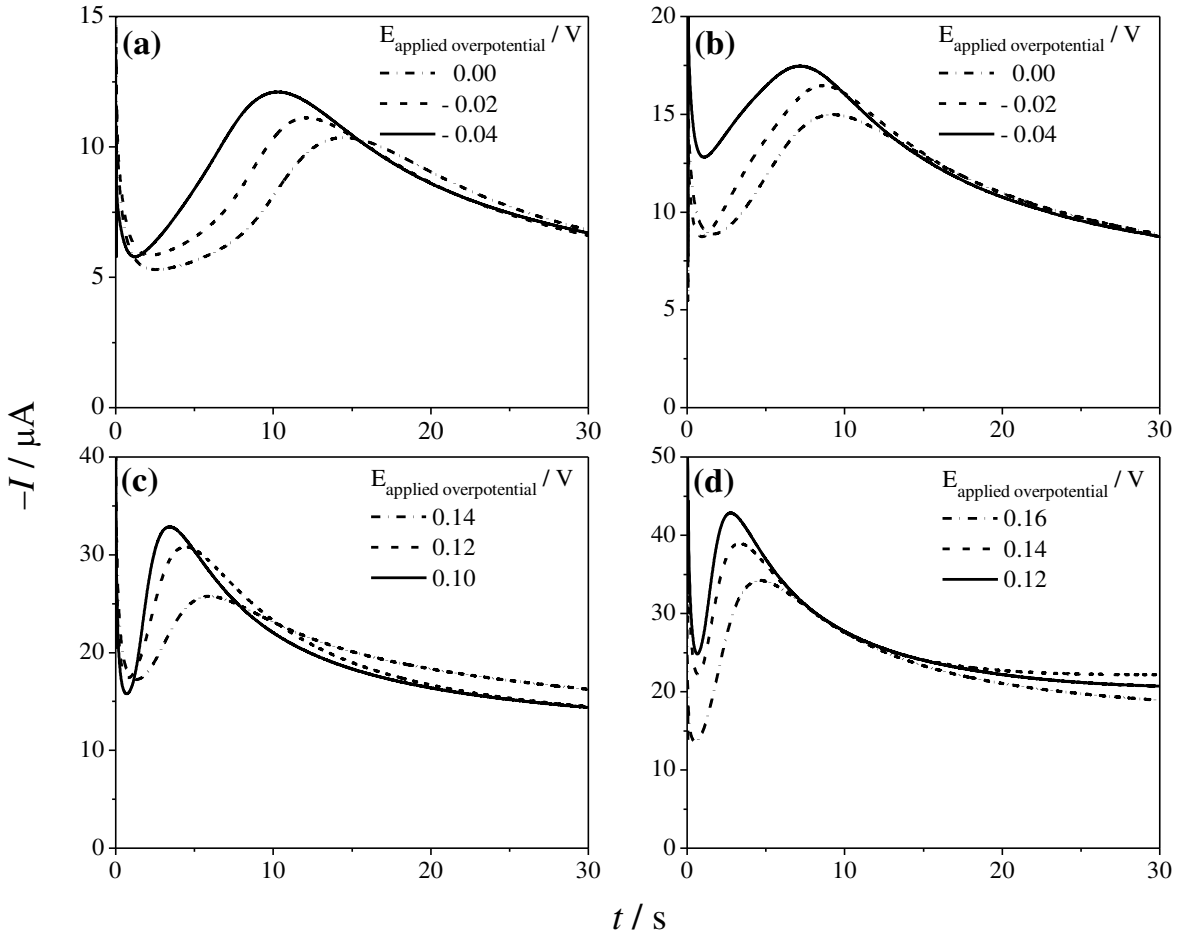

Source: Author

It is also observed in the Figs. 7 and 8 that there is an induction time, t_0, preceding the start of nucleation process. Then, before the analyses of the nucleation-growth mechanism the

delay time was estimated from the intercept of linear regression of the plots $(I/I_m)^2$ or $(I/I_m)^{2/3}$ versus t. Therefore, the axis of time was redefining as $t' = t - t_0$ and $t_m' = t_m - t_0$. The obtained values of the induction time and others kinetic parameters extracted from current-times curves are shown in Table 1.

Figure 8 - Current-time transients for the reduction of Te^{4+}/Te on Au substrate obtained from 1ChCl:2U containing 0.05 mol L^{-1} $TeCl_4$ at (a) 30, (b) 45 and (c) 60 °C.

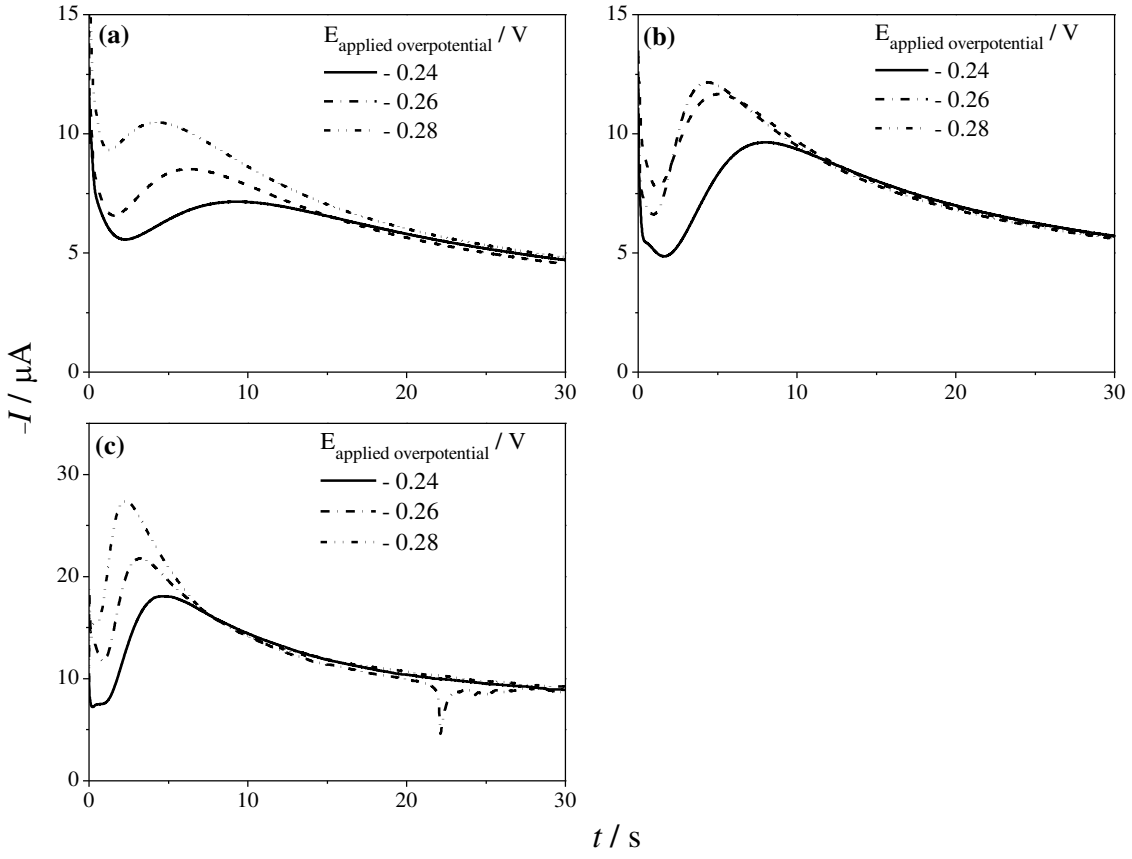

Source: Author.

Therefore, the comparisons between the dimensionless current-time transients curves, obtained from current-time transients' data (Fig. 7a-d) and Fig. 8a-c) with those generated from the theoretical S-H model (eqs. 4.1 and 4.2) are plotted in Figs. 9a-d and Figs. 10a-c. It can be noted that the nucleation and growth mechanism, related to the electrodeposition of Te on Au surface, from both 1ChCl:2EG and 1ChCl:2U mixtures, fits reasonably close to the three-dimensional progressive nucleation with diffusion-controlled

growth, regardless the bath temperature, which is in good concordance with the AFM analyses

Figure 9 - Comparison of the dimensionless experimental curves derived from Fig. 7a-d with those simulated by S-H model for electrodeposition of Te on Au from 1ChCl:2EG containing 0.05 mol L^{-1} $TeCl_4$ and at (a) 30°C, (b) 45°C, (c) 60 °C, and (d) 80 °C.

.

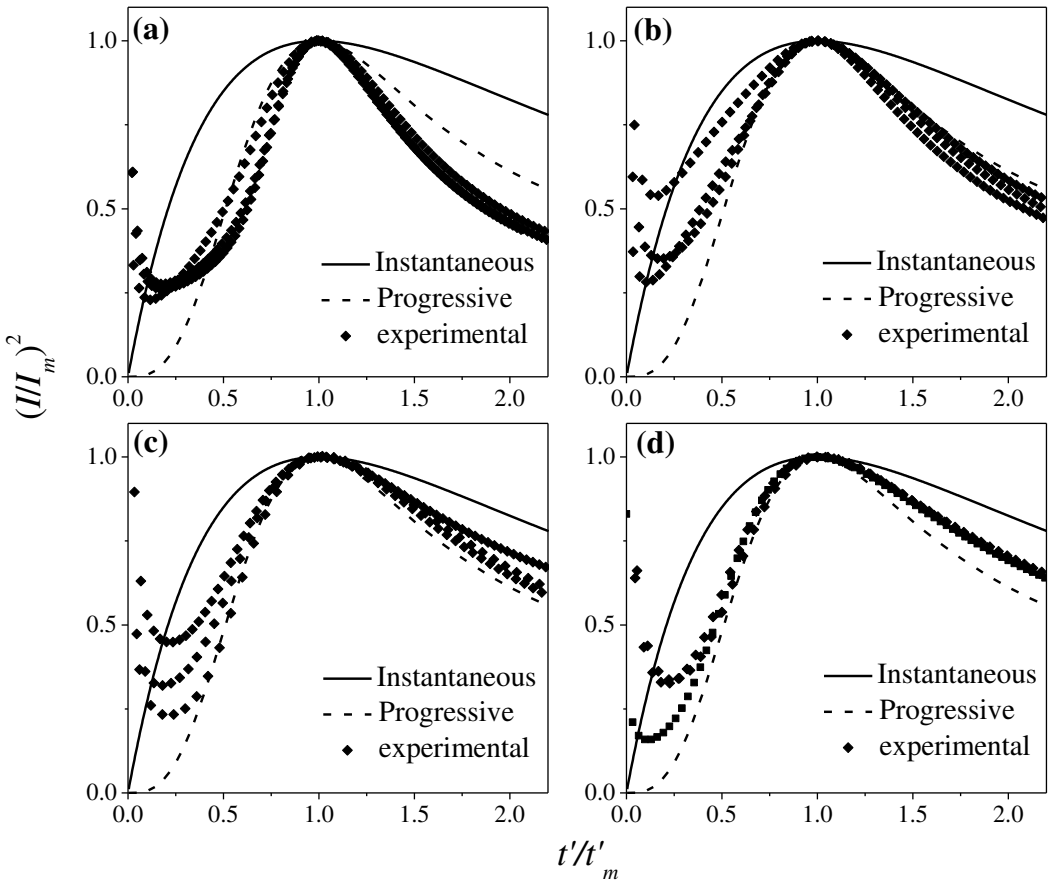

Source: Author.

The calculated data from S-H model agree with previously finding for the electrocrystallisation of Te on glassy carbon electrode in the chloroaluminate molten salt (JENG; SUN, I-Wen, 1997). On the other hand, Tsai *et al*., (TSAI *et al.*, 2014) reported that the Te nucleation on Ni electrode surface, from imidazolium-based RTIL solution, followed three-dimensional instantaneous nucleation with diffusion-controlled growth. Similar nucleation-growth mechanism were also observed for Te on glassy carbon substrate in TeO_2-silica sol solution and TeO_2-aqueous electrolyte (FENG, Y.; GU, 2013). Therefore, the comparison between the results obtained in this investigation and those previously published

in literature (FENG, Y.; GU, 2013; JENG; SUN, I-Wen, 1997; TSAI *et al.*, 2014), suggest that the nucleation mechanism is affected by the plating solutions and the substrate surface.

Figure 10 - Comparison of the dimensionless experimental curves derived from Fig. 8a-c with those simulated by S-H model for electrodeposition of Te on Au from 1ChCl:2U containing 0.05 mol L^{-1} $TeCl_4$ and at (a) 30, (b) 45, and (c) 60 °C.

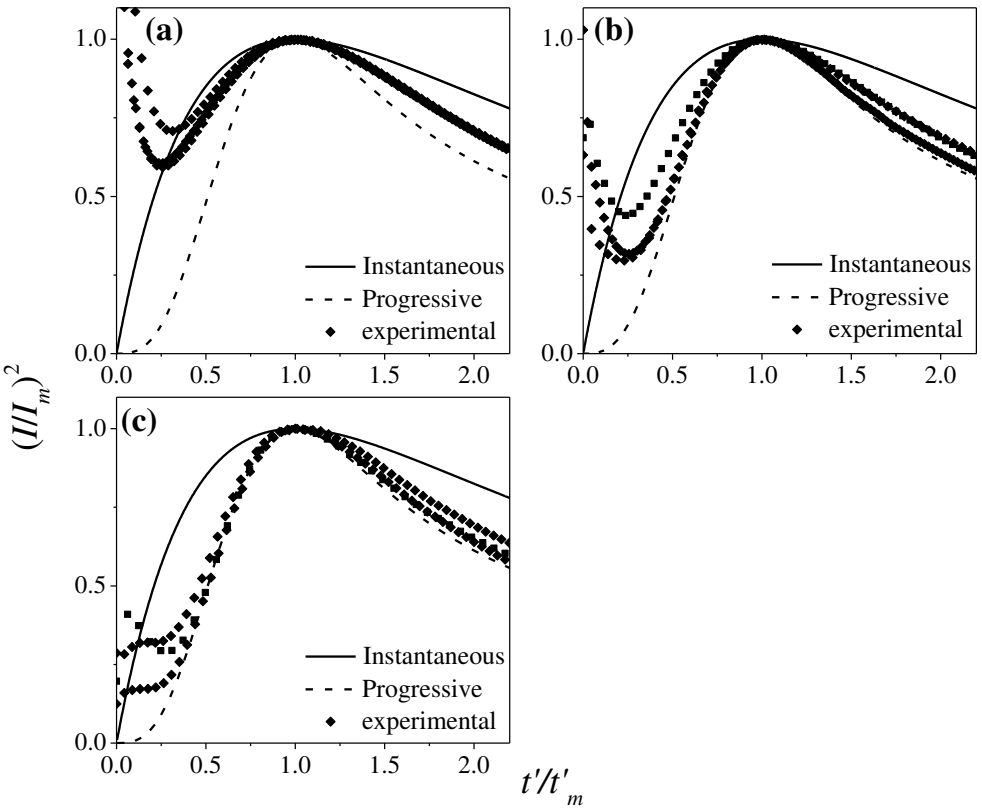

Source: Author.

Scharifker and Hill (SCHARIFKER; HILLS, 1983) have also shown that the number density of active on the substrate surface can be determined the rising portion of the potentiostatic current transients, as described by the equation below:

$$I(t) = \frac{2}{3}\frac{zFAN_{\infty}\pi(2Dc)^{3/2}M^{1/2}}{\rho^{1/2}}t^{3/2} \qquad 4.3$$

here, $I(t)$ is the current at time t, zF is the molar charge of the electrodepositing species, D is the diffusion coefficient, c is the metal ion bulk concentration, M and ρ is the molecular

weight and the density of the deposited material, respectively, A is the steady state nucleation rate constant per site and N_∞ is the number density of active sites.

The steady state nucleation rate (AN_∞) estimated during early stages of nucleation at different applied overpotentials are shown in Table 1. Overall, the value of AN_∞ increased when either the nucleation potentials were shifted in direction to more negative values or the bath temperature was raised. In addition, the deposition charges, obtained by integrated area under the current-times curves (Figs. 7 and 8) and listed in Table 2. It can be seen that the deposition charges increased with the bath temperature in both eutectic mixtures, additionally, the charges calculated from Te electrodeposition in 1ChCl:2EG medium were slightly higher than ones obtained in 1ChCl:2Uelectrolyte at the range temperature investigated, which implied in the increase availability of Te^{4+} species over electrode surface and consequently increasing the current density, as seen in the Table 1.

In addition, the S-H model leads to determine the diffusion coefficient of electroactive species. The calculation depends on the nucleation mechanism of the metal specie, since there are two limiting approaches, as described above. Therefore, a progressive nucleation controlled by diffusion process the diffusion coefficient can be determined by the product of $j_m^2 t_m$, following the equation (4.4):

$$j_m^2 t_m = 0.2598(zFc)^2 D \qquad 4.4$$

where j_m is the maximum current density at maximum instant of time t_m and D is the diffusion coefficient, all the others variables have their meaning showed above in this Chapter.

The values of $j_m^2 t_m$ obtained from potentiostatic current transients (Figs. 7 and 8) can be also seen in the Table 1 and the average diffusion coefficient of Te^{4+} ions in both DESs are shown in Table 3. It is worth noting that diffusion coefficient of Te^{4+} species increased with temperature, probably, due to the decrease of the viscosity of the plating solution (ABBOTT, A. P. *et al.*, 2003; ABBOTT, A. P.; BOOTHBY; *et al.*, 2004; GHAREH BAGH *et al.*, 2015; KAREEM *et al.*, 2010; MJALLI *et al.*, 2014).

Moreover, the diffusion coefficient of any electroative metal species in solution can be evaluated by the well-known Cottrell´s equation:

$$I(t) = nFac(D/\pi)^{1/2} t^{-1/2} \quad 4.5$$

here, *a* is the geometric area of the working electrode (7.85×10^{-3} cm^2), *n* is the number of electrons transferred in the electrochemical reaction and *F* is the Faraday´s constant and all the others variables have their meaning elsewhere in this Chapter. The Cottrellian profiles obtained for Te^{4+} species in 1ChCl:2EG and 1ChCl:2U are shown in Figures 11 and 12, respectively.

The diffusion coefficients obtained by the Cottrell' method are also displayed in Table 3. The values of diffusion coefficients obtained upon the S-H model are around twice larger than those ones evaluated by Cottrell's equation. This apparently disagreement could be related to the existence of more than one Te^{4+} complex species in solution. It is reported that in basic cloroaluminate molten salt (JENG; SUN, I-Wen, 1997) and in piperidinium-based ILs (THIEBAUD *et al.*, 2016), Te^{4+} species can exist as $[TeX_6]^{2-}$, where X = Cl or Br. However, in DES beyond the Cl^- ions, there are EG, or U, molecules which can also coordinate with Te ions. The EG molecules have two coordinate sites located in O atom, while the coordinate sites in U molecules are located over the O and N atoms. Therefore, in 1ChCl:2EG may be exists a competition between Cl^- ions and EG molecules to coordinate with Te^{4+} ions in solution. Similar situation is expected to Cl^- ions and U molecules in 1ChCl:2U. These complexes maybe exhibit different rates of electron transfer reactions, therefore, producing parallel reactions during the reduction of Te on Au substrate.

In addition, a comparison between the values for diffusion coefficients of Te^{4+} species obtained by either S-H model or Cottrell's equation in 1ChCl:2EG and 1ChCl:2U at 30 °C with values reported in the literature is done in Table 3. As can be seen, the values are in same order of magnitude to reported by Jeng and Sun (JENG; SUN, I-Wen, 1997) in cloroaluminate molten salt but two order lesser than those reported in aqueous solution (FENG, Y.; GU, 2013; FRANTZ *et al.*, 2015) and sol electrolyte (FENG, Y.; GU, 2013).

Table 1 - Experimental data extracted from the current-time transients for Te nucleation on Au substrate from DESs.

1ChCl:2EG containing 0.05 mol L^{-1} $TeCl_4$							
Temperature / °C	$E_{applied\ overpotential}$ / V	t_m / s	t_o	t'_m	j_m / A cm^{-2}	$j_m^2\ t_m$/ A^2 s cm^{-4}	AN_∞ / cm^{-2} s^{-1}
30	0.00	14.43	0.24	14.19	1.32×10^{-3}	2.51×10^{-5}	46.55×10^{3}
	–0.02	12.18	0.32	11.86	1.42×10^{-3}	2.45×10^{-5}	37.29×10^{3}
	–0.04	10.31	0.46	9.85	1.42×10^{-3}	2.45×10^{-5}	73.44×10^{3}
45	0.00	8.15	0.54	7.61	1.91×10^{-3}	4.07×10^{-5}	50.05×10^{3}
	–0.02	6.94	0.73	6.21	2.09×10^{-3}	4.03×10^{-5}	54.58×10^{3}
	–0.04	5.72	0.75	4.94	2.23×10^{-3}	3.84×10^{-5}	58.25×10^{3}
60	0.14	5.94	0.60	5.34	3.28×10^{-3}	6.40×10^{-5}	75.26×10^{3}
	0.12	4.43	0.48	3.95	3.92×10^{-3}	6.82×10^{-5}	18.95×10^{4}
	0.10	3.34	0.33	3.01	4.18×10^{-3}	5.84×10^{-5}	37.91×10^{4}
80	0.16	4.65	0.35	4.30	4.36×10^{-3}	8.85×10^{-5}	18.84×10^{4}
	0.14	3.31	0.46	2.85	4.96×10^{-3}	8.15×10^{-5}	25.89×10^{4}
	0.12	2.70	0.45	2.25	5.45×10^{-3}	8.03×10^{-5}	35.96×10^{4}
1ChCl:2U containing 0.05 mol L^{-1} $TeCl_4$							
30	–0.24	9.48	0.74	8.74	9.11×10^{-4}	7.87×10^{-6}	19.45×10^{4}
	–0.26	6.43	0.73	5.70	1.08×10^{-3}	7.50×10^{-6}	42.26×10^{4}
	–0.28	4.32	0.83	3.49	1.34×10^{-3}	7.76×10^{-6}	47.20×10^{4}
45	–0.24	8.59	0.45	8.14	1.21×10^{-3}	1.26×10^{-5}	31.63×10^{4}
	–0.26	5.12	0.59	4.53	1.48×10^{-3}	1.12×10^{-5}	69.32×10^{4}
	–0.28	4.33	0.42	3.91	1.55×10^{-3}	1.04×10^{-5}	12.00×10^{5}
60	–0.24	4.77	0.29	4.48	2.30×10^{-3}	2.52×10^{-5}	65.78×10^{4}
	–0.26	3.26	0.36	2.90	2.78×10^{-3}	2.52×10^{-5}	10.94×10^{5}
	–0.28	2.32	0.45	1.87	3.48×10^{-3}	2.81×10^{-5}	20.85×10^{5}

Table 2 - Deposition charge for the reduction of Te^{4+}/Te on Au substrate calculated from the integration of current-times curves.

1ChCl:2EG system		
Temperature / °C	$E_{\text{applied overpotential}}$ / V	$-Q$ / μC
30	0.00	224.0
	–0.02	236.0
	–0.04	260.0
45	0.00	364.0
	–0.02	376.0
	–0.04	382.0
60	0.14	576.0
	0.12	587.0
	0.10	591.0
80	0.16	707.0
	0.14	774.0
	0.12	780.0
1ChCl:2U system		
30	–0.24	168.0
	–0.26	183.0
	–0.28	210.0
45	–0.24	212.0
	–0.26	235.0
	–0.28	236.0
60	–0.24	361.0
	–0.26	365.0
	–0.28	415.0

Source: Author.

Table 3 - Comparison between the diffusion coefficients of Te^{4+} species obtained in this Thesis with those already reported in the literature.

Reference	D / cm^2 s^{-1}	Method	System	T / °C
This work	$2.55 \pm 0.33 \times 10^{-7}$	S-H model	$TeCl_4$ in 1ChCl:2EG	30
This work	$3.70 \pm 0.12 \times 10^{-7}$	S-H model	$TeCl_4$ in 1ChCl:2EG	45
This work	$6.60 \pm 0.50 \times 10^{-7}$	S-H model	$TeCl_4$ in 1ChCl:2EG	60
This work	$8.62 \pm 0.46 \times 10^{-7}$	S-H model	$TeCl_4$ in 1ChCl:2EG	80
This work	$7.97 \pm 0.16 \times 10^{-8}$	S-H model	$TeCl_4$ in 1ChCl:2U	30
This work	$1.20 \pm 0.10 \times 10^{-7}$	S-H model	$TeCl_4$ in 1ChCl:2U	45
This work	$2.53 \pm 0.30 \times 10^{-7}$	S-H model	$TeCl_4$ in 1ChCl:2U	60
This work	$1.21 \pm 0.04 \times 10^{-7}$	Cottrell	$TeCl_4$ in 1ChCl:2EG	30
This work	$2.27 \pm 0.07 \times 10^{-7}$	Cottrell	$TeCl_4$ in 1ChCl:2EG	45
This work	$3.10 \pm 0.15 \times 10^{-7}$	Cottrell	$TeCl_4$ in 1ChCl:2EG	60
This work	$4.50 \pm 0.15 \times 10^{-7}$	Cottrell	$TeCl_4$ in 1ChCl:2EG	80
This work	$4.50 \pm 0.75 \times 10^{-8}$	Cottrell	$TeCl_4$ in 1ChCl:2U	30
This work	$8.96 \pm 0.06 \times 10^{-8}$	Cottrell	$TeCl_4$ in 1ChCl:2U	45
This work	$4.97 \pm 0.30 \times 10^{-7}$	Cottrell	$TeCl_4$ in 1ChCl:2U	60
(JENG; SUN, I-Wen, 1997)	1.75×10^{-7}	Rotating disk electrode	$TeCl_4$ in $AlCl_3$-MEIC (44.4/55.6 m/o)	30
(FENG, Y.; GU, 2013)	3.18×10^{-6}	S-H model modified	TeO_2-SiO_2 sol (TEOS:C_2H_5OH:EG:H_2O:HCl:TeO_2)	RT
(FENG, Y.; GU, 2013)	3.25×10^{-6}	S-H model modified	TeO_2 aqueous solution	RT
(FRANTZ *et al.*, 2015)	$6.9 \pm 0.2 \times 10^{-6}$	Sand-Bard method	$HTeO_2^+$ in acid aqueous solution	RT

Source: Author.

Figure 11 - Current-time transients for the reduction of Te^{4+}/Te on Au substrate obtained from 1ChCl:2EG at diffusional control (a) 30, (b) 40, (c) 60 and (d) 80 °C. Cottrell plots are showed as insert.

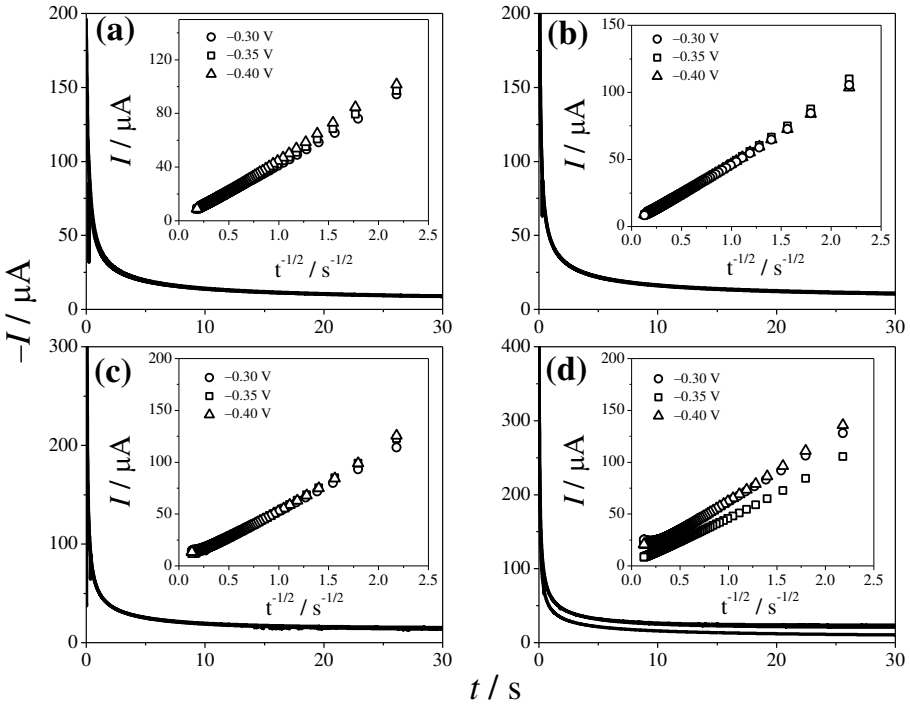

Source: Author.

Figure 12 - Current-time transients for the reduction of Te^{4+}/Te on Au substrate obtained from 1ChCl:2U at diffusional control at (a) 30, (b) 40, and (c) 60. Cottrell plots are showed as insert.

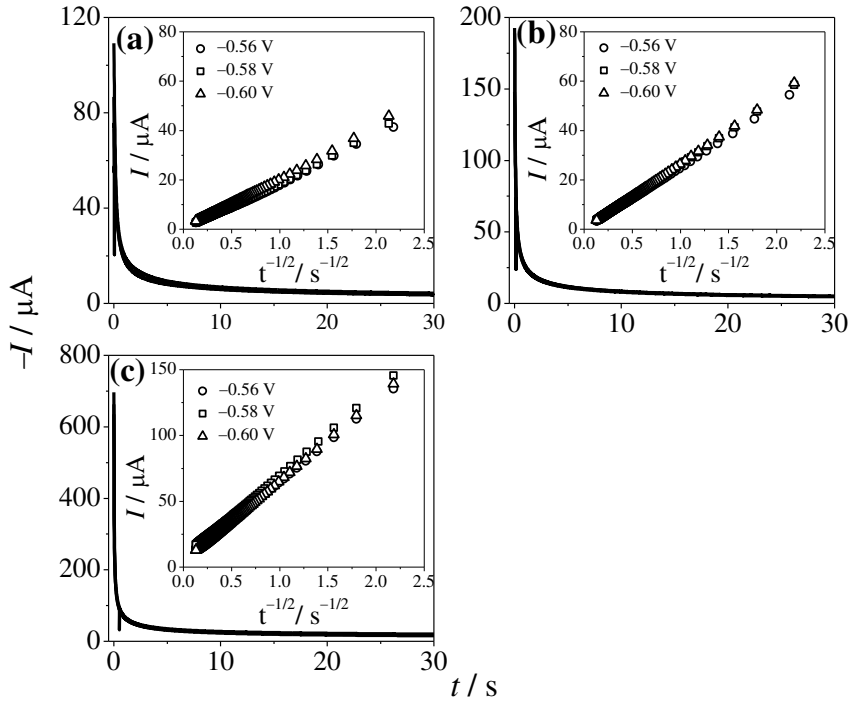

Source: Author.

4.2.4. Dynamic viscosity

An important thermoproperty of solutions is the viscosity. The dynamic viscosity of 1ChCl:2EG and 1ChCl:2U containing 0.05 mol L^{-1} $TeCl_4$ was measured. In general, the viscosity of liquids can be describe by the Arrhenius equation (GHAREH BAGH *et al.*, 2015; KAREEM *et al.*, 2010; MJALLI *et al.*, 2014).

Figure 13a-b gives the experimental results for both eutectic mixtures. The straight line observed in this figure revealed that the viscosity decrease exponentially with the temperature raises following an Arrhenius behaviour, which is in good agreement with findings of Mjalli and co-workers (GHAREH BAGH *et al.*, 2015; KAREEM *et al.*, 2010; MJALLI *et al.*, 2014). The reduction of the viscosity with increasing temperature suggests an improving the mass transport into electrolyte.

In addition, thermal effect on the dynamic viscosity can be evaluate considering the slope of straight line obtained by linear regression of data found in the Fig. 13a-b. The product between the slopes of straight line times the ideal gas constant has the physical significance of activation-like energy (GHAREH BAGH *et al.*, 2015). According to Mjalli *et al.*, (MJALLI *et al.*, 2014) higher viscosity activation energy indicates a higher energy barrier to be overcome by mass transport. Thus, the like-activation energy of viscosity was 27.1 and 49.5 kJ mol^{-1} for 1ChCl:2EG and 1ChCl:2U, respectively, suggesting that the drive force to move a molecule in 1ChCl:2U is higher than in 1ChCl:2EG. This is reflected upon the slightly difference of diffusion coefficient of Te^{4+} species in both electrolytes, see Table 3.

The relationship between the diffusion coefficient (D) and viscosity is given by the Stokes-Einstein equation:

$$D = \frac{k_B T}{6\pi a \eta} \qquad 4.6$$

where k_B is the Boltzmann constant, T is the absolute temperature, a is the solvodynamic radius and η is the dynamic viscosity. A good linearity is present by the Stokes-Einstein plots for both 1ChCl:2EG and 1ChCl:2U containing Te^{4+} ions, as shown in Fig. 14a-b. For these plots, the diffusion coefficient values calculated by through Cottrell's method were used.

Figure 13 - Arrhenius' plot for dynamic viscosity of (a) 1ChCl:2EG and (b) 1ChCl:2U containing 0.05 mol L^{-1}.

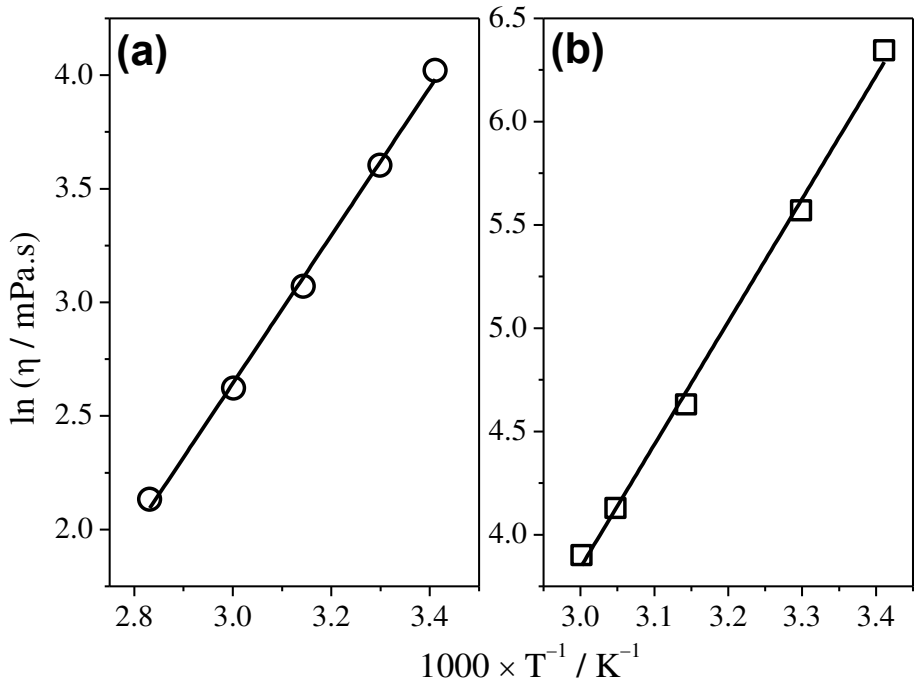

Source: Author.

Thus, it is clearly noted that there is a good concordance between the experimental results of the Te^{4+} species in both DESs plating solution with the Stokes-Einstein model. However, the applicability of this equation in non-aqueous electrolytes is still under debate.

According to Huang *et al*., (HUANG, X.-J. *et al.*, 2009) the Stokes-Einstein relationship depends on the species sizes. They reported that in studies of cobaltocenium hexafluorophosphate, ferrocene and N,N,N′,N′-tetramethyl-p-phenylenediamine in ILs, the Stokes-Einstein relation holds well for these molecules. In contrast, in case of small molecular such as, H_2, SO_2 and H_2S no apparent linear correlation is observed. In addition, the Stokes-Einstein relation is based on a large sphere moving in an incompressible continuum (BOCKRIS; REDDY; GAMBOA-ALDECO, 1998), which is a rough approximation to describe ILs and DESs.

The effects of bath temperature on density and viscosity of electrolytes, additionally, Stokes-Einstein product ($\eta D / T$) and solvodynamic radius can be seen in Table 4. The increase of the bath temperature promotes a decrease in the density of electrolytes. In

case of 1ChCl:2EG the property changes from 1.1273 g cm^{-3} at 20 °C to 1.0825 g cm^{-3} at 100 °C, while for 1ChCl:2U a variation from 1.1929 at 20 °C to 1.1712 at 60 °C was observed, which was followed by reduction in dynamic viscosity of solution, for 1ChCl:2EG the changes from 0.058 to 0.0064 Pa·s, whereas in 1ChCl:2EG changes 0.5695 to 0.0494 Pa·s was observed, respectively, over the same range of temperatures.

Therefore, with the increasing in bath temperature a volume expansion of the electrolytes is expected, thereby reducing the density and also hence the diffusion of Te^{4+} species. For 1ChCl:2EG, as the bath temperature increase the Stokes-Einstein products reduced, increasing the solvodynamic radius, therefore, suggesting a change in complexation of Te^{4+} ions. In fact, it hydrodynamic radius changed from 0.499 nm at 30 °C to 0.684 nm at 80 °C. Similar behaviour was observed in 1ChCl:2U, where the solvodynamic radius increased from 0.188 nm to 0.253 nm at temperature of 30 and 45°C, respectively. On the other hand, when the bath temperature increased to 60 °C, the hydrodynamic radius was calculated to be around 0.099 nm (Table 4), which is quite close to effective ionic radius of Te^{4+} in crystalline phase (0.052–0.097 nm) (SHANNON, 1976), indicating that Te^{4+} ions could be exist in 1ChCl:2U without complexing agents, additionally, this reduction in solvodynamic radius of Te^{4+} may be related with formation of the white precipitate observed at temperature higher than 60 °C.

Figure 14 - Stokes-Einstein plots of (a) 1ChCl:2EG and (b) 1ChCl:2U both contains 0.05 mol L^{-1} $TeCl_4$.

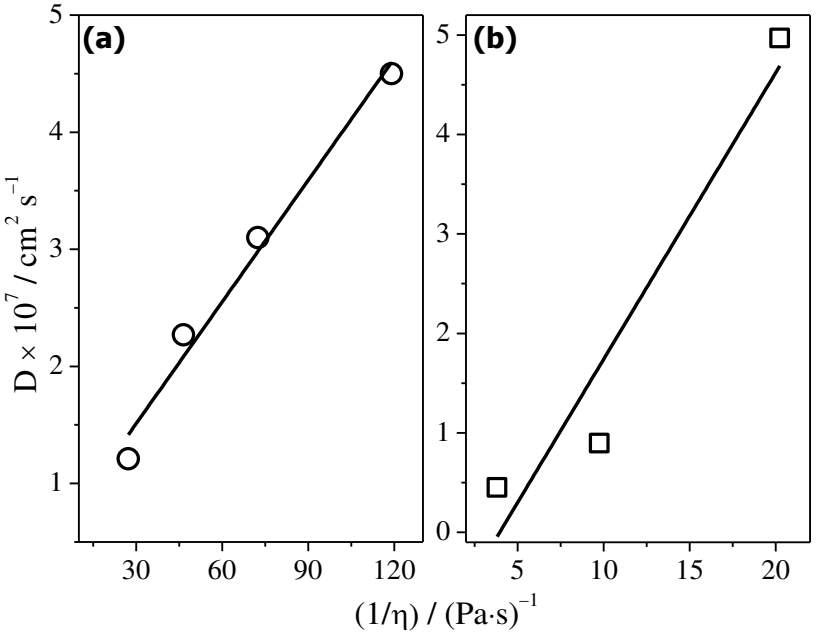

Table 4 - Effect of temperature on diffusion coefficients of Te^{4+} species, density and viscosity of 1ChCl:2EG and 1ChCl:2U.

Temperature / K	ρ / g cm^{-3}	$D \times 10^7$ / cm^2 s^{-1}	η / Pa·s	(η D / T) × 10^{10} / g cm s^{-2} K^{-1}	a / nm
1ChCl:2EG containing 0.05 mol L^{-1} $TeCl_4$					
293	1.1273	–	0.0558	–	–
303	1.1216	1.21	0.0367	1.46	0.499
318	1.1132	2.27	0.0215	1.53	0.477
333	1.1048	3.10	0.0138	1.28	0.572
353	1.0938	4.50	0.0084	1.07	0.684
373	1.0825	–	0.0064	–	–
1ChCl:2U containing 0.05 mol L^{-1} $TeCl_4$					
293	1.1929	–	0.5695	–	–
303	1.1874	0.450	0.2625	3.90	0.188
318	1.1793	0.896	0.1025	2.89	0.253
333	1.1712	4.970	0.0494	7.37	0.099

*obs.: 0.1 Pa·s = 1 g cm^{-1} s^{-1}
Source: Author.

Furthermore, the diffusion coefficients of Te^{4+} showed in Table 3 for both eutectic mixtures were well-fitted with an Arrhenius-like law, as shown in Figure 15a-b. From the slope of the straight line, obtained from plot of natural logarithm of the diffusion coefficients (ln *D*) *versus* the inverse of the absolute temperature (1/T), leads to estimate the apparent activation energy for the diffusion of Te^{4+} species in both DESs. Although, the values of diffusion coefficients predicted by S-H model and Cottrell´s equation were a little different (Table 3) the slope of the straight lines of ln *D* calculated *vs* 1000/*T* were quite closed, as can be seen in Figure 15a-b. For Te^{4+} species in 1ChCl:2EG, the calculated values of the apparent activation energy were 22.20 and 22.55 kJ mol^{-1} for S-H model and Cottrell´s models, respectively. On the other hand, for Te^{4+} species in 1ChCl:2U, the obtained values were 59.20 and 57.80 kJ mol^{-1}, respectively, which are in well agreement with the activation-like energy of viscosity previously discussed.

Figure 4.13 - Arrhenius' plots showing for the Te^{4+} species diffusion coefficient in (a) 1ChCl:2EG and (b) 1ChCl:2U solutions.

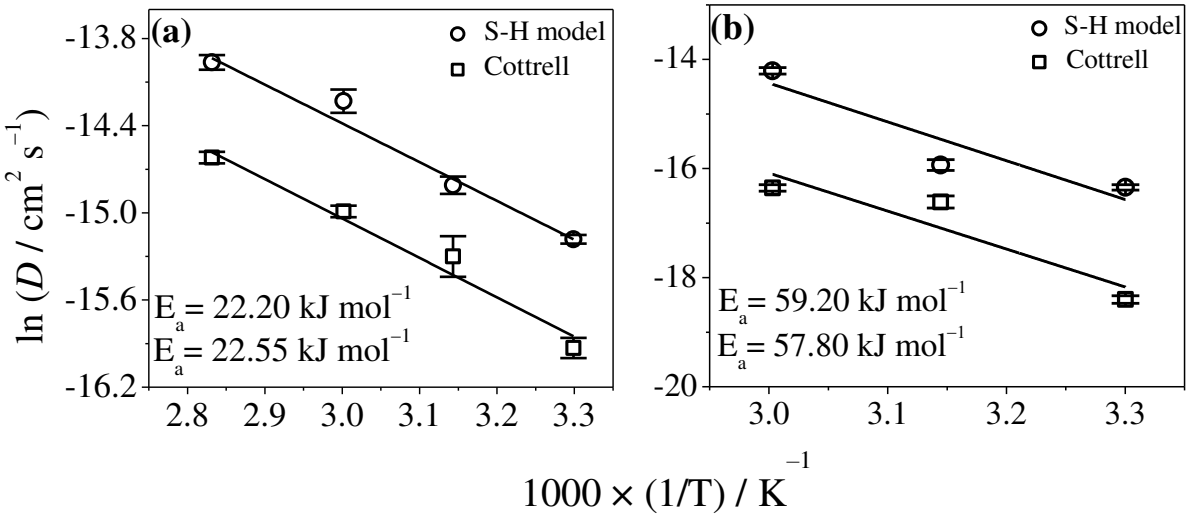

Source: Author.

4.2.5. SEM examination

Te films were electrodeposited on Au/FTO surface under potentiostatic control corresponding to the potential of the *c*1 peak displayed in the cyclic voltammograms, which were recorded at each working temperature (Fig. 4a-b). In order to lead the comparisons between all the investigated conditions the electrodeposition experiments were carried out a constant charge density of 0.5 C cm^{-2}. The electrodeposits produced were adherent to electrode surface with a dark appearance and metallic shine.

Figure 16a-b shows the surface morphology of Te films as-deposited on Au-coated FTO electrode from 1ChCl:2EG at 30 and 100 °C, while surface morphology of the Te films electrodeposited from 1ChCl:2U plating solution at 30 and 60 °C are shown in Figure 16c-d. The SEM examination revealed that the all obtained Te films have similar morphology, characterised by hexagonal rods-like, which are better evidenced in the SEM images obtained for the Te electrodeposited from 1ChCl:2U eutectic mixture.

Furthermore, an analysis of the histogram plots, displayed in Fig. 17, show that the Te rods diameters decrease with the rising of the bath temperature. For Te nanorods electrodeposited in 1ChCl:2EG the changes from 134 ±40 to 94 ±21.5 nm over the range temperature investigated. In contrast, the variation was from 88.5 ±20 to 80 ±19 nm for nanorods deposited in 1ChCl:2U.

In addition, these histograms also reveal that all the diameter values are in nanometric scale, characterising the formation of a 1-D Te nanostructured film. These results are in close agreement with previous findings for template-free electrodeposition of Te nanowires in a piperidinium-based ionic liquid (SZYMCZAK *et al.*, 2012; THIEBAUD *et al.*, 2016; THIEBAUD; LEGEAI; STEIN, 2016). The formation of template-free 1-D nanostructure electrodeposited metals and alloys have been already observed in ILs (HSIEH, Y. T. *et al.*, 2014; YANG, J.-M.; GOU; SUN, I-Wen, 2010) and DES (ALCANFOR *et al.*, 2017) plating solutions. The formation of these anisotropic nanostructures maybe associated with the presence of adsorption of chemical species on the electrode surface, which may acts as growth preferential agents (AL-SALMAN *et al.*, 2015).

Figure 16 - SEM micrographs of Te nanorods arrays on Au-coated FTO substrate grew under potentiostatic control from 1ChCl:2EG at (a) 30 °C (E_{peak}= –0.22 V), (b) 100 °C (E_{peak}= –0.07 V) and 1ChCl:2U at (c) 30 °C (E_{peak}= –0.48 V) and (d) 60 °C (E_{peak}= –0.43 V).

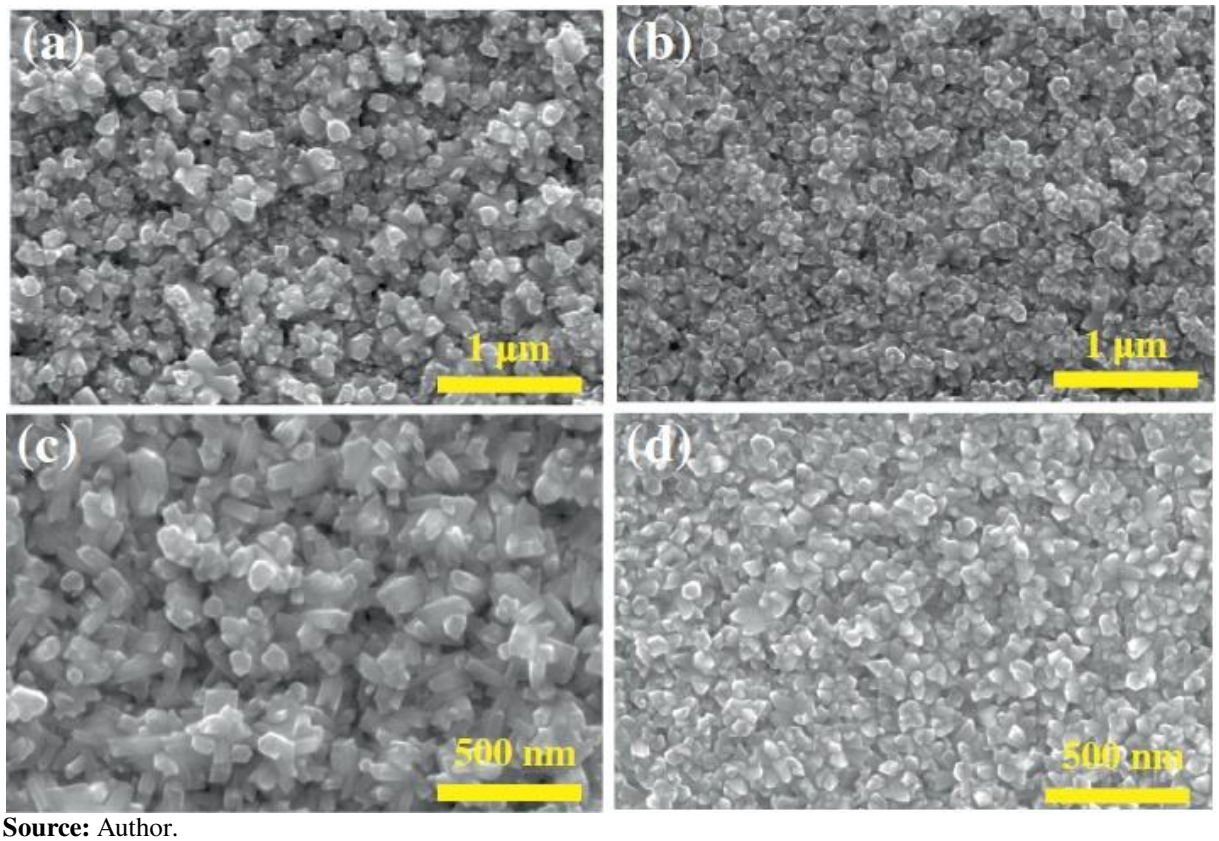

Source: Author.

Szymczak *et al.*, (SZYMCZAK *et al.*, 2012) reported that bromide ions may favour adsorption of Te adatoms on particular growth sites to template-free electrodeposition Te nanowires in piperidinium-based IL. In addition, Thiebaud and co-workers (THIEBAUD *et al.*, 2016) revealed that the dimensions and the morphology of Te nanowires were affected by bromine content in electrochemical bath, additionally, the researchers observed that halide ions do not play the role of capping agents. Moreover, Hsieh *et al.*, (HSIEH, Y. T. *et al.*, 2014) studied template-free Co wires in 1-ethyl-3-methylimidazolium chloride IL and proposed that after reduction of Co^{2+} chloride complex ions to Co nuclei on the substrate surface, the concentration of the Co ions around the adjacent growing Co nuclei is rapidly reduced inhibiting further nucleation there. Thereby, the one-dimensional nanostructure grows along the vertical direction faster than the lateral direction. On the other hand, Vieira *et al.*, (VIEIRA, L; SCHENNACH; GOLLAS, B., 2016; VIEIRA, Luciana; WHITEHEAD; GOLLAS, B. R., 2015) investigated glassy carbon electrode/1ChCl:2EG interface using *in-*

situ spectroelectrochemistry and observed that as the electrode is negatively polarized the Ch^+ cations become more strongly adsorbed on electrode surface forming a compact layer. In general, the anisotropic structure of Te crystal leads a 1-D growth under appropriate conditions (HE *et al.*, 2017), therefore, it is presumably that at sufficient negative potential, the Ch^+ ions adsorbed on electrode surface as well as other molecules such as, EG and U can be act as capping agents, which allow the formation of 1-D nanostructures.

Figure 17 - Histogram of diameter distribution of the Te nanorods arrays on Au-coated FTO substrate obtained from DESs (a) 1ChCl:2EG and (b) 1ChCl:2U at several temperatures.

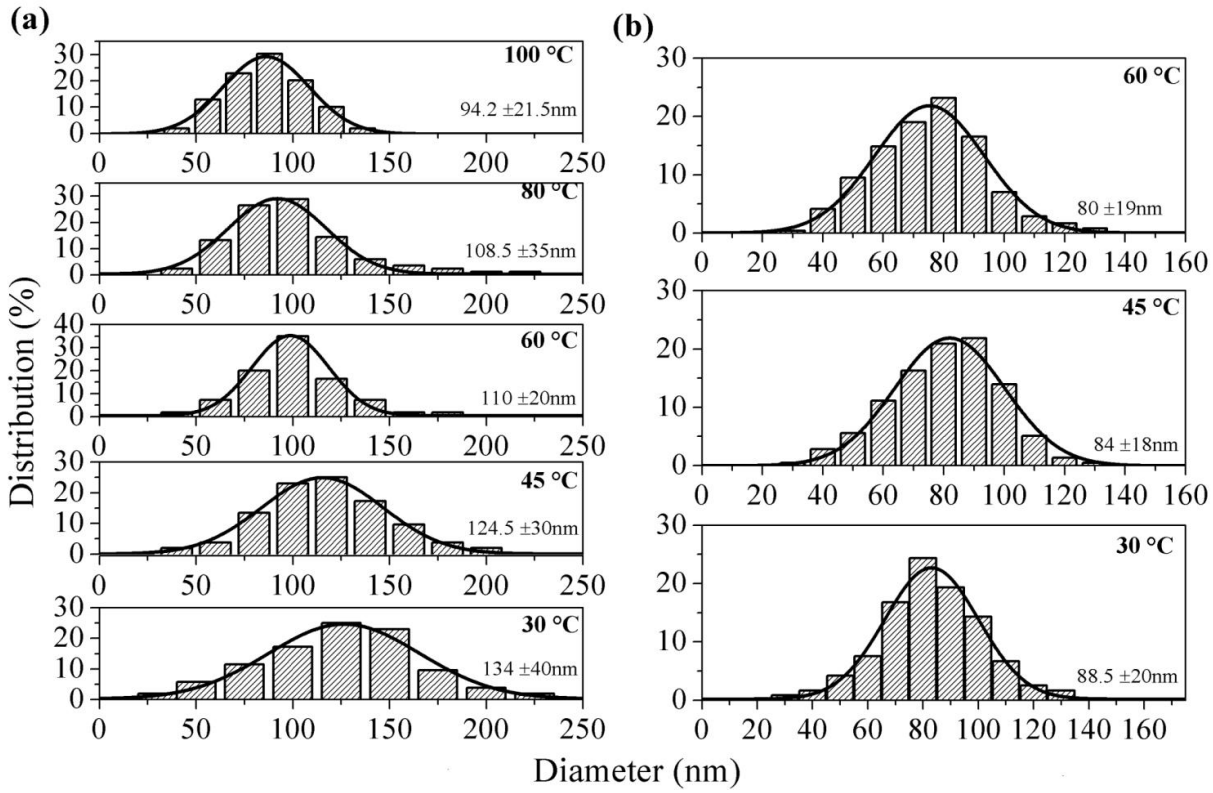

Source: Author.

4.2.6. XRD analyses

XRD analyses were carried out to assess the crystallinity of Te film electrodeposited on Au/FTO substrate. The obtained diffraction patterns are shown in Figure 17. The XRD patterns exhibited characteristics diffraction peaks corresponding to hexagonal crystal structure of Te (space group $P3_121$ [152]), which can be index with ICSD #40008 card file. Additionally, peaks attributed to the Au (ICSD #64701) and SnO_2 from FTO (ICSD #39177) are also displayed in these diffractograms confirming the thin nature of Te film.

Moreover, one can be seen that there are changes in the relative intensity of the diffraction peaks of Te as the temperature increases, which is suggesting that Te nanorods grew under preferential orientation.

Figure 18 - XRD pattern of the Te nanorods arrays on Au-coated FTO substrate obtained from (a) 1ChCl:2EG and (b) 1ChCl:2U at several different temperatures. The (*) is corresponding to FTO peaks and (‡) is indicating the Au peaks position.

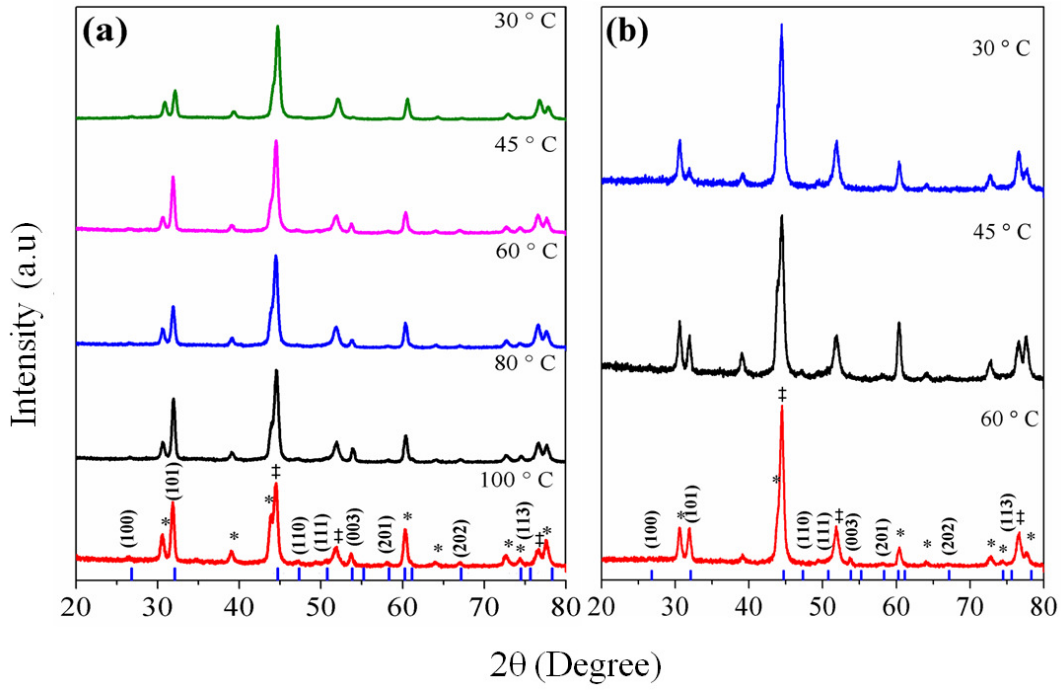

Source: Author.

4.2.7. TEM examination

The SEM images and XRD results suggests that the Te single-crystalline growth with the preferred orientation. Therefore, transmission electron microscopy analyses were conducted and the micrographs of the Te nanorods are shown in the Figure 19. In this image the morphology of nanorods are showed in (a), (b), (c), (d) and (e), while the fast Fourier transform (FFT) analysis of lattice fringes are identified in (I) and (II). On the other hand, inverse FFT are presented in (I') and (II'), finally *d*-space is presented for Te nanorods electrodeposited from either DES 1ChCl:2EG at 30, 60, 100 or 1ChCl:2U at 30 and 60 °C, respectively.

The morphology of the nanorods was further confirmed and the outer diameter for nanorods observed in the Fig. 19a-e was found to be approximately 29, 9, 5, 65 and 13 nm, respectively. In addition, the lattice fringes observed in the Te nanostructures were investigate in order to confirm the preferential growth evidenced by XRD results.

So, a fast Fourier transform (FFT) analysis of two selected regions indicated by I and II circles (Fig. 19a-e) was firstly obtained. The FFT patterns are presented besides each TEM image and, except by sample 5, it exhibits the crystalline nature of the Te nanostructures. Moreover, it is worth to mention that the same pattern is observed for I and II regions, which evidences a similar arrangement of the atoms. Subsequently, an inverse FFT (I' and II') was carried out to reconstruct the images. Finally, the fit profile of the lattice fringes was obtained and the interplanar distance values (d_{hkl}) for I and II regions were calculated to be in the range of 0.365–0.471 (FU, G. *et al.*, 2016). However, this wide range was caused by the sample 5 due to amorphous nature of this Te nanorod with great number of structural defects. Most of the values for other samples are near 0.386 (Fit profiles from Fig. 19a-d, which can be attributed to the (100) planes (ICSD #40008 card file). These results proof the preferential growth of the crystalline Te nanorods through [001] direction.

Figure 19 - TEM of Te nanorods obtained in 1ChCl:2EG (a), (b), and (c) and in 1ChCl:2U.

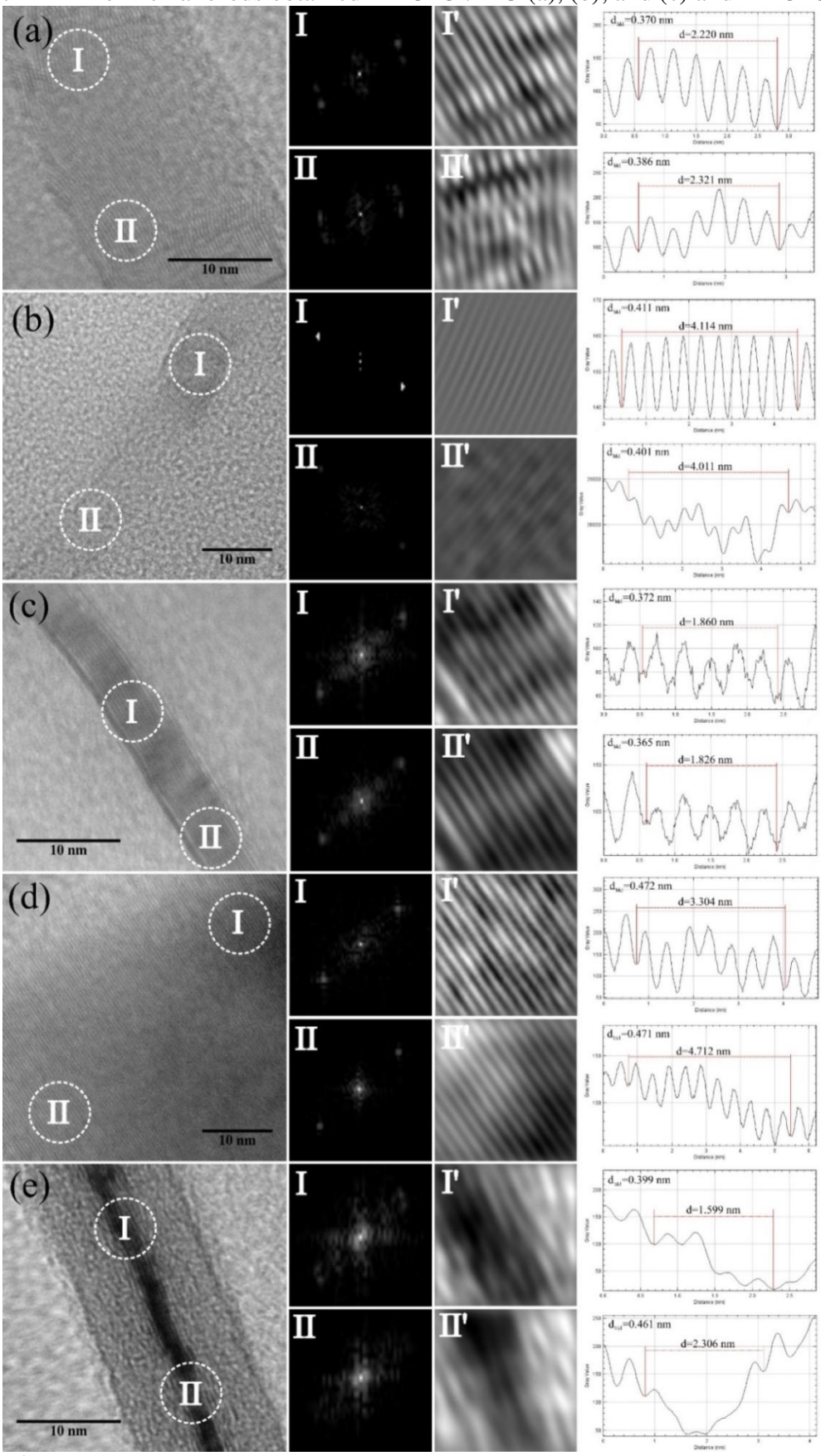

Source: Author.

4.3. CONCLUSION

Tellurium was successful electrodeposited on gold surface from plating solutions prepared by the choline chloride-urea and choline chloride-ethylene glycol mixtures. Te electrocrystallisation on Au surface followed a three-dimensional progressive mechanism with diffusion-controlled growth limited regardless the nature of DESs investigated. The diffusion coefficients of Te^{4+} species calculated by S-H and Cottrell´s models were slightly from each other; however, they were well fitted by a like-Arrhenius equation in both eutectic mixtures. The apparent activation energies were 22.20 and 22.55 kJ mol^{-1} for Scharifker-Hills and Cottrell´s models, respectively, in 1ChCl:2EG. On the other hand, in 1ChCl:2U these values were 59.20 and 57.80 kJ mol^{-1}. The surface morphology of the Te electrodeposited films were characterize by the presence of hexagonal Te rods, which were uniformly distributed on the Au-coated FTO surface. Finally, the Te rods were characterized as been 1D nanostructured that grew perpendicular of (100) planes following preferential growth direction of [001].

5. ELECTRODEPOSITION OF CdTe ON Au FROM CHLORIDE-ETHYLENE GLYCOL BASED EUTECTIC MIXTURE

In this chapter, the applicability of deep eutectic solvent (DES) for the CdTe thin films electrodeposition on Au is examined with a focus on the use of choline chloride-ethylene glycol based DES, as main chemical agent, over the following operational condition: molar ration of 1:2, at a temperature range of 30, 60, and 80 °C, under atmosphere conditions without any further heat treatment. The electrochemical results have shown that the formation of CdTe occurs at same region of reduction of Cd^{2+} to Cd. Furthermore, the temperature-dependence dynamic viscosity of the plating solution was found to fit an Arrhenius-type equation to given an activation-like energy of 25.4 $kJ \cdot mol^{-1}$. The density of the electrolytes decreases linearly as a function of the absolute temperature. XRD revealed that polycrystalline of CdTe films grew preferentially oriented along the (111) and (311) planes with the crystallite in nanosize regime. In addition, SEM examination demonstrated that surface morphology of CdTe coatings exhibits a uniform distribution of spherical-like clusters with large agglomerated crystallite increasing as the temperature goes up. Finally, it was found a blue shift in the optical band gap of the CdTe films which could be associated to the quantum-confinement effects.

5.1. INTRODUCTION

Over the last three decades, tremendous attention has been given to the II-VI semiconductors compounds because of their wide applications in the high technology industry. These materials are crucial for the manufacture of laser sources, radiation detectors, electro-luminescent displays, light-emitting diodes, photovoltaic, optoelectronic, magnetic, and thermoelectric devices (BRITT; FEREKIDES, 1993; ISHII; AMAGASU; NOMURA, 2019; MINGO, 2004; MIROV, S. *et al.*, 2013; MOHAMED *et al.*, 2014; SCHAFFNER *et al.*, 2011). Among these materials, cadmium telluride (CdTe) is one of the most promising semiconductors because of its direct band-gap energy around 1.45 – 1.50 eV, at room temperature; long with its high absorption coefficient around 10^4 – 10^5 cm^{-1} (ADACHI; KIMURA; SUZUKI, 1993; FENG, L. *et al.*, 2005; HERNANDEZ-CALDERON, 2002; KOKATE *et al.*, 2007; MYERS; EDWARDS; SCHETZINA, 1981; RAKHSHANI, 1997; TOMA *et al.*, 2014), which leads to its utilisation in the photovoltaic field (BRITT; FEREKIDES, 1993; SCHAFFNER *et al.*, 2011; TOMA *et al.*, 2014). In 2016, the American

Company First Solar confirmed the achievement of 22.1% conversion efficiency for thin films of CdTe solar cells in laboratory scale (GREEN *et al.*, 2018), establishing a competitive growth in comparison to the traditional multicrystalline Si technology that reported in a record efficiency of 22.3% (GREEN *et al.*, 2018).

In the literature, there are several methods used for the preparation of CdTe thin films, including the well-established the vacuum-based techniques (BRITT; FEREKIDES, 1993; MOHAMED *et al.*, 2014; SCHAFFNER *et al.*, 2011), even requiring high temperature and expensive apparatus. Equally important, also exist the solution-based approaches (CAO, X. *et al.*, 2008; HODES, 2007; YONG *et al.*, 2010), less expensive than the previous one. Nevertheless, long deposition time and/or annealing treatment are demanded. In this scenario, a low-cost and quick deposition technique is essential. In this scenario, a low-cost and quick deposition technique is essential. Electrodeposition is a well-established technique for production of metallic coatings at large scale and more recently, turns up as powerful tool to the growth of semiconductor materials, for instance II-VI compounds (LINCOT, 2005). Traditionally, the electrochemical deposition of CdTe thin films is performed in aqueous medium either in acid solutions (SINGH, R. R.; PAINULY; PANDEY, R. K., 2009; ŞIŞMAN; DEMIR, 2011) or in alkaline electrolytes (DERGACHEVA; STATSYUK; FOGEL', 2004; SHAN *et al.*, 2016). However, aqueous plating solutions have a narrow electrochemical window that promotes the formation of hydrogen gas on the electrode surface during the electrochemical deposition which affects the quality of produced films.

Independently, Lade (LADE; UPLANE; LOKHANDE, 2000) and Pandey (PANDEY, R. K.; MAFFI; BICELLI, 1994) demonstrated the possibility of obtaining CdTe thin films using ethylene glycol-based baths but the deposition current density higher than 1 mA cm^{-2} and/or elevated bath temperature (160 °C) to films' preparation become the process unfeasible. On the other hand, Room-Temperature Ionic Liquids (RTILs/ILs) emerge as extraordinary electrochemical medium to electrodeposition of metals and alloys because of their wide range of potential, high thermal stability, low vapour pressure, high electrical conductivity, and high solubility of metal salts (SIMKA; PUSZCZYK; NAWRAT, 2009b). Recently, several researches have been conducted the electrodeposition of CdTe from RTILs electrolytes (CHAUHAN, K R *et al.*, 2014; CHAUHAN, Khushbu R; PATEL, D. B.; MUKHOPADHYAY, Indrajit, 2015; HSIU; SUN, I.-W., 2004; WALDIYA; BHAGAT; MUKHOPADHYAY, Indrajit, 2018, 2019). Hsiu and Sun (HSIU; SUN, I.-W., 2004) first

investigated the electrochemical behaviour of Cd^{2+} and Te^{4+} species in 1-ethyl-3-methylimidazolium chloride/tetrafluoroborat IL and reported the deposition of stoichiometric CdTe coatings at 140 °C. Chauhan *et al.*, (CHAUHAN, K R *et al.*, 2014) carried out the potentiostatically electrodeposition of CdTe thin films in a 1-butyl-3-methyl-imidazolium chloride IL bath at 80 °C, their results showed that after 1 h of deposition films with typical thickness around 2.7 µm and optical band gap of 1.44 eV were obtained. Waldiya and co-workers (WALDIYA; BHAGAT; MUKHOPADHYAY, Indrajit, 2019) claimed that CdTe thin films with band gap energy of 1.49 eV were galvanostatically deposited from 1-butyl-3-methylimidazolium chloride at 80 °C employing a current density of 745 µA cm^{-2}. However, the properties of RTILs are sensible to the moisture reducing their shelf time at atmosphere conditions (ENDRES, Frank; ABEDIN, Sherif Zein EL, 2006). Moreover, it been found that RTILs could be hazardous to aquatic environments and very poor biodegradable (ROMERO *et al.*, 2008), limiting their industrial applications.

In this context, Deep Eutectic Solvents (DESs) have been presented as an interesting alternative to the RTILs (SMITH; ABBOTT, A. P.; RYDER, 2014; WAGLE; ZHAO, H.; BAKER, 2014; ZHANG, Q. *et al.*, 2012), especially because of their unique physicochemical properties, such as: biodegradability and nontoxicity, higher sensibility to water content, and low-price (SMITH; ABBOTT, A. P.; RYDER, 2014; WAGLE; ZHAO, H.; BAKER, 2014; ZHANG, Q. *et al.*, 2012), which is very attractive to market outlook. In general, the DESs can be obtained by simply mixing together a halite salt with the hydrogen bonding donor molecule under appropriate proportions. One of the most studied DES is formed by mixing choline chloride (ChCl) and ethylene glycol (EG), in molar ratio of 1:2.

Several researchers have used DESs in the electrodeposition process for II-VI semiconductors compounds. Dale *et al.*, (DALE, Phillip J. *et al.*, 2007) successfully electrodeposited at 100 °C the CdS, CdSe, and ZnS semiconductors on fluorine-doped tin oxide (FTO) substrate using eutectic mixture of ChCl and urea (U), at a molar ratio of 1:2, that is 1ChCl:2U. The films obtained showed optical band gap in agreements with the values found in the literature. Catrangiu and co-workers (CATRANGIU, A. S. *et al.*, 2016) reveled that ZnTe with 1:1 stoichiometry can be deposited on Pt electrode from 1ChCl:2EG at 60 °C. Golgovici and Visan (GOLGOVICI, Florentina; VISAN, Teodor, 2012) reported the electrodeposition of CdTe films on Pt from 1ChCl:2U in the temperature range from 25 up to 60 °C . The authors suggested that the deposition of CdTe from the eutectic mixture occurs on

a Te-covered Pt substrate. Golgovici and Buda (GOLGOVICI, F.; BUDA, M., 2013; GOLGOVICI, Florentina; BUDA, Mihai, 2013) demonstrated that nanostructured CdTe films can be electrodeposited on Cu substrate at 60 °C using a eutectic electrolyte based on ChCl and malonic acid in molar ratio of 1:1, namely 1ChCl:1Malonic.

Therefore, in this chapter the electrochemical behaviour of Te^{4+} and Cd^{2+} ions in 1ChCl:2EG were studied. In addition, CdTe thin films were electrochemically deposited on Au substrate at temperature of 30, 60, and 80 °C. A detailed morphological, structural, and optical characterisation of electrodeposited CdTe thin films was performed and discussed.

5.2. RESULTS AND DISCUSSION

5.2.1. Cyclic voltammetry studies

In order to obtain the electrochemical processes occurring on electrode surface cyclic voltammetry experiments were conducted. Cyclic voltammograms acquired for as-prepared 1ChCl:2EG blank solution (dashed line) and containing 0.2 mmol L^{-1} $TeCl_4$ (solid line) on Au electrode at 30 °C are displayed in Figure 20. In the blank solution, a cathodic process can be seen in the forward scan at 0.5 V due to the reduction reaction of tri-chloride to chloride ions. Haerens *et al.*, (HAERENS *et al.*, 2009) demonstrated the formation of the Cl_3^- ions during the electrolysis of 1ChCl:2EG. The presence of these spices was also reported by Sun *et al.*, (SUN, H. *et al.*, 2005) in RTIL after long periods of electrolysis. Further, the additional cathodic shoulders also observed in voltammetric profile recorded for the blank solution, are perhaps associated to Au-catalyzed organic reactions. Furthermore, it can be observed a sweep change direction over negative potential (below –1.0 V), increasing the current. This behaviour could be related to the reduction of hydroxyl groups of EG, choline ions (Ch^+), and/or residual water molecules (VIEIRA, Luciana; WHITEHEAD; GOLLAS, B. R., 2014).

Figure 20 - Cyclic voltammograms obtained for Au electrode in 1ChCl:2EG blank electrolyte (dashed line) and containing 0.2 mmol L^{-1} $TeCl_4$ (solid line).

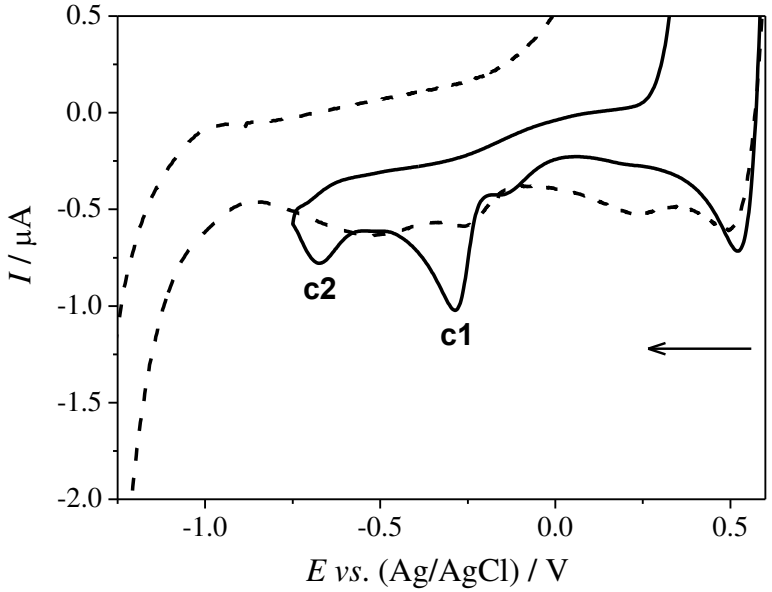

Source: Author.

On the other hand, in the electrolyte containing $TeCl_4$, the voltammogram obtained in forward sweep exhibits two well-established cathodic peaks. Similar voltammetric profiles have been reported in previous investigation for Te electrodeposition in DES based on ChCl with either EG or U, both at 1:2 molar ratio (SANTOS, L.P.M. *et al.*, 2019) and also announced in ILs electrolytes (HSIU; SUN, I.-W., 2004; SZYMCZAK *et al.*, 2012; THIEBAUD *et al.*, 2016; THIEBAUD; LEGEAI; STEIN, 2016; TSAI *et al.*, 2014). Therefore, the first electrochemical process *c*1 could be related to the follow reaction $Te^{4+} + 4e^{-} = Te$ and the second one *c*2 corresponding to the stripping reaction $Te + 2e^{-} = Te^{2-}$.

Moreover, cyclic voltammogram result for 1ChCl:2EG containing 20 mmol L^{-1} $CdCl_2$ (solid line) on Au substrate at 30 °C is displayed in Figure 21. In the forward direction, a Faradaic process can be observed at –1.0 V. This electrochemical process occurs at more negative potential than those of the Te redox couples (as showed in Fig. 20), and it can be attributed to $Cd^{2+} + 2e^{-} = Cd$ (DALE, Phillip J. *et al.*, 2007; HSIU; SUN, I.-W., 2004). It is worth mention that no current loop between the forward and reverse scans was observed, suggesting that Cd electrodeposition on Au in 1ChCl:2EG does not follow a three-dimensional nucleation and growth, as revealed in the inset of Figure 21. In addition, typical cyclic voltammograms were obtained for both ionic species at 60 and 80 °C.

Figure 21 - Cyclic voltammograms obtained for Au electrode in 1ChCl:2EG (a) blank electrolyte (dashed line) and containing 20 mmol L^{-1} $CdCl_2$ (solid line).

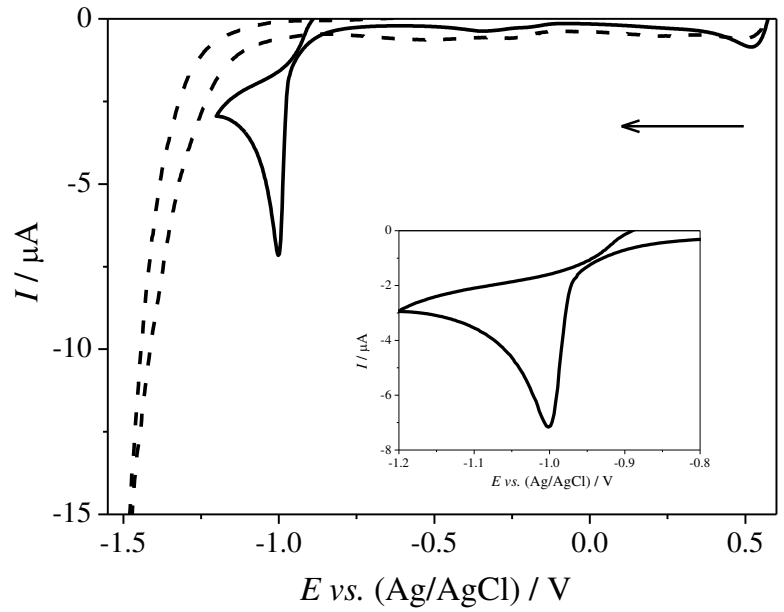

Source: Author

Figure 22 shows the cyclic voltammograms recorded at atmosphere pressure for 1ChCl:2EG containing 20 mmol L^{-1} $CdCl_2$ + 0.2 mmol L^{-1} $TeCl_4$ at temperature of 30 °C. In this voltammogram profile, the waves namely *c*1 and *c*2 correspond to the reductions of Te^{4+}/Te and Te/Te^{2-}, respectively, as described above (see Fig. 20). Furthermore, the cathodic wave *c*3 around –1.02 V, could be attributed to the reduction of Cd^{2+}/Cd and/or simultaneous formation of CdTe, following the electrochemical reaction Te + Cd^{2+} + $2e^-$ = CdTe. According to Golgovice and co-workers (GOLGOVICI, Florentina; BUDA, Mihai, 2013; GOLGOVICI, Florentina; VISAN, Teodor, 2012) that investigated the electrodeposition of CdTe films in 1ChCl:2U and 1ChCl:1Malonic, the growth of CdTe layer occurs on Te-covered substrate. In addition, similar deposition mechanism was observed for the electrochemical preparation of CdTe thin films in imidazolium based IL (CHAUHAN, K R *et al.*, 2014). Therefore, the electrodeposition indicated in the wave *c*3 (Fig. 22) might be the growth of CdTe thin film on previous deposited Te layer. Notably, the increase in the bath temperature to 60 and 80 °C promotes a slightly shifted in *c*3 peak position to values of –0.97 and –0.95 V, respectively, (not show data). These potentials were used for the electrodeposition of CdTe films on Au/FTO substrates from 1ChCl:2EG plating solution containing dissolved salts of Cd and Te at different temperatures. It is worth mentioning that

after electrodeposition, the electrode showed films grown with the dark appearance and well-adherent on substrate surface.

Figure 22 - Cyclic voltammograms obtained for Au electrode in 1ChCl:2EG containing a mixture of 20 mmol L^{-1} $CdCl_2$ + 0.2 mmol L^{-1} $TeCl_4$ at 30 °C.

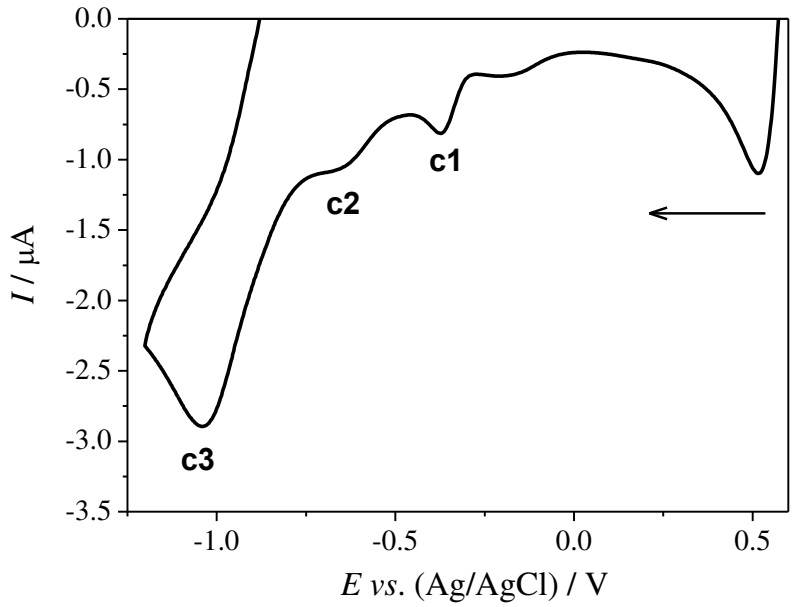

Source: Author

Table 5 - Effect of temperature on density, dynamic viscosity, diffusion coefficient of metals species of 1ChCl:2EG electrolytes.

1ChCl:2EG containing 20 mmol L^{-1} $CdCl_2$				
Temperature (K)	ρ (g cm^{-3})	η (mPa·s)[a]	$D_{Cd^{2+}} \times 10^7$ (cm^2 s)	$\left(\eta D_{Cd^{2+}}/T\right) \times 10^{10}$ (g cm s^{-2} K^{-1})
303	1.1157 ±0.0001	34.801 ±0.820	0.82	0.96
318	1.1073 ±0.0002	20.663 ±0.580	-	-
333	1.0990 ±0.0001	13.280 ±0.320	1.36	0.55
353	1.0879 ±0.0001	8.297 ±0.060	3.34	0.79
1ChCl:2EG containing 0.2 mmol L^{-1} $TeCl_4$				
Temperature (K)	ρ (g cm^{-3})	η (mPa·s)[a]	$D_{Te^{4+}} \times 10^7$ (cm^2 s)	$\left(\eta D_{Te^{4+}}/T\right) \times 10^{10}$ (g cm s^{-2} K^{-1})
303	1.1131 ±0.0003	34.028 ±1.870	1.21 (SANTOS, L.P.M. *et al.*, 2019)*	1.33
318	1.1047 ±0.0003	20.197 ±0.670	-	-
333	1.0964 ±0.0004	13.047 ±0.430	3.10 (SANTOS, L.P.M. *et al.*, 2019)	1.19
353	1.0852 ±0.0003	8.040 ±0.250	4.50 (SANTOS, L.P.M. *et al.*, 2019)	1.00
1ChCl:2EG containing 20 mmol L^{-1} $CdCl_2$ + 0.2 mmol L^{-1} $TeCl_4$				
Temperature (K)	ρ (g cm^{-3})	η (mPa·s)[a]	$D_{Cd^{2+}/Te^{4+}} \times 10^7$ (cm^2 s)	$\left(\eta D_{Cd^{2+}/Te^{4+}}/T\right) \times 10^{10}$ (g cm s^{-2} K^{-1})
303	1.1155 ±0.0002	31.479 ±0.230	1.20	1.25
318	1.1071 ±0.0001	18.795 ±0.160	-	-
333	1.0986 ±0.0002	12.214 ±0.150	3.02	1.12
353	1.0873 ±0.0002	7.551 ±0.066	4.47	0.96

[a]obs.: 1 Pa·s = 10 g cm^{-1} s^{-1}.

*These data reported in ref. (SANTOS, L.P.M. *et al*., 2019) are discussed in Chapter 4 of this thesis.

5.2.2. Viscosity and density of the electrolytes

Viscosity and density are two important thermophysical properties of a solution which affects other properties and have an important role in defining the nature of substances. Therefore, before the examination of the surface morphology of the electrodeposited CdTe films, the effect of temperature in density (ρ) and dynamic viscosity (η) of the 1ChCl:2EG mixture containing either 20 mmol L^{-1} $CdCl_2$ or 0.2 mmol L^{-1} $TeCl_4$ or yet 20 mmol L^{-1} $CdCl_2$ + 0.2 mmol L^{-1} $TeCl_4$ were investigated. The results are listed in Table 5. Therefore, when electrochemical bath temperature increases, there are a decreasing in both density and dynamic viscosity, as expected for regular liquids. For instance, a decrease in the viscosity of 1ChCl:2EG solutions around 76% can be observed in the temperature range studied. In case of the plating solution the viscosity changes from 31.479 to 7.551 mPa·s. In addition, Figure 23a shows that the dynamic viscosity data are well-fitted by an Arrhenius-like equation:

$$ln\ \eta = ln\ \eta_0 + E_\eta/RT \tag{5.1}$$

where η_0 is a constant, R is the ideal gas constant (8.314 $J \cdot K^{-1} \cdot mol^{-1}$), and T is the absolute temperature (ABBOTT, A. P.; CAPPER; *et al.*, 2004; ABBOTT, A. P.; CAPPER; GRAY, 2006; BAGH *et al.*, 2015; BOCKRIS; REDDY; GAMBOA-ALDECO, 1998; MJALLI *et al.*, 2014). The term E_η is associated to the activation-like energy of viscous flow, which indicate the energy required to overcome the mass transport (MJALLI *et al.*, 2014). This fit supports that the electrolytes' viscosity decays exponentially with the bath temperature. From these results, it could be stated that E_η parameter is constant (~25.4 $kJ \cdot mol^{-1}$, for the plating solution) for the temperature range studied.

Furthermore, regarding density, the influence of temperature is quite narrow, with a maximum variation of 2.5 %, for instance; for the plating solution the density changes from 1.1155 to 1.0873 $g \cdot cm^{-3}$ at 30 and 80 °C, respectively. Moreover, it was found that the experimental density decreases linearly as a function of absolute temperature as shown in Fig. 23b, these data is well-correlated to a linear equation:

$$\rho = a + bT \tag{5.2}$$

where *a* and *b* are fitting constants. These parameters are summarised in Table 6, along with the correlation coefficient (R^2). As seen so far, the increases in bath temperature promote a thermal expansion in the volume of the plating solutions, which lead to a considerable increase in the species' mobility in the bulk of the 1ChCl:2EG that should be reflected in the diffusion coefficient of ions (*D*).

Figure 23 - (a) Arrhenius' plot of dynamic viscosity and (b) density as function of absolute temperature for 1ChCl:2EG containing either 20 mmol L–1 $CdCl_2$ (hollow circle), 0.2 mmol L^{-1} $TeCl_4$ (hollow triangle), and 20 mmol L^{-1} $CdCl_2$ + 0.2 mmol L^{-1} $TeCl_4$ (hollow)

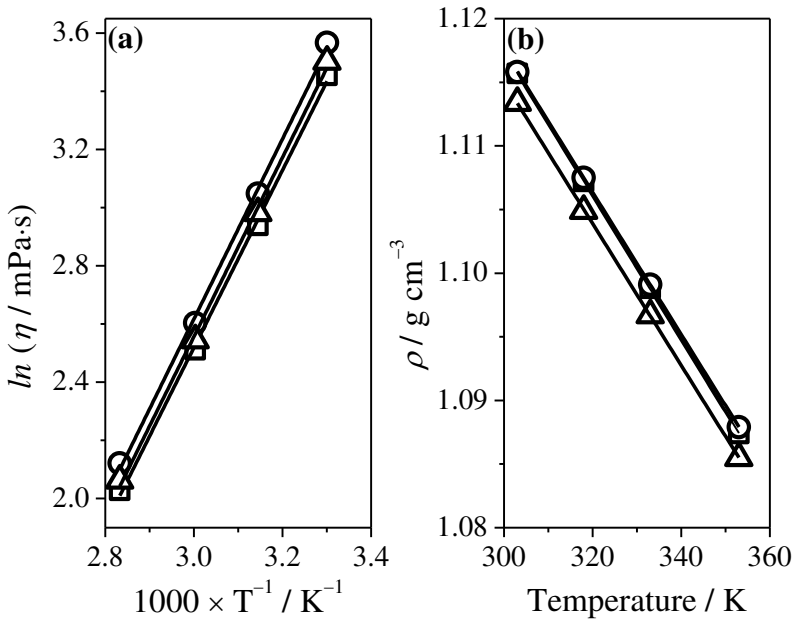

Source: Author

Table 6 - Values of fitting parameters for density of 1ChCl:2EG electrolytes.

1ChCl:2EG containing	Data fitting		
	a (g cm^{-3})	$b \times 10^4$ (g cm^{-3} K^{-1})	R^2
20 mmol L^{-1} $CdCl_2$	1.282	–5.580	0.999
0.2 mmol L^{-1} $TeCl_4$	1.285	–5.583	0.999
20 mmol L^{-1} $CdCl_2$ + 0.2 mmol L^{-1} $TeCl_4$	1.287	–5.656	0.999

Source: Author.

The diffusion coefficient of any electroactive metallic species in solution can be calculated electrochemically employing the well-known Cottrell´s equation (BARD; FAULKNER, 2001).

$$I(t) = nFac\left(D/\pi\right)^{1/2} t^{-1/2} \tag{5.3}$$

where *a* is the geometric area of the working electrode, *n* is the number of electrons transferred in the electrochemical reaction, *F* is the Faraday constant (96 485 $C \cdot mol^{-1}$), *c* is the bulk concentration of electroactive specie, and *t* is the time. Therefore, the Cottrellian profiles recorded for electrodeposition of Cd^{2+} ions on Au electrode in 1ChCl:2EG are shown in Figure 24 and the calculated values for diffusion coefficient this specie is showed in Table 1. As expected, the diffusion coefficient of Cd^{2+} ions increases by increasing temperature, suggesting an enhancement of the mass transport due to the reduction on electrolytes viscosity.

Figure 25 shows that the diffusion coefficient experimental data obeys an Arrhenius-like law, allowing estimate the activation-like energy, e.g., 23.76 $kJ \cdot mol^{-1}$ for diffusion Cd^{2+} species in 1ChCl:2EG, which is slightly higher than the values of 22.55 $kJ \cdot mol^{-1}$ found for the diffusion of Te^{4+} in 1ChCl:2EG that is reported in the Chapter 4 of this thesis. The diffusion coefficient of Te^{2+} species in 1ChCl:2EG is also included in Table1.

However, it is important to mention that diffusion coefficient is easily obtained for systems containing a single electroactive ion, by chronoamperometry method. Therefore, for electrolytes with more than one electroactive specie, such as 1ChCl:2EG containing 20 mmol L^{-1} $CdCl_2$ + 0.2 mmol L^{-1} $TeCl_4$, this electrochemical technique is not the more appropriate. According to Li and Gregory (YUAN-HUI; GREGORY, 1974) in such systems the diffusion coefficient can be estimated knowing the concentration and the diffusion coefficient of the individual species in the electrochemical bath and their concentration, according to equation (5.4):

$$D_{Cd^{2+}/Te^{4+}} = \frac{\left(z_{Cd^{2+}} c_{Cd^{2+}} + z_{Te^{4+}} c_{Te^{4+}}\right) D_{Cd^{2+}} D_{Te^{4+}}}{z_{Cd^{2+}} c_{Cd^{2+}} D_{Cd^{2+}} + z_{Te^{4+}} c_{Te^{4+}} D_{Te^{4+}}} \tag{5.4}$$

where $z_{Cd^{2+}}$, $z_{Te^{4+}}$, $c_{Cd^{2+}}$, and $c_{Te^{4+}}$ are the charge and concentration of each species in the solution, respectively. The results obtained from the equation (5.4) are displayed in Table 5. It is observed that $D_{Cd^{2+}/Te^{4+}}$ decreases with the increasing of the temperature, as noticed for diffusion coefficient of Cd^{2+} and Te^{4+} species. Moreover, Figure 26 shows that this diffusion coefficient also be adjusted by an Arrhenius-type approaches, revealing an activation-like energy of 23.66 kJ·mol^{-1}. This value is quite close to found previously for the diffusion of Cd^{2+} ions in 1ChCl:2EG. This result is expected since the molar ratio of Cd^{2+}/Te^{4+} is 100:1.

Figure 25 - Current-time transients for the reduction of Cd^{2+}/Cd on Au/FTO substrate obtained from DES 1ChCl:2EG containing 0.02 mol L^{-1} $CdCl_2$.

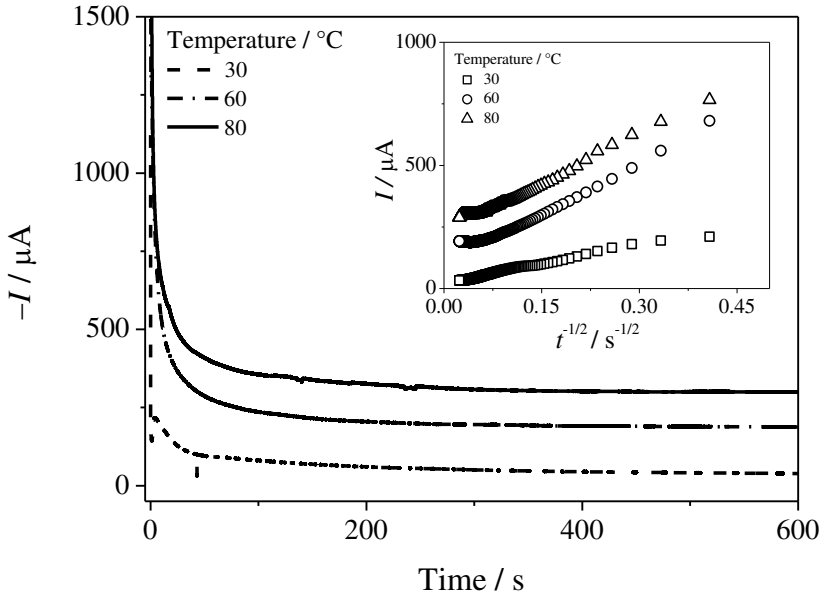

Source: Author.

Figure 26 - Arrhenius' plot for experimental of $D_{Cd^{2+}}$ (hollow circle) and $D_{Cd^{2+}/Te^{4+}}$ (hollow square) in 1ChCl:2EG.

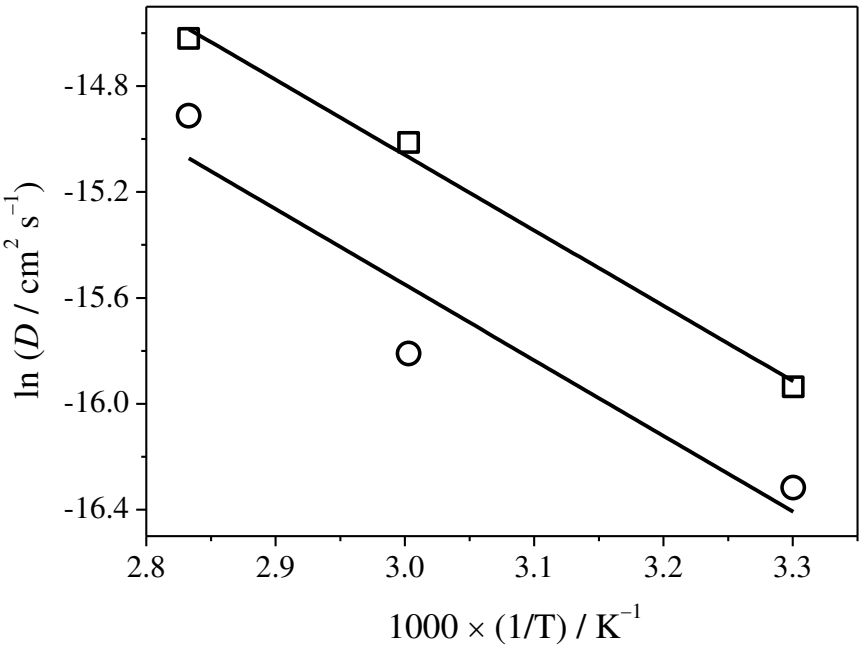

Source: Author

So far, it was pointed out that the increasing the bath temperature promotes the increases of the mobility of species in the bulk of the 1ChCl:2EG. The relationship between the dynamic viscosity of solvent and the diffusion coefficient of any metallic ion in solution is ascribed according to the Stokes-Einstein equation (BOCKRIS; REDDY; GAMBOA-ALDECO, 1998):

$$D = \frac{k_B T}{6\pi r \eta} \tag{5.5}$$

where k_B is the Boltzmann constant (1.38×10^{-23} $m^2 \cdot kg \cdot s^{-2} \cdot K^{-1}$), T is the absolute temperature, and r is the solvodynamic radius. The Stokes-Einstein plots for 1ChCl:2EG containing 20 mmol L^{-1} $CdCl_2$ and 20 mmol L^{-1} $CdCl_2$ + 0.2 mmol L^{-1} $TeCl_4$ are shown in Figure 27.

Figure 27 - Stokes-Einstein's plots for 1ChCl:2EG containing either 20 mmol L^{-1} $CdCl_2$ (hollow circle) or 20 mmol L^{-1} $CdCl_2$ + 0.2 mmol L^{-1} $TeCl_4$ (hollow square).

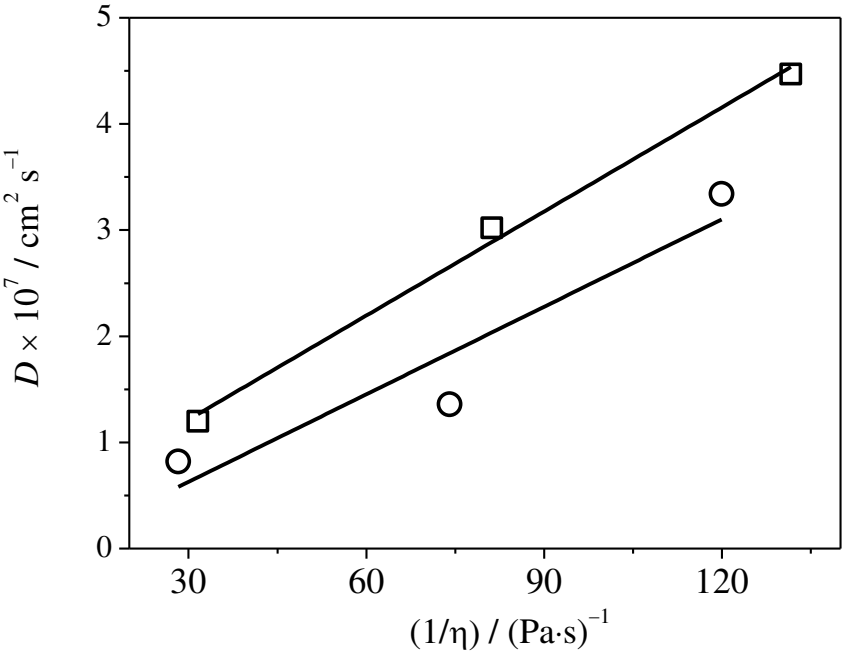

Source: Author

According to the Figure 27, there is a good linearity in both cases. Huang *et al.*, (HUANG, X.-J. *et al.*, 2009) demonstrated that the applicability of the Stokes-Einstein relation in RTILs is molecular-size dependent. These authors reported a linear correlation in Stokes-Einstein plots for large molecules, such as cobaltocenium hexafluoro-phosphate, ferrocene, and *N*,*N*,*N*′,*N*′-tetram-ethyl-p-phenylenediamine. Nevertheless, for single small molecules, such as SO_2 and H_2S, this correlation was not observed. They suggest that some chemical interactions can occur with the RTIL or the molecules size are too small for it application. The results obtained in previous results reported in the Chapter 4 and the currently investigation (see Fig. 26), suggest that Stokes-Einstein relation holds to metallic species in DES. In addition, the Stokes-Einstein product $(\eta D/T)$ was determined, as seen in Table 5. According to the equation (5.5), the solvodynamic radius is reciprocal to this product. In fact, the solvodynamic radius of Cd^{2+} species in solution changed from 0.767 to 0.926 nm at 30 and 80 °C, respectively. Similar behaviour is observed in the solvodynamic radius of Te^{4+} species, which increased from 0.552 to 0.730 nm at same range temperature.

5.2.3. SEM examination of CdTe films

The morphology of the CdTe films electrodeposited under potentiostatic control at temperatures of 30, 60, and 80 °C are shown in Figure 28a-c. SEM micrographs in the low magnification mode revealed that the surface of electrodes was completely covered by the deposit. Additionally, the images also suggest that the coatings are rough because of the uniform distribution of small spherical-like particles containing large agglomerated crystallite clusters grown on the substrate.

Moreover, the high magnification view (seen in the inset of Figure 28a-c) indicates that the formation of CdTe layers followed a predominant cluster growth mechanism, as reported by Chauhan *et al.* (CHAUHAN, K R *et al.*, 2014) for electrodeposition of CdTe on FTO in IL-based on butyl methyl imidazolium at 80 °C. Thereby, the first electrodeposited CdTe nanoparticles grew simultaneous in the lateral directions. This coalescence process established interconnections of them to form a CdTe layer. In the course of the electrodeposition, a new clusters layer was formed over this previous one, as revealed in the inset of Figure. 28a-c.

Figure 29a-c gives the histograms of the electrodeposited CdTe clusters. It can be seen that clusters size range changes with the bath temperature. Crystalline agglomerates size ranging from 115 up to 335 nm for deposition at 30 °C. Otherwise, it is observed higher size for 60 °C between 134 to 430 nm. Finally, the electrodeposition at 80 °C leads to the formation of clusters raging from 80-520 nm. The existence of big clusters during the electrochemical deposition at the higher temperature further support this growth mechanism (Fig. 28a-c).

Figure 28 - SEM micrographs of CdTe electrodeposited on Au-coated FTO substrate from 1Ch:2EG at (a) 30 °C (E_{peak} = –1.02 V), (b) 60 °C (E_{peak} = –0.97 V), (c) 80 °C (E_{peak} = –0.95 V), and (d) EDS spectrum for sample showed in (a). Inset: SEM micrographs of high magnification.

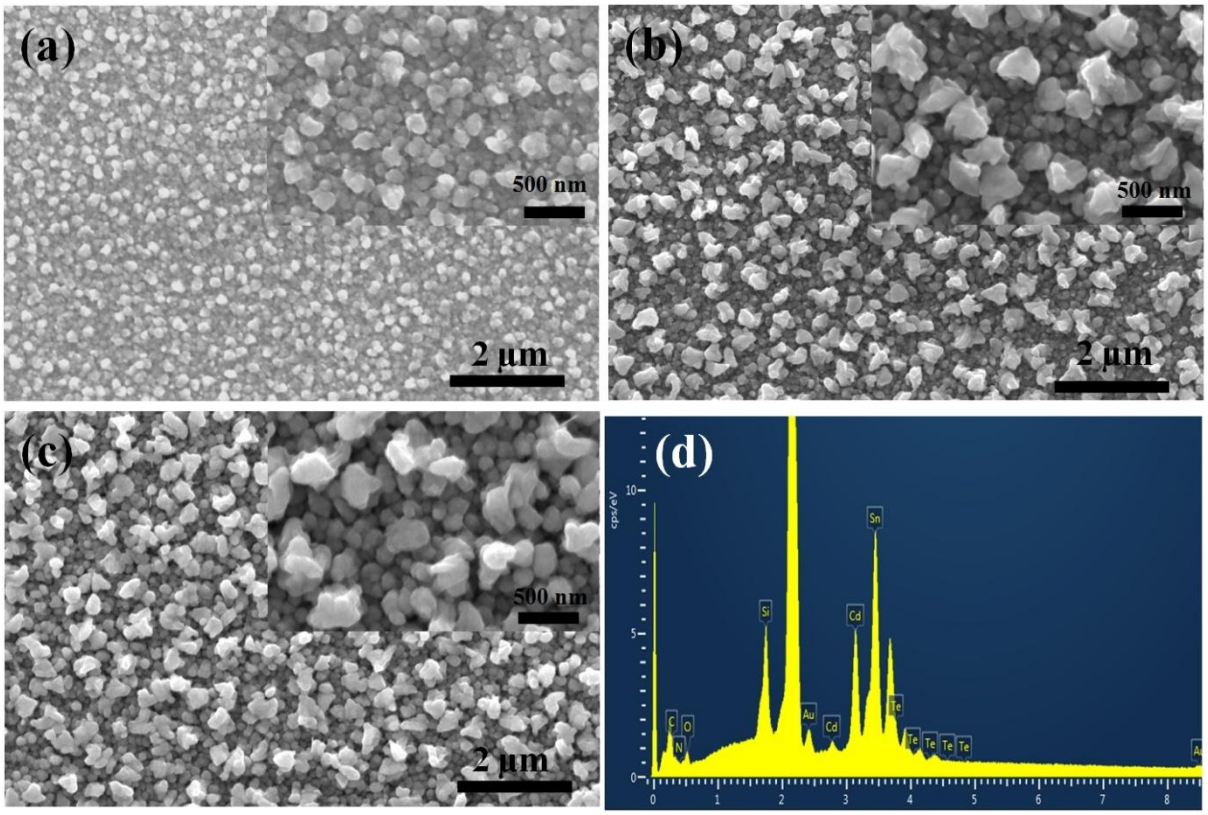

Source: Author.

The elemental chemical composition of CdTe films electrodeposited in 1ChCl:2EG was investigated by EDS. Figure 28d gives the EDS spectrum for CdTe sample electrodeposited at 30 °C and Table 7 shows the chemical composition of films. It can be seen that the increase of the bath temperature leads the formation of Te-rich films, in spite of the fact that in all conditions the composition of films is nearly stoichiometric. The Te-enrichement of CdTe films can be understood in terms of the diffusion coefficient. As reported in Table 5, the diffusion coefficient of Te^{4+} species is slightly higher than calculated to diffusion of Cd^{2+} ions. Moreover, less energy is required to move Te^{4+} species in 1ChCl:2EG, as previously demonstrated.

Figure 29 - Histogram of CdTe clusters size electrodeposited on Au-coated FTO substrate from 1Ch:2EG at (a) 30, (b) 60, and (c) 80 °C.

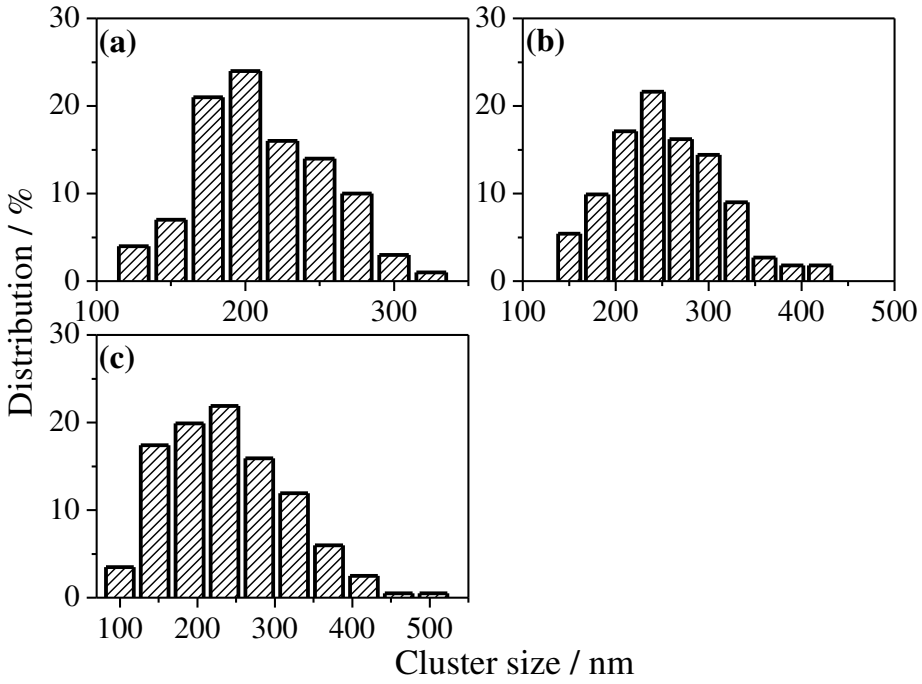

Source: Author.

Table 7 - Elemental chemical composition of CdTe films electrodeposited in 1ChCl:2EG.

Temperature (°C)	Deposition potential (V)	Cd weight %	Te weight %
30	–1.02	52.38	47.62
60	–0.97	42.86	57.14
80	–0.95	41.30	58.70

Source: Author

5.2.4. X-ray diffraction analysis CdTe films

XRD analyses were performed in order to reveal the crystal structure of CdTe samples, as well as, the growth orientation of films. The XRD recorded for as-electrodeposited CdTe films are shown in Figure 30. The patterns exhibit five pronounced diffraction peaks clearly observed at 2θ = 30.60, 35.05, 50.84, 60.43, and 63.91° which can be indexed to the (111), (200), (220), (311), and (222) crystallographic planes, respectively. These reflections planes can be attributed to the cubic crystal structure of CdTe (space group *Fm-3m*, #225), as confirmed by the ICSD collection code 620524. This result is in good

agreement with previous study (CHAUHAN, Khushbu R; PATEL, D. B.; MUKHOPADHYAY, Indrajit, 2015).

Figure 30 - XRD pattern CdTe thin film electrodeposited on Au-coated FTO substrate from 1Ch:2EG at (a) 30 °C (E_{peak} = –1.02 V), (b) 60 °C (E_{peak} = –0.97 V), and (c) 80 °C (E_{peak} = –0.95 V). The (*) is corresponding the SnO_2 phase from FTO.

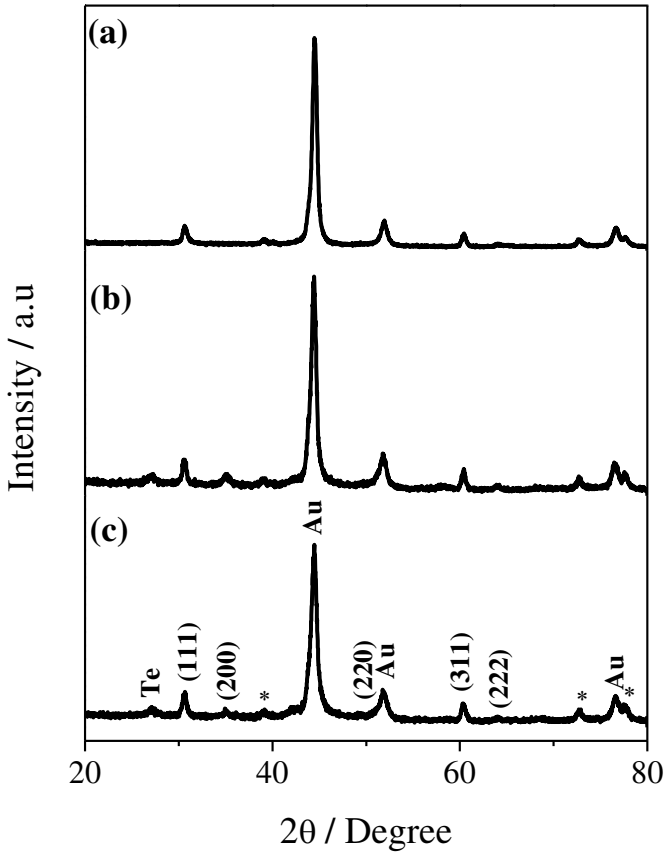

Source: Author.

Furthermore, diffraction peaks corresponding to the face centred cubic of Au (space group *Fm-3m*, #225) and the tetragonal crystal structure of SnO_2 (space group $P4_2/mnm$, #136) from the substrate can also be observed in the patterns presented in Figure 30. These phases can be fitted with the ICSD collection codes 64701 and 39177, respectively.

The XRD also revealed a single reflection peak located at 2θ = 27.06°, associated with (100) plane of hexagonal of elemental Te (space group $P3_121$, 152) in the CdTe electrodeposited films at 60 and 80 °C. This crystal structure was index with the ICSD

collection code 40008. The presence of Te in the films obtained at 60 and 80 °C corroborate with findings for chemical composition of films.

In order to obtain information about the preferential growth orientation of CdTe films, the texture coefficient (*TC*) was calculated by the following equation (HARRIS, 1952):

$$TC(hkl) = \frac{\frac{I_{(hkl)}}{I_{0(hkl)}}}{\frac{1}{N}\sum_{1}^{N}\frac{I_{(hkl)}}{I_{0(hkl)}}} \tag{5.6}$$

where $I_{(hkl)}$ and $I_{0(hkl)}$ are measurements of intensity of a specific diffraction peak and the standard integrated intensity from the ICSD card file for the same reflection plane, respectively, and N is the number of diffraction peaks considered in the calculation (HARRIS, 1952). The results of *TC* are shown in Fig. 31. This result suggests that the CdTe films growth preferential oriented along the (111) and (311) planes under the investigation conditions.

Figure 31 - Texture coefficient of the CdTe thin film electrodeposited on Au/FTO from 1ChCl:2EG.

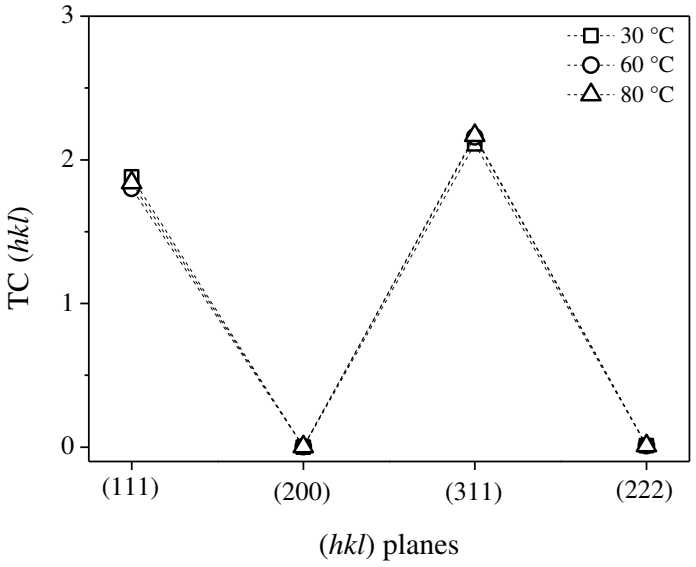

Source: Author.

Therefore, the full-width at half maximum (FWHM) of those crystallographic planes were taken into account to calculation of crystallite size. Thereby, the crystallite size of the material (D) is related to the FWHM of the diffraction peaks by the Scherrer´s equation (CULLITY, 1978):

$$D = \frac{0.9\lambda}{\beta \cos\theta} \tag{5.7}$$

where λ is the X-ray wavelength of the Co $K\alpha$ (0.1789 nm), β is the FWHM and θ is the Bragg´s angle (CULLITY, 1978). The results show that the CdTe crystallites sizes are in nanometer scale at all deposition conditions, as can be seen in Table 8.

Table 8 - Values of crystallite size, thickness, absorption coefficient at absorption edge, and the optical band gap energy of CdTe films eletrodeposited on Au/FTO in 1ChCl:2EG.

Temperature (°C)	$D_{(111)}$ (nm)	$D_{(311)}$ (nm)	d (μm)	$\alpha \times 10^{-4}$ (cm^{-1})	E_{gap} (eV)
30	19.65	42.40	1.34	4.98	1.79
60	22.69	41.40	1.87	4.45	1.68
80	20.89	38.36	2.77	4.23	1.57

Source: Author

5.2.5. Optical characterisation of CdTe films

In addition, the optical properties of CdTe films were investigated in the wavelength range from 300 to 1000 nm. The UV-vis spectra were acquired in diffuse reflectance mode, thus, the Kubelka-Munk transformation was used to obtained the absorbance data (PEREIRA *et al.*, 2018):

$$F(R) = \frac{(1-R)^2}{2R} \tag{5.8}$$

where R is the reflectance and $F(R)$ is the Kubelka-Munk function which is proportional to absorption coefficient (α). The absorbance spectra of as-grown CdTe thin films are displayed in Fig. 32a. As can be seen, the spectra show a broad absorption band covering in the range of near-ultraviolet and visible-light regions. The absorption band becomes narrower around 390

nm in the near-ultraviolet range of spectrum for the film electrodeposited at 80 °C. Moreover, the samples exhibit a gradually higher absorption intensities with bath temperature in the spectral range conducted.

Figure 32 - (a) UV-vis absorption spectra of CdTe thin films electrodeposited on Au-coated FTO substrate from 1Ch:2EG and (b) Tauc´s plot.

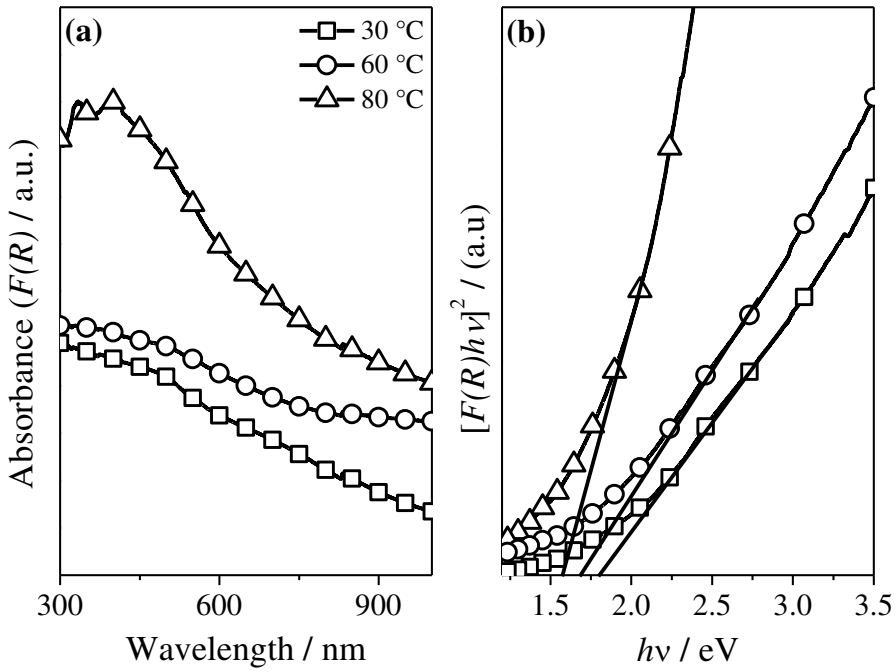

Source: Author.

According to Chander *et al.*, (CHANDER, Subhash *et al.*, 2017) the increase in absorbance can be related to changes in surface roughness which might be attributed to the effects on the propagation of the incident light owing to the light scattering. Furthermore, Patel *et al.*, (PATEL, S. L. *et al.*, 2019) reported that the improvement in the optical absorbance of heat-treated CdTe thin films is due to the increment in grain size. This way, perhaps the presence of large CdTe large nodular agglomerates grown at 60 and 80 °C (see Fig. 28b and c) and thickness change of films could be responsible for the increase in the absorption intensity of films.

Moreover, the absorption coefficient was determined from the absorbance spectra by the Lambert's law (RAZMJOO; BAHROLOLOOM; NAJAFISAYAR, 2017; ŞIŞMAN; DEMIR, 2011):

$$\alpha = 2.3026\left(\frac{F(R)}{d}\right) \tag{5.9}$$

where d is the CdTe films nominal thickness obtained from the current-time deposition curves. The Faraday's law was used to estimate the film thickness, considering a current efficiency of 100% (ŞIŞMAN; DEMIR, 2011; WALDIYA; BHAGAT; MUKHOPADHYAY, Indrajit, 2019):

$$d = \frac{Mit}{nF\rho a} \tag{5.10}$$

where M_{CdTe} = (M_{Cd}·x_{Cd}+ M_{Te}·x_{Te}) is the weight average molecular weight of CdTe films calculated, M_j and x_j are the molecular weight and weight percent of each species in the films in accordance with Table 7, i is the current that flows in the system, t is the time, n is the number of electron involved, F is the Faraday's constant, ρ is the density of material also determined based on Table 7, and finally, a is the electrode geometric area. The values of films thicknesses are shown in Table 8 and support their films nature. Further, it can be observed that the thickness increases with temperature. This result is suggesting that there is a mass transport enhancement in the electrochemical bath because of the increase of temperature, as shown in Figs. 23 and 25, and Table 5. Moreover, the high values of the absorption coefficient obtained at absorption edge (in order of 10^5 cm^{-1}) are consistent with the semiconductor nature of CdTe (ADACHI; KIMURA; SUZUKI, 1993; KOKATE *et al.*, 2007; MYERS; EDWARDS; SCHETZINA, 1981; RAKHSHANI, 1997). Additionally, it is observed a slightly decrease in absorption coefficient with thickness, as reported in Table 5.4.

One of the most important properties of a semiconductor material is the optical band gap (E_{gap}). It is well-known that in semiconductor materials the absorption coefficient and the electronic energy of the optical band gap are related by equation below (JIANG *et al.*, 2016; PEREIRA *et al.*, 2018; RAZMJOO; BAHROLOLOOM; NAJAFISAYAR, 2017; ŞIŞMAN; DEMIR, 2011):

$$\alpha h\nu = c\left(h\nu - E_{gap}\right)^N \tag{5.11}$$

where *c* is an absorption constant, *hv* is the incident photon energy, and finally, *N* has a value depending on the type of transition (JIANG *et al.*, 2016; PEREIRA *et al.*, 2018), in the present case, is equal to 1/2, since CdTe is the direct band semiconductor compound (RAZMJOO; BAHROLOLOOM; NAJAFISAYAR, 2017; ŞIŞMAN; DEMIR, 2011).

Therefore, the optical band gap energy was calculated from the Tauc's plot, i.e., first extrapolation the linear of plotting of $[F(R)hv]^2$ *vs*. *hv* and then measuring its intercept with the energy axis, as shown in Fig. 32b. The obtained values for the band gap energy of electrodeposited CdTe films are shown in Table 8. As it can be seen, there is a decreasing of the gap energy with the temperature. This result could be associate to the increasing of the thickness of the film as the temperature increases, as reported in ref. (ŞIŞMAN; DEMIR, 2011).

On the other hand, it can also be found that in all investigated conditions that the films have shown a blue shift in the optical band gap. Therefore, considering the E_{gap} as fundamental absorption that corresponds to electron excitation from the valence band, formed by filled Te 5*p* orbitals to the conduction band, formed by empty Cd 5*s* orbitals ($1S_{3/2}$-$1S_e$ transitions) (MASTAI; HODES, 1997; WEI, S. H.; ZUNGER, 1988). Thereby, the extending of E_{gap}, in comparison to bulk CdTe band gap at room temperature (*ca.* 1.50 eV) (FENG, L. *et al.*, 2005; TOMA *et al.*, 2014), could be associated with the quantum-confinement effect because of the existence of nanocrystalline material (MASTAI; HODES, 1997). The variations found in this study was 0.29, 0.18, and 0.07 eV for CdTe samples electrodeposited at 30, 60, and 80 °C, respectively. The present results are in agreement with previous findings (SINGH, R. R.; PAINULY; PANDEY, R. K., 2009; ŞIŞMAN; DEMIR, 2011). Singh *et al.*, (SINGH, R. R.; PAINULY; PANDEY, R. K., 2009) observed that the energy band shift increased as a function of reduction in the range of particle size of electrodeposited nanocrystalline CdTe films. In addition, these authors proposed that the blue shift in absorption edge is size-dependent which was correlated with theoretical approaches, such as effective mass approximation and tight-binding model.

5.3. CONCLUSION

In summary, the eutectic mixture based on choline chloride and ethylene glycol, in a molar ratio of 1:2, was successfully used for the electrodeposition of CdTe films on Au substrate at 30, 60, and 80 °C under atmosphere conditions. The cyclic voltammogram performed on Au electrode from the plating solution containing Te^{4+} and Cd^{2+} species presented in forward sweep three cathodic waves that correspond; the first one was the reduction of Te^{4+} to elemental Te, via one-step with four electrons transfer, the second one was attributed to the stripping reaction of Te to Te^{2-}, and finally the last one was assigned to the reduction of Cd^{2+} to Cd and the simultaneous formation of CdTe. The temperature-dependence dynamic viscosity of the electrolytes was fitted by an Arrhenius-like equation. For the plating solution, the activation-like energy of viscous flow was 25.4 $kJ \cdot mol^{-1}$. While the density of the electrolytes decreases linearly as a function of the absolute temperature. Clearly, characterisation through XRD revealed that the CdTe films had the polycrystalline cubic crystal structure, preferentially oriented along the (111) and (311) planes, with the crystallite in nanoscale regime. In addition, SEM examination demonstrated that surface morphology of as-electrodeposited CdTe coatings exhibits a uniform distribution of spherical-like clusters with large agglomerated crystallite which increase as the temperature increased. Finally, it was found a blue shift in the optical band gap of the CdTe thin films which could be the quantum-confinement effects.

6. CONCLUSIONS

This study explored the electrochemistry of Te^{4+} and the production and characterisation of Te films nanostructured on Au substrate from deep eutectic solvents based on either choline chloride and ethylene glycol or choline chloride and urea. Moreover, electrodeposition and characterisation of CdTe films were conducted in choline chloride and ethylene glycol based eutectic mixture. The following conclusions can be drawn:

- Tellurium was successful electrodeposited on Au surface from chloride-urea and choline chloride-ethylene glycol based plating solutions;
- The electrochemical reduction of Te^{4+} into elemental Te occurred on Au surface via one-step with four electrons transfer;
- The formation of Te^{2-} species was observed by the reduction of Te previous deposited in both eutectic mixtures;
- Te electrocrystallisation on Au surface in both proceeded via a three dimensional progressive nucleation and growth mechanism;
- The diffusion coefficients of Te^{4+} species can be described by an Arrhenius-like equation in both eutectic mixtures. The apparent activation energies were 22.20 and 22.55 kJ mol^{-1} for Scharifker-Hills and Cottrell´s models, respectively, in 1ChCl:2EG. In case of 1ChCl:2U values were 59.20 and 57.80 kJ mol^{-1};
- Te electrodeposited films were characterised by the presence of hexagonal Te rods, which were uniformly distributed on the electrode surface;
- Te rods were characterised as been 1D nanostructured that grew perpendicular of (100) planes following preferential growth direction of [001];
- CdTe films on Au substrate were successfully used for the electrodeposition from the eutectic mixture based on choline chloride and ethylene glycol, in a molar ratio of 1:2;
- The formation of CdTe occurred simultaneous the reduction of Cd^{2+} to Cd;
- CdTe films presented a cubic crystal structure and grew preferentially oriented along the (111) and (311) planes in nanoscale regime;
- CdTe films exhibited a uniform distribution of spherical-like clusters with large agglomerated crystallite
- The optical band gap of the CdTe films showed a blue shift which could be the quantum-confinement effects.

7. SCIENTIFIC PRODUCTION

The results presented in this Thesis allow the production of two scientific publications:

Santos, L.P.M., Freire, R.M., Michea, S., Denardin, J.C., Araújo, D.B., Barros, E.B., Correia, A.N. and de Lima-Neto, P., *Journal of Molecular Liquids*, **288** (2019), 111038.
Santos, L.P.M., Feitosa, F.X., de Sant'Ana, H.B., Correia, A.N. and de Lima-Neto, P., *Journal of Molecular Liquids*, MOLLIQ_2019_5601, **under decision**.

In addition, over the period comprised from 2015 up to 2019 which cover period of doctoral formation some collaboration with group mates and other colleagues were conducted which generate the following publications:

Figueredo-Sobrinho, F.A., **Santos, L.P.M.**, Leite, D.S., Craveiro, D.C., Santos, S.H., Eguiluz, K.I., Salazar-Banda, G.R., Maciel, C.D., Coutinho-Neto, M.D., Homem-de-Mello, P. and de Lima-Neto, P., 2016. *Physical Chemistry Chemical Physics*. **18** (2016), 7242;
Masoumi, M., **Santos, L.P.M.**, Bastos, I.N., Tavares, S.S., da Silva, M.J. and de Abreu, H.F., *Materials & Design*, **91** (2016) 90;
Béreš, M., Wu, L., **Santos, L.P.M.**, Masoumi, M., da Rocha Filho, F.A.M., da Silva, C.C., de Abreu, H.F.G. and da Silva, M.G., *International Journal of Hydrogen Energy*, **42** (2017) 14786;
Urcezino, A.S., **Santos, L.P.M.**, Cassiano, P.N.S., Correia, A.N. and de Lima-Neto, P., *Journal of the Brazilian Chemical Society.* **28** (2017), 1193;
Alcanfor, A.A., **Santos, L.P.M.**, Dias, D.F., Correia, A.N. and de Lima-Neto, P., *Electrochimica Acta*, **235** (2017), 553;
Avelino, A.F., Araújo, W.S., Dias, D.F., **Santos, L.P.M.**, Correia, A.N. and de Lima-Neto, P., *Electrochimica Acta*, **286** (2018) 339
Bezerra-Neto, J.R., Sousa, N.G., **Santos, L.P.M.,** Correia, A.N. and de Lima-Neto, P., *Physical Chemistry Chemical Physics*. **20** (2018) 9321;
Pereira, M.S., Ribeiro, T.S., Lima, F.A.S., **Santos, L.P.M.**, Silva, C.B., Freire, P.T.C. and Vasconcelos, I.F., *Journal of Nanoparticle Research.* **20** (2018) 212;
Gomes da Silva, M.J., Cardoso, J.L., Carvalho, D.S., **Santos, L.P.M.**, Herculano, L.F.G., de Abreu, H.F.G. and Pardal, J.M., *International Journal of Hydrogen Energy*. **44** (2019) 18606;

REFERENCES

ABAD, B. *et al.* Thermoelectric properties of electrodeposited tellurium films and the sodium lignosulfonate effect. **Electrochimica Acta**, v. 169, p. 37–45, 2015.

ABAD, B. *et al.* Thermoelectric properties of electrodeposited tellurium films and the sodium lignosulfonate effect. **Electrochimica Acta**, v. 169, p. 37–45, 2015.

ABBOTT, A. P. *et al.* Novel solvent properties of choline chloride/urea mixtures. **Chemical Communications**, n. 1, p. 70–71, 2003.

ABBOTT, A. P.; BOOTHBY, D.; *et al.* Deep eutectic solvents formed between choline chloride and carboxylic acids : versatile alternatives to ionic liquids. **Journal of the American Chemical Society**, v. 126, n. 29, p. 9142–9147, 2004.

ABBOTT, A. P.; CAPPER, G.; *et al.* Ionic liquid analogues formed from hydrated metal salts. **Chemistry - A European Journal**, v. 10, n. 15, p. 3769–3774, 2004.

ABBOTT, A. P.; CAPPER, G.; GRAY, S. Design of improved deep eutectic solvents using hole theory. **Chemphyschem: a European journal of chemical physics and physical chemistry**, v. 7, n. 4, p. 803–806, 2006.

ABBOTT, A. P.; FRISCH, G.; RYDER, K. S. Electroplating using ionic liquids. **Annual Review of Materials Research**, v. 43, n. 1, p. 335–358, 2013.

ABEDIN, S Zein El *et al.* Ionic liquids as green electrolytes for the electrodeposition of nanomaterials. **Green Chemistry**, v. 9, n. 6, p. 549–553, 2007.

ADACHI, S.; KIMURA, T.; SUZUKI, N. Optical properties of CdTe: experiment and modeling. **Journal of Applied Physics**, v. 74, n. 5, p. 3435–3441, 1993.

AGAPESCU, C. *et al.* Electrodeposition of bismuth, tellurium, and bismuth telluride thin films from choline chloride–oxalic acid ionic liquid. **Journal of Applied Electrochemistry**, v. 43, n. 3, p. 309–321, 2013.

AL-SALMAN, R. *et al.* Template-free electrochemical synthesis of high aspect ratio Sn nanowires in ionic liquids: a general route to large-area metal and semimetal nanowire arrays? **Chemistry of Materials**, v. 27, n. 11, p. 3830–3837, 2015.

ALCANFOR, A. A. C. *et al.* Electrodeposition of indium on copper from deep eutectic solvents based on choline chloride and ethylene glycol. **Electrochimica Acta**, v. 235, p. 553–560, 2017.

APPLEBY, D. *et al.* Room-temperature ionic liquids as solvents for electronic absorption spectroscopy of halide complexes. **Nature**, v. 323, n. 6089, p. 614–616, 1986.

BAGH, F. S. G. *et al.* Zinc (II) chloride-based deep eutectic solvents for application as electrolytes: preparation and characterization. **Journal of Molecular Liquids**, v. 204, p. 76–83, 2015.

BARD, A. J.; FAULKNER, L. R.. **Electrochemical Methods:** Fundamentals and applications**,** 2nd ed.; New York: Wiley, 2001.

BOCKRIS, J. O.; REDDY, A. K. N.; GAMBOA-ALDECO, M. **Modern electrochemistry: an introduction to an interdisciplinary area**. New York: Plenum Press New York, 1998.

BRADLEY, A. J. L. The crystal structures of the rhombohedral forms of selenium and tellurium. **The London, Edinburgh, and Dublin Philosophical Magazine and Journal of Science**, v. 48, n. 285, p. 477–496, 1924.

BRASIL, M. M. E. **Balanço Energético Nacional 2019**. Rio de Janeiro, 2019.

BRITT, J.; FEREKIDES, C. Thin-film CdS/CdTe solar cell with 15.8% efficiency. **Applied physics letters**,. v. 62, p. 2851–2852, 1993.

BUSTAMANTE, M. L.; GAUSTAD, G. Challenges in assessment of clean energy supply-chains based on byproduct minerals: A case study of tellurium use in thin film photovoltaics. **Applied Energy**, v. 123, p. 397–414, 2014.

CAMACHO-ESPINOSA, E. *et al.* All-sputtered CdTe solar cell activated with a novel method. **Solar Energy**, v. 193, p. 31–36, 2019.

CAO, X. *et al.* From CdTe nanoparticles precoated on silicon substrate to long nanowires and nanoribbons: oriented attachment controlled growth. **Crystal Growth and Design**, v. 8, n. 2, p. 575–580, 2008.

CATRANGIU, A.-S. *et al.* Studies of antimony telluride and copper telluride films electrodeposition from choline chloride containing ionic liquids. **Thin Solid Films**, v. 611, p. 88–100, 2016.

CATRANGIU, A. S. *et al.* Electrochemical deposition of zinc telluride thin films from ethaline ionic liquid. **Chalcogenide Letters**, v. 13, n. 5, p. 187–199, 2016.

CHANDER, Subhash *et al.* Enhancement of optical and structural properties of vacuum evaporated CdTe thin films. **Materials Chemistry and Physics**, v. 185, p. 202–209, 2017.

CHAUHAN, K R *et al.* Preparation of CdTe thin film by electrodeposition in butyl methyl imidazolium bath at 80 °C. **Journal of Electroanalytical Chemistry**, v. 713, p. 70–76, 2014.

CHAUHAN, Khushbu R; PATEL, D. B.; MUKHOPADHYAY, Indrajit. In situ growth of CdTe nanostructures from a novel electrodeposition bath: tuning of electrical properties and reuse of ionic liquid. **New Journal of Chemistry**, v. 39, n. 3, p. 1979–1985, 2015.

CHEN, H. *et al.* The fabrication of Te nanowires with different orientations by vacuum vapor deposition. **Physics Letters A**, v. 362, n. 1, p. 61–65, 2007.

CHEN, Q.; SANDERSON, M.; ZHANG, C. Nonlinear terahertz response of HgTe/CdTe quantum wells. **Applied Physics Letters**, v. 107, n. 8, p. 81111-1–81111-4, 2015.

CHUM, H. L. *et al.* Electrochemical scrutiny of organometallic iron complexes and hexamethylbenzene in a room temperature molten salt. **Journal of the American Chemical Society**, v. 97, n. 11, p. 3264–3265, 1975.

CULLITY, B. . **Elements of Diffraction**. 2nd. ed. New York: Addison-Wesley Publishing Company, Inc., 1978.

DALE, Phillip J. *et al.* Synthesis of cadmium and zinc semiconductor compounds from an ionic liquid containing choline chloride and urea. **Thin Solid Films**, v. 515, n. 15 SPEC. ISS., p. 5751–5754, 2007.

DERGACHEVA, M. B.; STATSYUK, V. N.; FOGEL', L. A. Electrodeposition of CdTe films from ammonia-chloride buffer electrolyte. **Russian Journal of Applied Chemistry**, v. 77, n. 2, p. 226–230, 2004.

DEVILLANOVA, F. A.; DU MONT, W.-W. **Handbook of Chalcogen Chemistry: New Perspectives in Sulfur, Selenium and Tellurium**. 2nd ed. Cambridge, UK: The Royal Society of Chemistry, vol. 1, 2013.

DEVILLANOVA, F. A.; DU MONT, W.-W. **Handbook of Chalcogen Chemistry: New Perspectives in Sulfur, Selenium and Tellurium**. 2nd ed. Cambridge, UK: The Royal Society of Chemistry, vol. 2, 2013.

DORANTES-DÁVILA, J.; PASTOR, G. M. Magnetic anisotropy of one-dimensional nanostructures of transition tetals. **Physical Review Letters**, v. 81, n. 1, p. 208–211, 1998.

ENDRES, Frank.; ABBOTT, A.; MACFARLANE, D. **Electrodeposition from ionic liquids**. 2nd. ed. Weinheim: Wiley-VCH Verlag GmbH & Co. KGaA, 2017.

ENDRES, Frank; ABEDIN, Sherif Zein EL. Air and water stable ionic liquids in physical chemistry. **Physical Chemistry Chemical Physics**, v. 8, n. 18, p. 2101–2116, 2006.

ENERGY INFORMATION ADMINISTRATION, (EIA). **Annual energy outlook 2019: with projections to 2050**. United States Energy Information Administration, 2019.

EUROSTAT. ICT sector-value added, employment and R&D. **Europe Union**, 2018.

FENG, L. *et al.* The electrical, optical properties of CdTe polycrystalline thin films deposited under Ar-O_2 mixture atmosphere by close-spaced sublimation. **Thin Solid Films**, v. 491, p. 104–109, 2005.

FENG, Y.; GU, M. The electrochemical behavior of tellurium on GCE in sol and solutions. **Electrochimica Acta**, v. 90, p. 416–420, 2013

.

FRANTZ, C. *et al.* Electrodeposition of PbTe thin films: electrochemical behavior and effect of reverse pulse potential. **Electrochimica Acta**, v. 173, p. 490–496, 2015.

FU, G. *et al.* Novel hydrogel-derived bifunctional oxygen electrocatalyst for rechargeable air cathodes. **Nano Letters**, v. 16, n. 10, p. 6516–6522, 2016.

GALIŃSKI, M.; LEWANDOWSKI, A.; STEPNIAK, I. Ionic liquids as electrolytes. **Electrochimica Acta**, v. 51, n. 26, p. 5567–5580, 2006.

GAMBARDELLA, P. *et al.* One-dimensional metal chains on Pt vicinal surfaces. **Physical Review B**, v. 61, n. 3, p. 2254–2262, 2000.

GAMBARDELLA, P. *et al.* Ferromagnetism in one-dimensional monatomic metal chains. **Nature**, v. 416, n. 6878, p. 301–304, 2002.

GAUTAM, U. K.; RAO, C. N. R. Controlled synthesis of crystalline tellurium nanorods, nanowires, nanobelts and related structures by a self-seeding solution process. **Journal of Materials Chemistry**, v. 14, n. 16, p. 2530-2535, 2004.

GE, M. *et al.* A review of one-dimensional TiO_2 nanostructured materials for environmental and energy applications. **Journal of Materials Chemistry A**, v. 4, n. 18, p. 6772–6801, 2016.

GHAREH BAGH, F. S. *et al.* Zinc (II) chloride-based deep eutectic solvents for application as electrolytes: Preparation and characterization. **Journal of Molecular Liquids**, v. 204, p. 76–83, 2015.

GOLGOVICI, F.; BUDA, M. Some properties of nanostructured CdTe films from choline chloride - malonic acid ionic liquid. **Chalcogenide Letters**, v. 10, n. 9, p. 325–334, 2013.

GOLGOVICI, Florentina *et al.* Surface characterization of BiSbTe thermoelectric films electrodeposited from chlorides aqueous solutions and choline chloride based ionic liquids. **Materials Chemistry and Physics**, v. 126, n. 3, p. 700–706, 2011.

GOLGOVICI, Florentina; BUDA, Mihai. Electrodeposition of nanostructured CdTe films using choline chloride - Malonic acid ionic liquid. **Revista de Chimie**, v. 64, n. 8, p. 791–795, 2013.
GOLGOVICI, Florentina; VISAN, Teodor. Electrodeposition behaviour of cadmium telluride from choline chloride-urea ionic liquids. **Chalcogenide Letters**, v. 9, n. 4, p. 165–174, 2012.

GOODENOUGH, J. B. Rechargeable batteries: challenges old and new. **Journal of Solid State Electrochemistry**, v. 16, n. 6, p. 2019–2029, 2012.

GORIPARTI, S. *et al.* Review on recent progress of nanostructured anode materials for Li-ion batteries. **Journal of Power Sources**, v. 257, p. 421–443, 2014.

GRAEDEL, T. E. *et al.* On the materials basis of modern society. **Proceedings of the National Academy of Sciences of the United States of America**, v. 112, n. 20, p. 6295–6300, 2015.

GREEN, M. A. *et al.* Solar cell efficiency tables (version 53). **Progress in Photovoltaics: Research and Applications**, v. 27, p. 3–12, 2018.

HAERENS, K. *et al.* Electrochemical decomposition of choline chloride based ionic liquid analogues. **Green Chemistry**, v. 11, n. 9, p. 1357-1365, 2009.

HARRIS, G. B. X. Quantitative measurement of preferred orientation in rolled uranium bars. **Philosophical Magazine**, v. 43, n. 336, p. 113–123, 1952.

HE, Z. *et al.* Emerging tellurium nanostructures: controllable synthesis and their applications. **Chemical Society Reviews**, v. 46, n. 10, p. 2732–2753, 2017.

HERNANDEZ-CALDERON, I. Optical properties and electronic structure of wide band gap II-VI semiconductors. *In*: TAMARGO, Maria (org.) **II VI Semiconductor Materials and Their Applications**. New York: Taylor & Francis, 2002, p. 113–170.

HODES, G. Semiconductor and ceramic nanoparticle films deposited by chemical bath deposition. **Physical Chemistry Chemical Physics**, v. 9, n. 18, p. 2181–2196, 2007.

HOLDREN, J P. **Materials Genome Initiative for Global Competitiveness**. Washington, USA: National Science and Technology Council (NSTC), 2011.

HOLDREN, John P. **Materials Genome Initiative for Global Competitiveness**. Washington, USA: National Science and Technology Council (NSTC), 2011.

HSIEH, Y. T. *et al.* Speciation of cobalt-chloride-based ionic liquids and electrodeposition of Co wires. **Electrochimica Acta**, v. 117, p. 217–223, 2014.

HSIU, S.-I.; SUN, I.-W. Electrodeposition Behaviour of cadmium telluride from 1-ethyl-3-methylimidazolium chloride tetrafluoroborate ionic liquid. **Journal of Applied Electrochemistry**, v. 34, n. 10, p. 1057–1063, 2004.

HU, J.; ODOM, T. W.; LIEBER, C. M. Chemistry and physics in one dimension: synthesis and properties of nanowires and nanotubes. **Accounts of Chemical Research**, v. 32, n. 5, p. 435–445, 1999.

HUANG, X.-J. *et al.* The reduction of oxygen in various room temperature ionic liquids in the temperature range 293−318 K: exploring the applicability of the Stokes− Einstein relationship in room temperature ionic liquids. **The Journal of Physical Chemistry B**, v. 113, n. 26, p. 8953–8959, 2009.

ISHII, K.; AMAGASU, R.; NOMURA, I. Investigation of the n-side structures of II-VI compound semiconductor optical devices on InP substrates. **Journal of Crystal Growth**, v. 512, p. 96–99, 2019.

JENG, E. G.; SUN, I-Wen. Electrochemistry of tellurium(IV) in the basic aluminum chloride-1-methyl-3-ethylimidazolium chloride room temperature molten salt. **Journal of The Electrochemical Society**, v. 144, p. 2369–2374, 1997.

JIAN-MIN, S. *et al.* Construction of unconventional hexapod-like tellurium nanostructure with morphology-dependent photoluminescence property. **Journal of Physical Chemistry C**, v. 113, n. 22, p. 9502–9508, 2009.

JIANG, J. *et al.* Shift of optical absorption edge in SnO_2 films with high concentrations of nitrogen grown by chemical vapor deposition. **Journal of Applied Physics**, v. 119, n. 24, p. 245703-1–245703-6, 2016.

JIN, Y.; KIM, J.; GUILLAUME, B. Review of critical material studies. **Resources, Conservation and Recycling**, v. 113, p. 77–87, 2016.

KANAGARAJ, A. B. *et al.* Electrochemically grown vertical CdTe nanowire arrays on a flexible/transparent substrate. **Materials Letters**, v. 253, p. 113–116, 2019.

KAREEM, M. A. *et al.* Phosphonium-based ionic liquids analogues and their physical properties. **Journal of Chemical & Engineering Data**, v. 55, n. 11, p. 4632–4637, 2010.

KOKATE, A. V. *et al.* Effect of annealing on properties of electrochemically deposited CdTe thin films. **Journal of Physics and Chemistry of Solids**, v. 68, n. 1, p. 53–58, 2007.

KOWALIK, R. *et al.* Analysis of tellurium thin films electrodeposition from acidic citric bath. **Applied Surface Science**, v. 388, p. 817–824, 2016.

KUMAR, N. *et al.* Optical and electrical vtudies of vertically oriented tellurium nanowire arrays produced by template electrodeposition. **Journal of Electronic Materials**, v. 44, n. 8, p. 2939–2945, 2015.

KUMARI, S. *et al.* Studies on CdSe/PVK nanocomposites films for electroluminescent display applications. **Optical Materials**, v. 97, p. 109319–109326, 2019.

LADE, S. J.; UPLANE, M. D.; LOKHANDE, C. D. Electrosynthesis of CdTe films from ethylene glycol bath. **Materials Chemistry and Physics**, v. 63, n. 2, p. 99–103, 2000.

LEE, Y.-C. *et al.* Fabrication of 3D macroporous structures of II-VI and III-V semiconductors using electrochemical deposition. **Langmuir**, v. 18, n. 25, p. 9942–9946, 2002.

LI, G. *et al.* Solvothermal synthesis of polycrystalline tellurium nanoplates and their conversion into single crystalline nanorods. **RSC Advances**, v. 4, n. 2, p. 954–958, 2014.

LI, J.-P. *et al.* Thermoelectric Properties of Ce_3Te_4 under High Pressure: First-Principles Calculation. **Materials transactions**, v. 58, n. 11, p. 1601–1605, 2017.

LIANG, F.; QIAN, H. Synthesis of tellurium nanowires and their transport property. **Materials Chemistry and Physics**, v. 113, n. 2–3, p. 523–526, 2009.

LIN, S. *et al.* Tellurium as a high-performance elemental thermoelectric. **Nature Communications**, v. 7, p. 10287–10293, 2016.

LINCOT, D. *et al.* Chalcopyrite thin film solar cells by electrodeposition. **Solar Energy**, v. 77, n. 6, p. 725–737, 2004.

LINCOT, D. Electrodeposition of semiconductors. **Thin Solid Films**, v. 487, n. 1, p. 40–48, 2005.

LIU, J.-W. *et al.* Mesostructured assemblies of ultrathin superlong tellurium nanowires and their photoconductivity. **Journal of the American Chemical Society**, v. 132, n. 26, p. 8945–8952, 2010.

LIU, J. W. *et al.* Systematic synthesis of tellurium nanostructures and their optical properties: from nanoparticles to nanorods, nanowires, and nanotubes. **ChemNanoMat**, v. 2, n. 3, p. 167–170, 2016.

LUEVANO, J.; DAMODARAN, C. A review of molecular events of cadmium-induced carcinogenesis. **Journal of Environmental Pathology, Toxicology and Oncology**, v. 33, n. 3, 2014.

MALAQUIAS, J. C. *et al.* Electrodeposition of Cu-In alloys from a choline chloride based deep eutectic solvent for photovoltaic applications. **Electrochimica Acta**, v. 103, p. 15–22, 2013.

MAMUR, H. *et al.* A review on bismuth telluride (Bi_2Te_3) nanostructure for thermoelectric applications. **Renewable and Sustainable Energy Reviews**, v. 82, p. 4159–4169, 2018.

MASTAI, Y.; HODES, G. Size quantization in electrodeposited CdTe nanocrystalline films. **Journal of Physical Chemistry B**, v. 101, n. 14, p. 2685–2690, 1997.

MINGO, N. Thermoelectric figure of merit of II-VI semiconductor nanowires. **Applied Physics Letters**, v. 85, n. 24, p. 5986–5988, 2004.

MIROV, S. *et al.* Frontiers of mid-infrared lasers based on transition metal doped II–VI semiconductors. **Journal of Luminescence**, v. 133, p. 268–275, 2013.

MJALLI, F. S. *et al.* Tetrabutylammonium chloride based ionic liquid analogues and their physical properties. **Journal of Chemical & Engineering Data**, v. 59, n. 7, p. 2242–2251, 2014.

MOHAMED, R. B. *et al.* Structural and magnetic properties of Co diffused CdTe nanocrystalline thin films deposited by electron beam evaporation. **Journal of Superconductivity and Novel Magnetism**, v. 27, n. 9, p. 2147–2152, 2014.

MOKARI, T.; ZHANG, Minjuan; YANG, Peidong. Shape, size, and assembly control of PbTe nanocrystals. **Journal of the American Chemical Society**, v. 129, n. 32, p. 9864–9865, 2007.

MYERS, T. H.; EDWARDS, S. W.; SCHETZINA, J. F. Optical properties of polycrystalline CdTe films. **Journal of Applied Physics**, v. 52, n. 1981, p. 4231–4237, 1981.

ÖKO-INSTITUT E.V. **Critical metals for future sustainable technologies and their recycling potential:** Sustainable innovation and technology transfer industrial sector studies. United Nations Environment Programme. Nairobi, 2009.

PANDEY, R. K.; MAFFI, S.; BICELLI, L. P. Evolution of the morphology, structure and composition of CdTe films potentiostatically electrodeposited from an ethylene glycol-based bath. **Materials Chemistry and Physics**, v. 37, n. 2, p. 141–148, 1994.

PANDEY, R Kumar; CHANDRA, S.; SAHU, S. N. **Handbook of semiconductor electrodeposition**. New York: Marcel Dekker, 1996.

PATEL, S. L. *et al.* Bi-incorporated CdTe thin films for solar cells: air annealing evolution to structural, optical, electrical and surface topographical properties. **Materials Letters**, v. 249, p. 29–32, 2019.

PEREIRA, M. S. *et al.* Synthesis and properties of $Sn_{1-x}Fe_xO_2$ nanoparticles obtained by a proteic sol–gel method. **Journal of Nanoparticle Research**, v. 20, n. 8, p. 1–10, 2018.

PETROLEUM, B. **BP Statistical Review of World Energy 2019**. London: UK, 2019.

QIAN, H. S. *et al.* High-quality luminescent tellurium nanowires of several nanometers in diameter and high aspect ratio synthesized by a poly (vinyl pyrrolidone)-assisted hydrothermal process. **Langmuir**, v. 22, n. 8, p. 3830–3835, 2006.

RAKHSHANI, A. E. Electrodeposited CdTe–optical properties. **Journal of Applied Physics**, v. 81, n. 12, p. 7988–7993, 1997.

RAZMJOO, O.; BAHROLOLOOM, M. E.; NAJAFISAYAR, P. The effect of current density on the composition, structure, morphology and optical properties of galvanostatically electrodeposited nanostructured cadmium telluride films. **Ceramics International**, v. 43, n. 1, p. 121–127, 2017.

REZENDE, S. M. **Materiais e dispositivos eletrônicos**. 2a. ed. São Paulo: Editora Livraria da Física, 2004.

RHEEM, Y. *et al.* Synthesis of tellurium nanotubes by galvanic displacement. **Electrochimica Acta**, v. 55, n. 7, p. 2472–2476, 2010.

ROMERO, A. *et al.* Toxicity and biodegradability of imidazolium ionic liquids. **Journal of Hazardous Materials**, v. 151, n. 1, p. 268–273, 2008.

ROSS, C. A. Patterned magnetic recording media. **Annual Review of Materials Research**, v. 31, n. 1, p. 203–235, 2001.

SANTOS, L.P.M. *et al.* Electrodeposition of 1-D tellurium nanostructure on gold surface from choline chloride-urea and choline chloride-ethylene glycol mixtures. **Journal of Molecular Liquids**, v. 288, n. 15, p. 111038, 2019.

SCHAFFNER, J. *et al.* 12% efficient CdTe/CdS thin film solar cells deposited by low-temperature close space sublimation. **Journal of Applied Physics**, v. 110, n. 6, p. 64508, 2011.

SCHARIFKER, B.; HILLS, G. Theoretical and experimental studies of multiple nucleation. **Electrochimica Acta**, v. 28, n. 7, p. 879–889, 1983.

SCHLESINGER, M.; PAUNOVIC, M. **Modern electroplating**. New Jersey: John Wiley & Sons, vol. 55, 2011.

SEN, S. *et al.* Synthesis of tellurium nanostructures by physical vapor deposition and their growth mechanism. **Crystal Growth and Design**, v. 8, n. 1, p. 238–242, 2008.

SHAN, B. *et al.* Electrodeposition of wurtzite CdTe and the potential dependence of the phase structure. **Materials Letters**, v. 166, p. 85–88, 2016.

SHANNON, R. D. Revised effective ionic radii and systematic studies of interatomic distances in halides and chalcogenides. **Acta crystallographica section A: crystal physics, diffraction, theoretical and general crystallography**, v. 32, n. 5, p. 751–767, 1976.

SHE, G. *et al.* Template-free electrodeposition of one-dimensional nanostructures of tellurium. **Crystal Growth & Design**, v. 9, n. 2, p. 663–666, 2009.

SHIVAGAN, D D *et al.* Electrodeposition of chalcopyrite films from ionic liquid electrolytes. **Thin Solid Films**, v. 515, p. 5899–5903, 2007.

SIMKA, W.; PUSZCZYK, D.; NAWRAT, G. Electrodeposition of metals from non-aqueous solutions. **Electrochimica Acta**, v. 54, p. 5307–5319, 2009.

SINGH, R. R.; PAINULY, D.; PANDEY, R. K. Synthesis and characterization of electrochemically deposited nanocrystalline CdTe thin films. **Materials Chemistry and Physics**, v. 116, p. 261–268, 2009.

ŞIŞMAN, I.; DEMIR, Ü. Electrochemical growth and characterization of size-quantized CdTe thin films grown by underpotential deposition. **Journal of Electroanalytical Chemistry**, v. 651, n. 2, p. 222–227, 2011.

SMITH, E. L.; ABBOTT, A. P.; RYDER, K. S. Deep Eutectic Solvents (DESs) and their applications. **Chemical Reviews**, v. 114, n. 21, p. 11060−11082, 2014.

SONG, J.-M. *et al.* Superlong high-quality tellurium nanotubes: synthesis, characterization, and optical property. **Crystal Growth & Design**, v. 8, n. 6, p. 1902–1908, 2008.

STEICHEN, M.; DALE, P. Synthesis of trigonal selenium nanorods by electrodeposition from an ionic liquid at high temperature. **Electrochemistry Communications**, v. 13, n. 8, p. 865–868, 2011.

STUKE, J. Recent progress in the physics of selenium and tellurium. *In*: COOPER, W. C. (Org.). **The Physics of Selenium and Tellurium**. Montreal, Canada: Pergamon Press, 1969, p. 380.

SU, C. J. *et al.* Electrodeposition of aluminum wires from the Lewis acidic $AlCl_3$/ trimethylamine hydrochloride ionic liquid without using a template. **Electrochemistry Communications**, v. 34, p. 170–173, 2013.

SUN, H. *et al.* Unusual anodic behaviour of chloride ion in 1-butyl-3-methylimidazolium hexafluorophosphate. **Electrochemistry Communications**, v. 7, n. 7, p. 685–691, 2005.

SZYMCZAK, J. *et al.* Template-free electrodeposition of tellurium nanostructures in a room-temperature ionic liquid. **Electrochemistry Communications**, v. 24, p. 57–60, 2012.

THE CONSUMER TECHNOLOGY ASSOCIATION. **U.S. Economic Contribution of the Consumer Technology Sector**, 2016.

THIEBAUD, L. *et al.* Electrodeposition of high aspect ratio single crystalline tellurium nanowires from piperidinium-based ionic liquid. **Electrochimica Acta**, v. 222, p. 528–534, 2016.

THIEBAUD, L.; LEGEAI, S.; STEIN, N. Tuning the morphology of Te one-dimensional nanostructures by template-free electrochemical deposition in an ionic liquid. **Electrochimica Acta**, v. 197, p. 300–306, 2016.

TOMA, O. *et al.* Optical, morphological and electrical studies of thermally vacuum evaporated CdTe thin films for photovoltaic applications. **Solar Energy**, v. 108, p. 51–60, 2014.

TSAI, R.-W. *et al.* Voltammetric study and electrodeposition of tellurium, lead, and lead telluride in room-temperature ionic liquid 1-ethyl-3-methylimidazolium tetrafluoroborate. **Electrochimica Acta**, v. 137, p. 49–56, 2014.

TSIULYANU, D. *et al.* Characterization of tellurium-based films for NO_2 detection. **Thin Solid Films**, v. 485, n. 1–2, p. 252–256, 2005.

U.S. DEPARTMENT OF ENERGY. **Basic research needs for solar energy utilization**. Washington, D.C., 2005.

U.S. DEPARTMENT OF ENERGY. **Critical Materials Strategy**. Washington, D.C., 2011.
URCEZINO, A. S. C. *et al.* Electrodeposition study of Ni coatings on copper from choline chloride-based deep eutectic solvents. **Journal of the Brazilian Chemical Society**, v. 28, n. 7, p. 1193–1203, 2017.

VIEIRA, L; SCHENNACH, R.; GOLLAS, B. The effect of the electrode material on the electrodeposition of zinc from deep eutectic solvents. **Electrochimica Acta**, v. 197, p. 344–352, 2016.

VIEIRA, Luciana; WHITEHEAD, A. H.; GOLLAS, B. R. Mechanistic studies of zinc electrodeposition from deep eutectic electrolytes. **Journal of the Electrochemical Society**, 2014. v. 161, n. 1, p. D7–D13.

VIEIRA, Luciana; WHITEHEAD, A. H.; GOLLAS, B. R. In situ PM-IRRAS of a glassy carbon electrode/deep eutectic solvent interface. **Physical Chemistry Chemical Physics**, v. 17, n. 19, p. 12870–12880, 2015.

VISWANATH, S. G.; JACHAK, M. M. The effect of concentration of glycerol and electric current on the morphology and particle size of electrodeposited cadmium powder. **Metallurgical and Materials Engineering**, v. 19, n. 2, p. 137–154, 2013.

WAGLE, D. V; ZHAO, H.; BAKER, G. A. Deep eutectic solvents : sustainable media for nanoscale and functional materials. **Accounts of Chemical Research**, v. 47, n. 8, p. 2299−2308, 2014.

WALDEN, P. Molecular weights and electrical conductivity of several fused salts. **Bull. Acad. Imper. Sci. (St. Petersburg)**, v. 1800, 1914.

WALDIYA, M.; BHAGAT, D.; MUKHOPADHYAY, Indrajit. Electrodeposition of CdTe from BmimCl: influence of substrate and electrolytic bath. **Journal of Electroanalytical Chemistry**, v. 814, n. February, p. 59–65, 2018.

WALDIYA, M.; BHAGAT, D.; MUKHOPADHYAY, Indrajit. Raman study of galvanostatically deposited CdTe thin films from BmimCl. **Physica B: Condensed Matter**, v. 568, p. 36–41, 2019.

WANG, J. *et al.* Vertically aligned CdTe nanorods array for novel three-dimensional heterojunction solar cells on Ni substrates. **Electrochimica Acta**, v. 258, p. 858–865, 2017.

WANG, Y. *et al.* Crystallinity and phase controlling of g-C_3N_4/CdS hetrostructures towards high efficient photocatalytic H_2 generation. **International Journal of Hydrogen Energy**, 2019.

WANG, Z. *et al.* Formation of single-crystal tellurium nanowires and nanotubes via hydrothermal recrystallization and their gas sensing properties at room temperature. **Journal of Materials Chemistry**, v. 20, n. 12, p. 2457–2463, 2010.

WEI, L. *et al.* Electrochemically shape-controlled synthesis in deep eutectic solvents: triambic icosahedral platinum nanocrystals with high-index facets and their enhanced catalytic activity. **Chemical Communications**, v. 49, n. 95, p. 11152–11154, 2013.

WEI, S. H.; ZUNGER, A. Role of metal d states in II-VI semiconductors. **Physical Review B**, v. 37, n. 15, p. 8958–8981, 1988.

WEIDMANN, E. J.; ANDERSON, J. C. Structure and growth of oriented tellurium thin films. **Thin Solid Films**, v. 7, n. 3–4, p. 265–276, 1971.

WILKES, J. S.; ZAWOROTKO, M. J. Air and water stable 1-ethyl-3-methylimidazolium based ionic liquids. **Journal of the Chemical Society, Chemical Communications**, n. 13, p. 965–967, 1992.

WU, L.-K. *et al.* Effect of tellurium on copper electrodeposition in copper sulfate-sulfuric acid system. **Journal of The Electrochemical Society**, v. 164, n. 7, p. D451–D456, 2017.

WU, Yiying *et al.* Inorganic semiconductor nanowires: rational growth, assembly, and novel properties. **Chemistry - A European Journal**, v. 8, n. 6, p. 1260–1268, 2002.

XIA, Younan *et al.* One-dimensional nanostructures: synthesis, characterization, and applications. **Advanced Materials**, v. 15, n. 5, p. 353–389, 2003.

YANG, J.-M.; GOU, S.-P.; SUN, I-Wen. Single-step large-scale and template-free electrochemical growth of Ni–Zn alloy filament arrays from a zinc chloride based ionic liquid. **Chemical Communications**, v. 46, n. 15, p. 2686–2688, 2010.

YEUNG, H. W. C. From followers to market leaders: asian electronics firms in the global economy. **Asia Pacific Viewpoint**, v. 48, n. 1, p. 1–25, 2007.

YONG, S. M. *et al.* One-step hydrothermal synthesis of CdTe nanowires with amorphous carbon sheaths. **Materials Letters**, v. 64, n. 14, p. 1551–1554, 2010.

YUAN-HUI, L.; GREGORY, S. Diffusion of ions in sea water and in deep-sea sediments. **Geochimica et cosmochimica acta**, v. 38, n. 5, p. 703–714, 1974.

YUE, D. *et al.* Structure and electrochemical behavior of ionic liquid analogue based on choline chloride and urea. **Electrochimica Acta**, v. 65, p. 30–36, 2012.

ZEIN EL ABEDIN, S.; ENDRES, F. Electrodeposition of nanocrystalline silver films and nanowires from the ionic liquid 1-ethyl-3-methylimidazolium trifluoromethylsulfonate. **Electrochimica Acta**, v. 54, n. 24, p. 5673–5677, 2009.

ZHANG, B. *et al.* 1D tellurium nanostructures: photothermally assisted morphology-controlled synthesis and applications in preparing functional nanoscale materials. **Advanced Functional Materials**, v. 17, n. 3, p. 486–492, 2007.

ZHANG, Q. *et al.* Deep eutectic solvents: syntheses, properties and applications. **Chemical Society Reviews**, v. 41, n. 21, p. 7108–7146, 2012.

ZHANG, Q. B.; HUA, Y. X. Electrochemical synthesis of copper nanoparticles using cuprous oxide as a precursor in choline chloride–urea deep eutectic solvent: nucleation and growth mechanism. **Physical Chemistry Chemical Physics**, v. 16, n. 48, p. 27088–27095, 2014.

ZHAO, A. *et al.* Ordered tellurium nanowire arrays and their optical properties. **Applied Physics A: Materials Science and Processing**, v. 80, n. 8, p. 1725–1728, 2005.

ZHOU, B. *et al.* A novel ultrasonic-assisted solution-phase approach for the fabrication of tellurium bundles of nanowhiskers. **Ultrasonics Sonochemistry**, v. 13, n. 4, p. 352–358, 2006.

ZHU, W. *et al.* Ultrasonic-induced growth of crystalline tellurium nanorods and related branched structures. **Journal of Crystal Growth**, v. 295, n. 1, p. 69–74, 2006.

ZHU, Y.-J. *et al.* Microwave-Assisted Synthesis of Single-Crystalline Tellurium Nanorods and Nanowires in Ionic Liquids. **Angewandte Chemie**, v. 116, n. 11, p. 1434–1438, 2004.